ANALYSIS AND TESTING OF AN INTEGRATED REFRIGERATION AND STORAGE SYSTEM FOR LIQUID HYDROGEN ZERO BOIL-OFF, LIQUEFACTION, AND DENSIFICATION

By

WILLIAM USILTON NOTARDONATO

A DISSERTATION PRESENTED TO THE GRADUATE SCHOOL
OF THE UNIVERSITY OF FLORIDA IN PARTIAL FULFILLMENT
OF THE REQUIREMENTS FOR THE DEGREE OF
DOCTOR OF PHILOSOPHY

UNIVERSITY OF FLORIDA

2006

To the men and women of NASA KSC and their operations contractors for their dedication and commitment in performing an often-unappreciated role of preparing and launching spacecraft.

ACKNOWLEDGMENTS

I have a number of people to thank from NASA Kennedy Space Center, including Roy Bridges, who set up the Kennedy Graduate Student Fellowship, Joe Porta, my boss, who let me take the time to do the research work; and a number of KSC cryogenic engineers who lent their expertise, including but not limited to Robert Johnson, James Fesmire, Zoltan Nagy, Carl Exline, Diane Stees, and Maria Littlefield. In addition, a number of industry sources, including people at PHPK, Praxair, Sierra Lobo, Air Liquide, and NIST have contributed their expertise. I am also particularly indebted to Dr. Jong Baik of the Florida Solar Energy Center, my partner, who did the laboratory set up and much of the testing, and Dr. Glen McIntosh of CTS, for significantly contributing to the design and fabrication of the cryostat.

I express my sincere gratitude to all my committee members for agreeing to take the time to help my work and review this document. Specifically, I wish to thank Dr. Peterson and Dr. Chung for all of their help and guidance while I was revising this dissertation, Dr. Chow for a number of discussions and projects worked between KSC and UCF, and Dr. Sullivan and Dr. Ingley for agreeing to step in late and take over for other departed members. I also would like to thank all the professors I had at UF for rekindling my desire for learning about advanced engineering concepts. Finally, and most importantly, I acknowledge and thank Dr. Sherif for his time, patience, and guidance over the past five years.

This work would not be possible without the support of my immediate family, and for this I am very grateful. I thank my parents Mary-Lou and Joe for all their support over the years and for stressing the value of a good education. I also recognize Loretta Parenteau for her support and help with my family during the year I was in Gainesville. Finally, and most importantly, I thank my wife Celeste for all of her patience, understanding, support, praise, motivation, and help over the past five years. I could not have done it without her.

TABLE OF CONTENTS

LIST OF TABLES

Table page

LIST OF FIGURES

Abstract of Dissertation Presented to the Graduate School
of the University of Florida in Partial Fulfillment of the
Requirements for the Degree of Doctor of Philosophy

ANALYSIS AND TESTING OF AN INTEGRATED REFRIGERATION AND STORAGE SYSTEM FOR LIQUID HYDROGEN ZERO BOIL-OFF, LIQUEFACTION, AND DENSIFICATION

By

William Usilton Notardonato

December 2006

Chair: S. A. Sherif
Major Department: Mechanical and Aerospace Engineering

While hydrogen was first liquefied in the laboratory by Sir James Dewar in 1898, it was not until the beginning of the space age in the 1950s that large-scale production of liquid hydrogen was common. Since then, the methods used by NASA to produce, liquefy, store and distribute hydrogen for launch vehicle applications have not changed. Specifically, gaseous hydrogen is produced from natural gas, liquefied in large scale plants by performing external work on the gas and then expanding it, transported to the launch site via tanker trucks and stored in large ground tanks in the saturated state until it is loaded into the vehicle during launch countdown. During the process, heat leak and tank pressurization create boil-off losses, and chill-down of the transport lines cause more product losses. Other handling issues, including low liquid density, large thermal transients, leakage and safety concerns, and two phase flow problems have given liquid hydrogen a reputation for being a difficult fluid to store and control.

This dissertation proposes a novel method of liquefying and storing hydrogen by incorporating a closed-cycle helium refrigerator into the storage tank. There are numerous advantages to this system. Localized production and liquefaction eliminates the need for transportation of hazardous liquid hydrogen, minimizes heat flow into the system, and reduces the number of personnel required at the launch site. Proper design of the refrigerator also allows for densification of the liquid, increasing the amount of propellant loaded into the flight tank. In addition, subcooling below the normal boiling point allows the liquid to store more refrigeration energy, leading to less boil off losses or eliminating boil off completely, and possible allowing for recovery of chill down losses. Subcooled propellants also provide greater thermal margin before onset of evaporation and two-phase flow. Details of these performance and economic benefits are provided in Chapter 2.

While there are benefits, refrigerated and subcooled cryogens behave in a different manner than saturated liquids. These behavior issues must be investigated before large-scale incorporation in future launch systems. The conservation equations have been presented, and simplification of these equations in a 2-dimensional transient mass and energy model has been developed. Chapter 3 presents some results of the predicted behavior. A small testbed has also been proposed, designed, and fabricated for experimental validation of this model, and initial testing has occurred to validate the proposed concepts of liquefaction, zero boil off and densification. Results of this initial round of tests are provided in Chapter 6.

CHAPTER 1
CURRENT STATE OF THE ART IN HYDROGEN LIQUEFACTION, ZERO BOIL-OFF, AND DENSIFICATION

Hydrogen has many favorable properties that make it attractive as a secondary energy carrier. Hydrogen is very abundant. It is believed to make up 90% of the mass in the universe, and is the ninth most common chemical element on Earth. Combustion of hydrogen is clean, with the major combustion products being water and heat.[1] With a higher heating value (HHV) of 142,000 J/g, hydrogen carries more energy per unit mass than other fuels.[2] This is particularly useful for space applications as liquid hydrogen/liquid oxygen rockets have the highest specific impulse of any combination of chemical propellant currently in use.[3] For this reason, NASA and the US Air Force (USAF) have been interested in hydrogen as a propellant for space vehicles since the late 1950s. More recently, there is much interest in using hydrogen as an energy carrier in transportation applications, including automobiles, busses, and aircraft.[4-5]

Use of hydrogen does have some negative aspects however. Hydrogen gas has very low mass density, so volumetric concerns limit it use to small applications. Hydrogen can be stored as a gas in a solid matrix such as metal hydrides, but these systems are not mass efficient for space use. The most practical storage method for hydrogen fuels has been as a low temperature liquid. Hydrogen has a normal boiling point (NBP) of 20.27 K, and the density at this point is 70.79 kg/m^3. Its critical point has a pressure of 1315 kPa and temperature of 33.2 K, and the triple point has a pressure of 7.2 kPa and a temperature of 13.9 K.[6] While NASA and USAF have pioneered methods

for large scale production, storage, and distribution of liquid hydrogen, there are issues that must still be addressed before liquid hydrogen gains more widespread use as a practical energy carrier. Hydrogen requires large quantities of energy to liquefy, and since it is stored far below ambient temperature, heat leaks into the storage vessels creating evaporation and product losses. In addition, although liquid hydrogen density is 789 times greater than gaseous hydrogen, it is still a very low-density fuel and requires large, well-insulated storage vessels. These issues will be addressed in the present chapter.

Hydrogen Liquefaction

One factor delaying development of widespread use of hydrogen in the economy is the difficulty of storing and distributing large quantities. Gaseous storage requires extremely large volumes and storage in a metal hydride requires heavy storage tanks and addition of energy to drive the hydrogen out of the storage state. Liquid hydrogen has the potential to eliminate these concerns, but the process of liquefying hydrogen is energy intensive. Many different cycles have been proposed and used for hydrogen liquefaction, ranging from small-scale laboratory use to large liquefaction plants capable of producing 60 tons per day of liquid hydrogen.[7] A challenge associated with liquid production and storage is the need for development of small- to medium-scale distributed liquefaction systems that have efficiencies of the same order of magnitude as the large-scale liquefaction plants. This allows for localized production of hydrogen gas optimized for the specific location coupled with localized efficient liquefaction for higher energy storage densities.[8]

Generalized descriptions of procedures for hydrogen liquefaction exist in cryogenic technology literature.[1,7,9] These methods all rely on taking a purified gas at room

temperature and cooling it to the extremely low temperature of 20.3 K, the normal boiling point of hydrogen. In order to compare these systems, the thermodynamically ideal process first must be identified. The optimum cycle from the thermodynamic perspective is the Carnot Cycle, which consists of two reversible isothermal processes and two reversible adiabatic processes. This cycle would be the ideal refrigeration cycle, however, the liquefaction process is not a closed cycle but an open cycle where mass is continuously liquefied at the cold end and must be re-supplied at the warm end. Therefore the ideal liquefaction process can be taken as the first two steps of the Carnot cycle, namely a reversible isothermal compression of the gas to a suitably high pressure, followed by an isentropic expansion where the gas completely condenses in the expander. Refer to Figure 1-1 for details on this process depicted on a T-s diagram.[9] However, the high pressure required for complete liquefaction of hydrogen, 10^5 bar, makes this process technically not feasible. The minimum work required for this ideal liquefier can be determined and used as a benchmark for comparison with real processes.

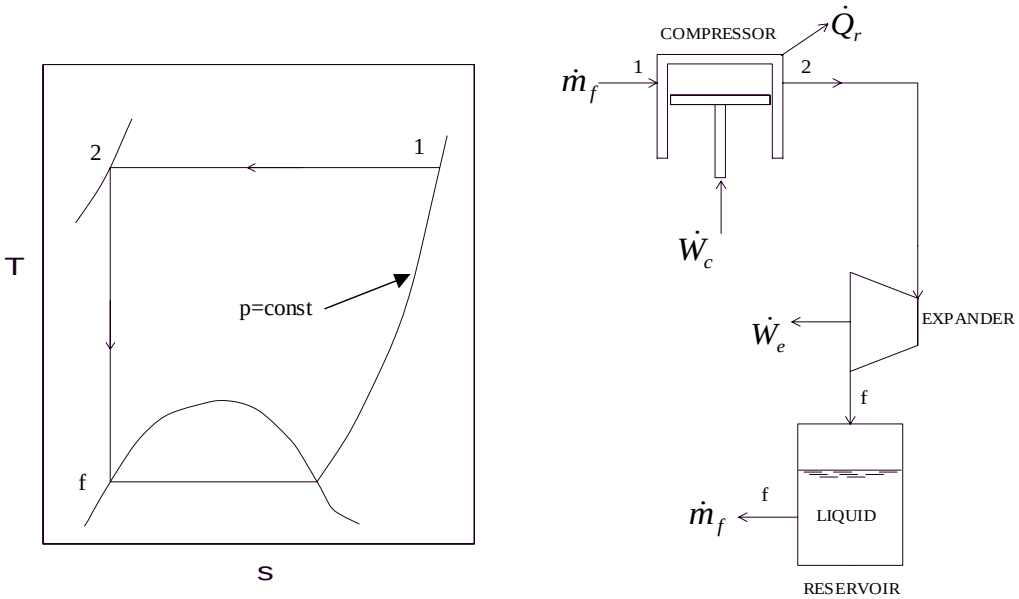

Figure 1-1 Ideal liquefaction process T-s diagram and system schematic

The First Law of Thermodynamics for steady flow with one inlet and one outlet, neglecting kinetic and potential energy change between the initial and final state, can be written as

$$\dot{Q} - \dot{W} = \dot{m}(h_3 - h_1) \qquad 1\text{-}1$$

From the Second Law of Thermodynamics for an ideal reversible process, an entropy balance on the heat exchange process gives

$$\dot{Q} = \dot{m}\int T \cdot ds \quad \text{or} \quad \dot{Q} = \dot{m}T_1(s_2 - s_1) \qquad 1\text{-}2$$

Combining equations 1-1 and 1-2 and knowing s_2 is equal to s_3 we find the minimum work required for liquefaction can be expressed as

$$-\frac{\dot{W}}{\dot{m}} = T_1(s_1 - s_3) - (h_1 - h_3) \qquad 1\text{-}3$$

From equation 1-3 we find the minimum work required to liquefy a gas (assuming the initial and final pressure are equal) depends on the initial state of the gas and the type of gas to be liquefied. Some common cryogenic fluids are listed in Table 1-1 along with their NBP and their ideal work of liquefaction. Note that hydrogen requires the highest work input for liquefaction, more than even liquid helium, which has the lowest NBP of any fluid.

Table 1-1 Ideal work of liquefaction for cryogenic fluids

Gas	Normal Boiling Point (K)	Ideal Liquefaction Work (J/g)
Helium 3	3.19	8178
Helium 4	4.21	6819
Hydrogen	20.27	12,019
Neon	27.09	1335
Nitrogen	77.36	768
Argon	87.28	479
Oxygen	90.18	636
Methane	111.7	1091

As an interesting side note regarding hydrogen storage for automotive use, US manufacturers tend to favor high-pressure hydrogen gas storage over liquid storage, which differs from some European auto manufacturers. Storage pressures range from the present 5000-psi systems to proposed 10000-psi systems.[10] Reasons cited for this preference include longer storage times, since there is no boil as with liquid systems, less systems complexity, and less energy input required. The advantages to liquid storage are greater energy density and hence greater range, and inherent purity of liquid hydrogen as opposed to gas.[9,11,12] Table 1-2 shows the relative energy costs associated with ideal liquefaction systems as compared to ideal gas compression systems for 5000 and 10000 psi. Ideal isothermal compression is given by the equation

$$W = P_o V_o \ln(P_1 / P_o) \qquad 1\text{-}4$$

although this is not attainable in real life. A more realistic process is the adiabatic compression process, expressed as

$$W = (\gamma / \gamma - 1) P_o V_o \{(P_1 / P_o)^{\gamma - 1 / \gamma} - 1\} \qquad 1\text{-}5$$

This table also shows the density of the product. From this table it is apparent that there is still significant energy cost associated with high-pressure gas storage.

Table 1-2 Ideal work input and density for liquefaction vs. pressurization of hydrogen

	Ideal Work Input	Density
	kJ/kg	kg/m^3
Liquid	12019	70.8
10000 psi fluid	8603	38.7
5000 psi fluid	7468	22.9

Now that a baseline liquefaction work requirement for ideal systems has been identified, actual liquefaction processes can be compared. A parameter called the Figure of Merit (FOM) is defined as ideal work required divided by the actual work required, and varies between 0 and 1.

Linde-Hampson Cycle

The most simple liquefaction system is the Linde-Hampson system, which uses a Joule Thomson (J-T) valve for isenthalpic expansion of the gas. The basic Linde-Hampson system is unacceptable for use in hydrogen systems because of that isenthalpic expansion, since the J-T coefficient for hydrogen at ambient temperature is negative. This means the expansion of hydrogen gas at ambient temperature will create a heating effect. It is not until the hydrogen gas reaches 205 K, its maximum inversion temperature that the J-T coefficient becomes positive and refrigeration may occur upon expansion. However, the Linde Hampson cycle will be discussed here because many of the same principles are used in other cycles.

A simple schematic of the Linde-Hampson cycle is shown in Figure 1-2[(9)], and the cycle state points are represented in the T-s diagram shown in Figure 1-3[(9)]. First, the gas is compressed isothermally from a low pressure P_1 to a high pressure P_2. The high-pressure warm gas stream then passes through an isobaric heat exchanger (HX), being cooled from the cold low-pressure gas stream. Next, the gas undergoes an isenthalpic expansion back to the original low pressure though a flow restriction, and enters the two-phase region. Here, some fraction of the process stream is withdrawn as a liquid, and the remaining vapor is used to cool the high-pressure gas stream before being re-compressed

for another round though the cycle. Make-up gas, equal in mass to the liquid withdrawn, is added prior to the compression step.

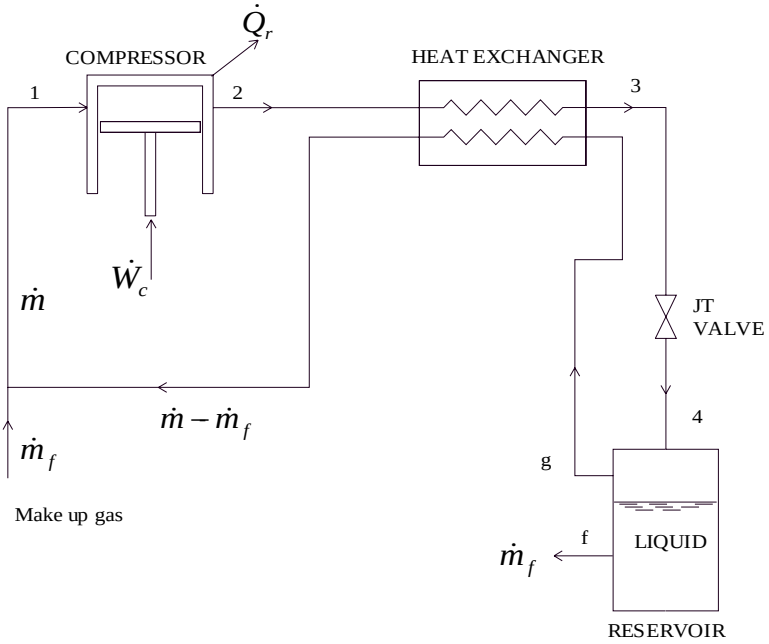

Figure 1-2 Linde Hampson schematic

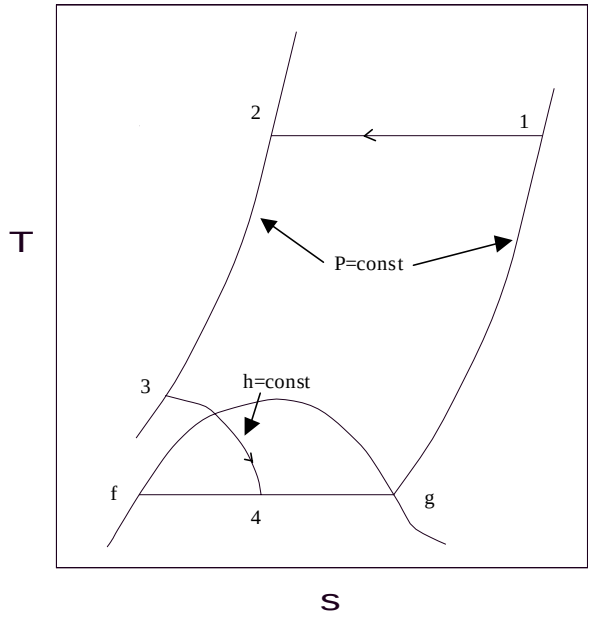

Figure 1-3 Linde Hampson T-s diagram

A control volume energy balance for the heat exchanger, expansion valve, and liquid tank, using the same assumptions as before, allows one to solve for the liquid yield.

$$y = \frac{\dot{m}_f}{\dot{m}} = \frac{h_1 - h_2}{h_1 - h_f} \tag{1-6}$$

Applying a similar energy balance to the compressor gives the work per unit mass liquefied to be

$$-\frac{\dot{W}}{\dot{m}_f} = (\frac{h_1 - h_f}{h_1 - h_2})[T_1 \cdot (s_1 - s_2) - (h_1 - h_2)] \tag{1-7}$$

This is an ideal analysis that does not take into account imperfect heat exchange, pressure drops in the system, heat leak into the system, and assumes isothermal compression. Nevertheless, this analysis will give a liquid yield of about 7% for liquid nitrogen systems, and has a typical LN_2 FOM of 0.115.

Pre-Cooled Linde-Hampson Cycle

The basic Linde-Hampson cycle can be used as a hydrogen liquefier if the high-pressure gas stream is cooled below the J-T inversion temperature prior to undergoing expansion in the valve. This system, referred to as the pre-cooled Linde-Hampson, is shown schematically in Figure 1-4[9] and the cycle state points are shown in Figure 1-5.[9] A secondary refrigerant, most commonly liquid nitrogen in either an open or closed cycle, is used to decrease the temperature of the gas prior to entering the recuperative heat exchanger. Again using an energy balance for the control volume including the two heat exchangers, expansion valve and receiver tank, a relation for the liquid yield can be found to be

$$y = \frac{h_1 - h_2}{h_1 - h_f} + \frac{\dot{m}_r}{\dot{m}} \frac{(h_a - h_c)}{(h_1 - h_f)} \tag{1-8}$$

and the ideal work requirement per mass of gas liquefied becomes

$$-\frac{\dot{W}}{\dot{m}_f} = \frac{1}{y}[T_1 \cdot (s_1 - s_2) - (h_1 - h_2) + \frac{\dot{m}_r}{\dot{m}}(h_b - h_a)] \qquad 1\text{-}9$$

The final term represents the additional work required by the refrigerant compressor. There are added complexities with this type of system, and careful design is required to find the optimum refrigerant flow rate. Typically this type of system will raise the FOM for a nitrogen liquefier to a value of 0.168. Variations on the pre-cooled Linde-Hampson include the Cascade cycle, where the refrigerant is pre-cooled by another cycle, which in turn could be pre-cooled by another cycle. A simple schematic of a cascade system is shown in Figure 1-6.[9]

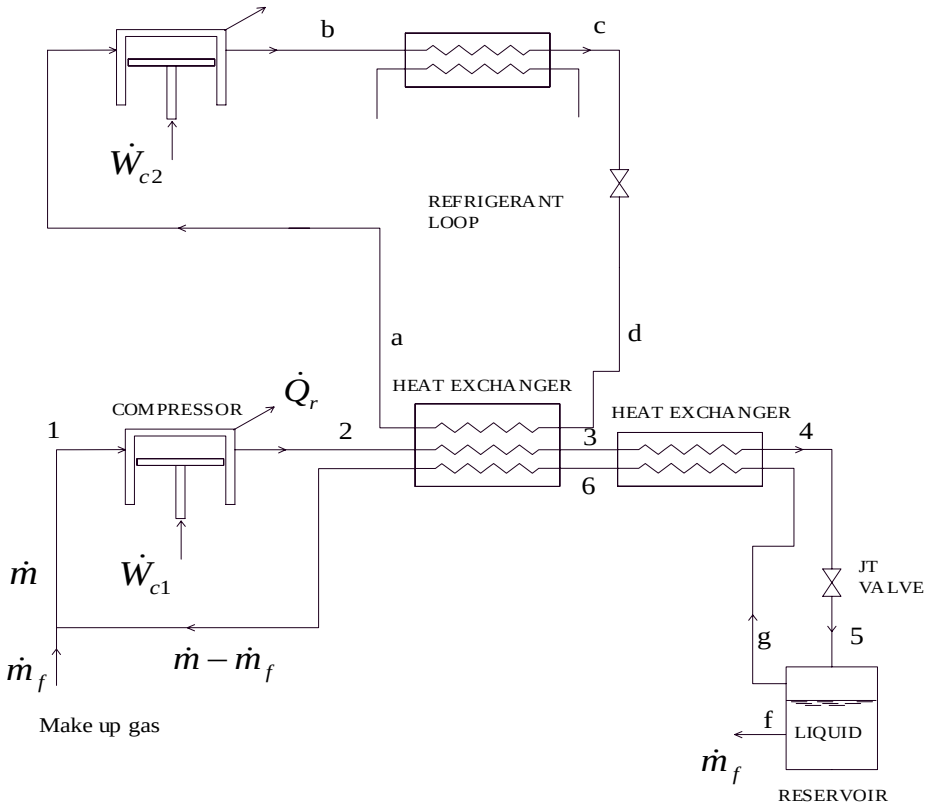

Figure 1-4 Pre-cooled Linde Hampson schematic

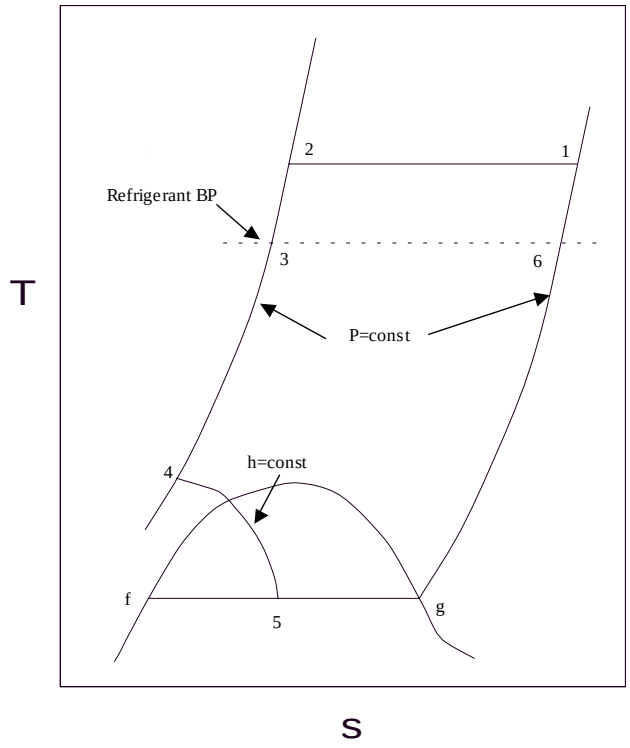

Figure 1-5 Pre-cooled Linde Hampson T-s diagram

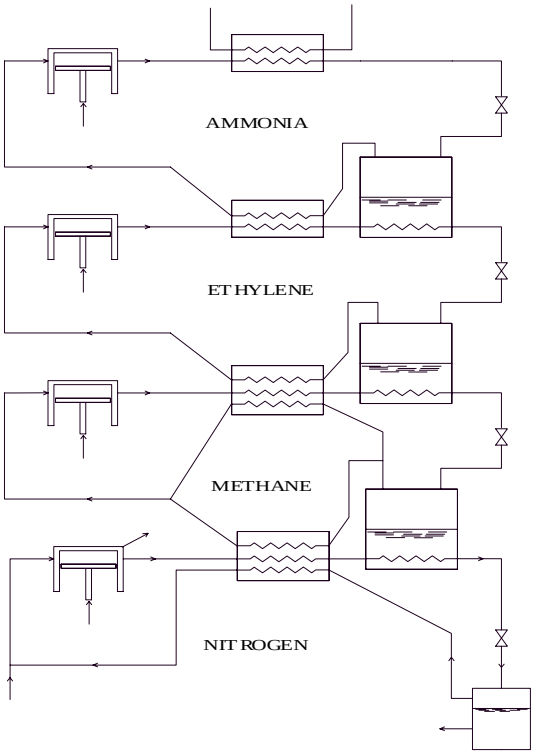

Figure 1-6 Cascade cycle schematic

Linde Dual Pressure Cycle

Another modification to the basic Linde-Hampson cycle is to add an intermediate pressure compression to the system, so not all the gas is compressed to the final pressure. This reduces the total work requirement somewhat and allows some of the heat to be removed from the gas at a higher temperature, making the process more efficient in terms of work required per unit mass liquefied. A schematic of the dual pressure cycle is shown in Figure 1-7[9] and the T-s diagram is shown in Figure 1-8.[9] The liquid yield is found to be

$$y = \frac{h_1 - h_3}{h_1 - h_f} - \frac{\dot{m}_i}{\dot{m}} \frac{(h_1 - h_2)}{(h_1 - h_f)} \qquad 1\text{-}10$$

And the ideal work per mass liquefied is

$$-\frac{\dot{W}}{\dot{m}_f} = \frac{1}{y}[T_1 \cdot (s_1 - s_2) - (h_1 - h_2) - \frac{\dot{m}_i}{\dot{m}}\{T_1(s_1 - s_2) - (h_1 - h_2)] \qquad 1\text{-}11$$

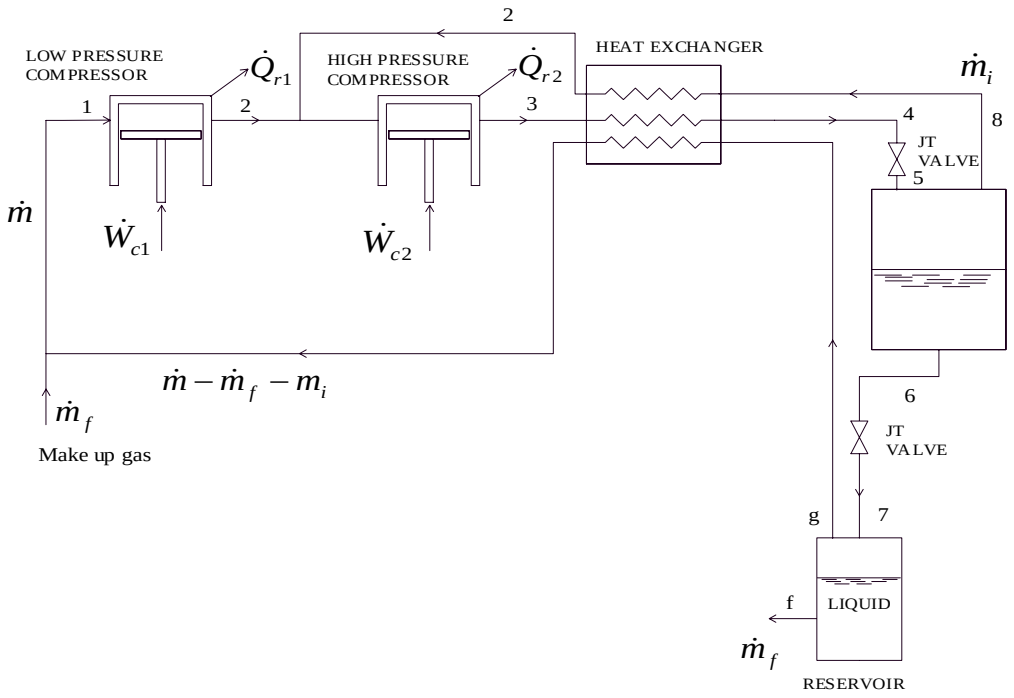

Figure 1-7 Linde dual pressure cycle schematic

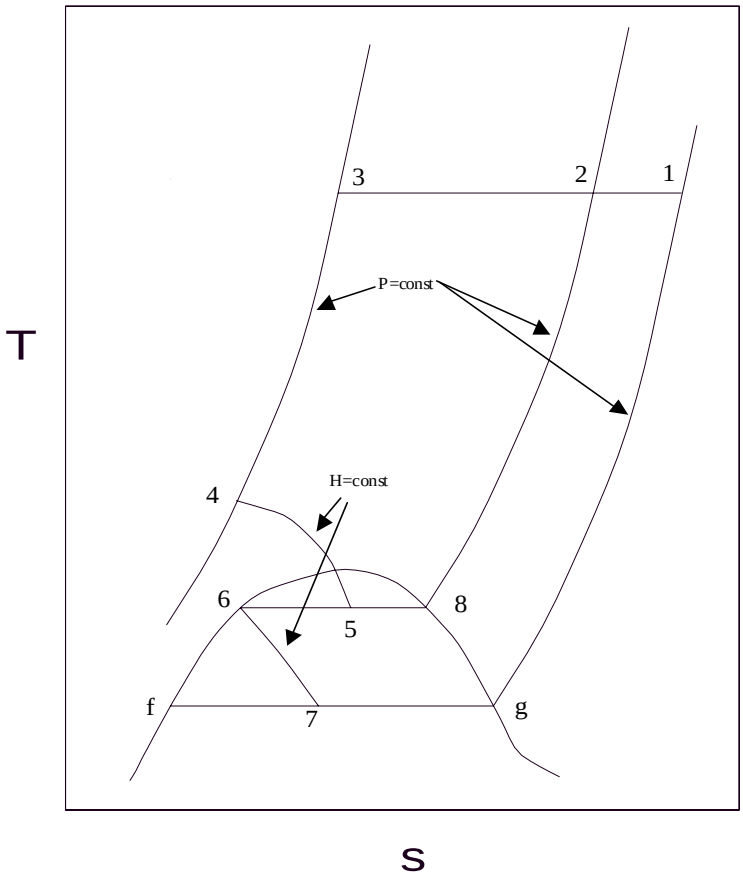

Figure 1-8 Linde dual pressure cycle T-s diagram

Claude Cycle

Another typical cryogenic liquefaction cycle, commonly used in hydrogen liquefiers, is the Claude cycle. This system is shown schematically in Figure 1-9[(9)] and the state points are shown in Figure 1-10.[(9)] The major difference between this and other cycles discussed so far is the first stage of expansion is done through a work-extracting turbine. This expansion is typically approximated as isentropic, and this allows the hydrogen to be cooled more efficiently than isenthalpic expansion, and cooling will occur no matter what the initial temperature. The refrigeration produced in the first stage expander is used to pre-cool the remained of the gas, so heat can be removed more efficiently at a higher temperature. A second stage J-T expansion is used for final

liquefaction, for simplicity since turbines typically cannot tolerate large liquid flow. An additional benefit of large scale Claude systems is the work produced in the turbine expander is used to help compress the gas, reducing the total work required. Liquid yield can be approximated as

$$y = \frac{h_1 - h_2}{h_1 - h_f} + \frac{\dot{m}_e}{\dot{m}} \frac{(h_3 - h_e)}{(h_1 - h_f)} \qquad 1\text{-}12$$

And the ideal work per unit mass liquefied is

$$-\frac{\dot{W}}{\dot{m}_f} = \frac{1}{y}[T_1 \cdot (s_1 - s_2) - (h_1 - h_2) - \frac{\dot{m}_e}{\dot{m}}(h_3 - h_e)] \qquad 1\text{-}13$$

There are many variations of the Claude cycle in use, not just for liquefaction of hydrogen but in many cases refrigeration of helium as well. This cycle can be combined in many ways with dual-pressure systems and pre-cooled systems. In some cases work is recovered in the outlet of the turbine but in others with work is dissipated in a braking system.

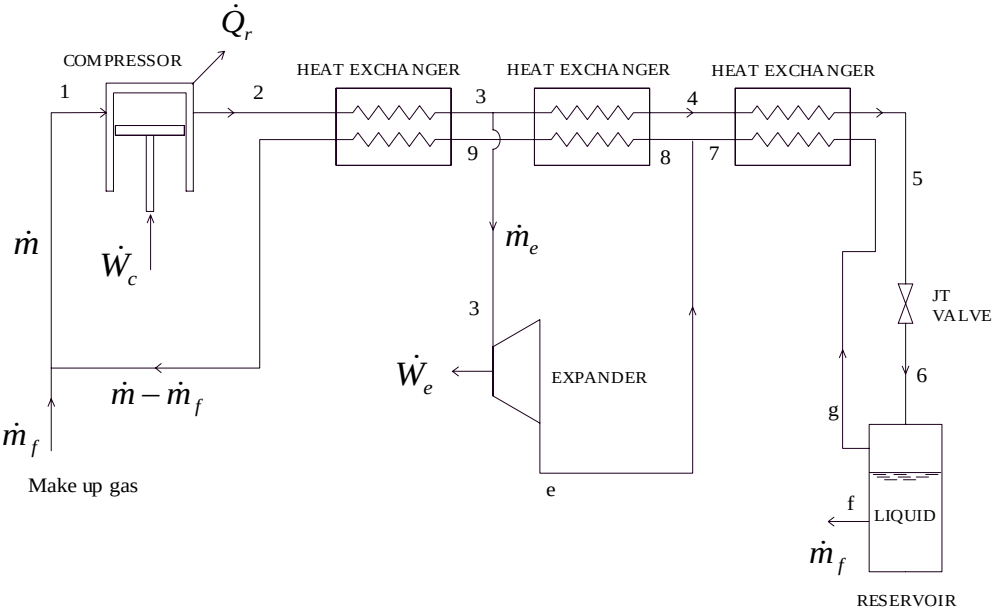

Figure 1-9 Claude cycle schematic

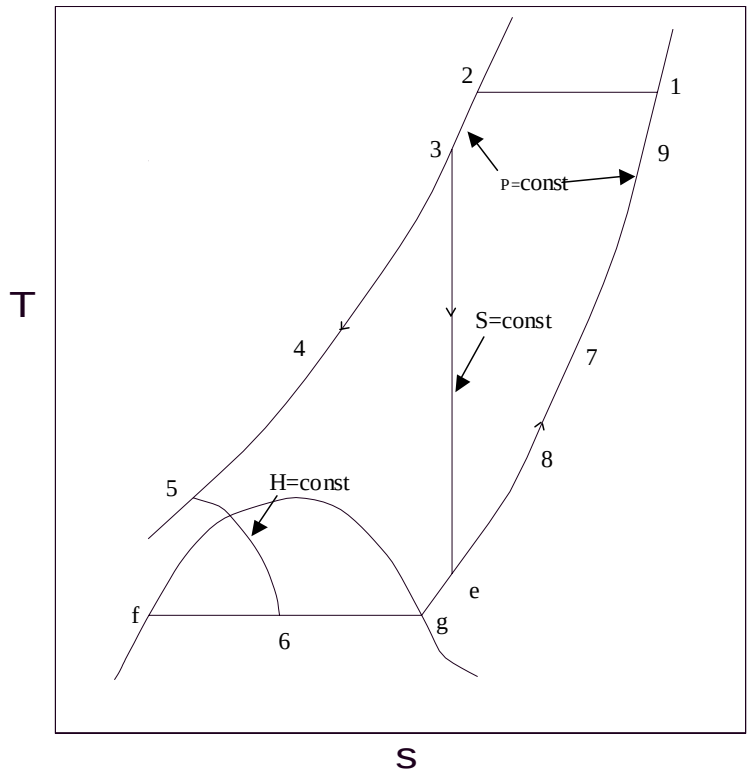

Figure 1-10 Claude cycle T-s diagram

Large Scale Hydrogen Liquefaction Plants

Several large-scale hydrogen liquefaction plants are in operation around the world and supply the majority of liquid hydrogen currently consumed. Details of the exact cycles used are considered proprietary but in general the plants use variations on the Claude cycle with a dual pressure system, and include several stages of isentropic turbine expansions before the final J-T expansion step for liquefaction.[1,7,13] These plants have been designed and optimized for the specific conditions of the local economy, and compromises between capital costs (typically the number of stages of turbine expansion and heat exchanger effectiveness) and operating costs (electrical input and maintenance) have been analyzed for economic efficiency. Generally, plants in the US also include a

liquid nitrogen pre-cooling stage while this practice has not been favored in Europe as much.

Surveys of existing large scale liquefaction plants as well as thermodynamic analysis has found that these systems typically operate at efficiencies approaching 40% of the Carnot ideal cycle.[14] This calculates that the total work required per mass of gas liquefied is typically around 30,000 kJ/kg. Obviously this is significant since this is approximately 22% of the HHV of the hydrogen.

Another factor to consider is the ortho-para conversion, and the energy associated with this exothermic reaction. Details of the ortho to para hydrogen conversion are given in Chapter 4. The optimum method of removing the heat of conversion is to use a catalyst to speed up the conversion process and remove the heat at the highest temperature possible. Current plants perform the catalyst step and heat removal in a number of discrete temperature points, but prototypes have been built and tested that perform conversion and heat removal in a continuous process.

Zero Boil Off

Ground Applications

One common feature of liquid hydrogen systems, indeed of cryogenic systems in general, is the fact that they are never in thermodynamic equilibrium with their surroundings. Heat transfer from the ambient temperature to the cryogenic storage temperature will always occur, no matter how good the thermal insulation systems are. If the liquid is subcooled, the heat leak increases the sensible heat of the liquid, and if the liquid is saturated the heat leak is absorbed by the latent heat of vaporization and boil off occurs. This boil off increases the vapor pressure in the tank until the maximum operating pressure is reached, and product losses occur as the excess vapor is vented

through the pressure relief system. As a side note, although the term boil off is in general use in the cryogenic industry to describe this product loss, heat leaks into the tank are typically so small that no nucleate boiling is actually occurring. A more accurate term would be surface evaporation.

Due to the cost of producing hydrogen from natural gas feedstock, liquefying it at a central plant, and then shipping it to the final destination, it appears economically attractive to ensure that boil off losses are minimized or perhaps even eliminated. NASA has been investigating zero boil off (ZBO) systems for many years at the Kennedy Space Center (KSC). Martin Marietta proposed a hydrogen reliquefier for the LC-39 complex in 1977 that would remove the heat that leaked into the tank by compressing the cold vapor at the top of the tank and then expanding it isenthalpically to obtain cooling in a modified basic Linde-Hampson system.[15] The compressors would operate at ambient temperature, with the compressor inlet stream cooling the compressor outlet stream, after the heat of compression was removed at ambient temperature. The compressor and coldbox were to be installed at the top of the LH2 tank at LC-39. Review of the thermodynamics and economics of the system indicated the approach was feasible, however the idea was never implemented because NASA management was concerned the work at the pads would impact the upcoming maiden launch of the Space Shuttle. In 1991, Ergenics Inc. proposed a system that would capture boil off losses in a metal hydride bed.[16] The captured gas would then be compressed in a hydride compressor, pre-cooled with liquid nitrogen, and expanded in a J-T expansion system. The analysis done indicated the system could be sized to capture not just the normal boil-off of the hydrogen tank, but also losses during tanker offload operations, from chill down of the

transfer lines as well as losses from tanker venting. This approach required the development of a large metal hydride storage system as well as a 2-ton per day liquefier that would only operate a few weeks per year. This proposal was rejected partly for the reason of complexity of a transient refrigeration system operating in batch processes, and concerns over reliability in such a design. At this same time, a Phase II SBIR contract was awarded to Hydrogen Consultants Inc. to prove the concept of a metal hydride compressor design that could run a J-T refrigeration system.[17] This system was sized to provide just enough refrigeration to overcome the steady heat leak into the tank, and the concerns over thermal transients was eliminated since the system was designed to operate continuously, using dual regenerative hydride beds. The program did produce working hardware, but there were technical issues with the J-T expansion device freezing and sticking during operation. In addition, the measured efficiency of the system was just 8.5% Carnot, poor by comparison with other cryogenic refrigerators. In all three cases discussed above, the hydrogen was allowed to vaporize, and then work was performed on the vapor to compress it prior to expansion and reliquefaction.

Despite the lack of success in creating a zero boil off system at KSC in the past, there are still sound economic advantages to recapturing hydrogen losses from boil off. In the case of liquid hydrogen at Kennedy Space Center a quick analysis shows the potential payoff for such a system.[18] Assume KSC pays a rough cost of $5.40 per kg of LH2 (not a true cost). This includes the cost to produce the hydrogen from the natural gas, cost to chill the hydrogen from its ambient temperature to a saturated vapor, cost to liquefy the vapor, the cost to ship the hydrogen to KSC in the tanker (plus losses in the transfer process), the cost to offload it to the KSC storage vessel, and profit for the

vendor. Now, after all the energy and effort that went into that process, every 20 J of heat that leaks into the storage vessel creates a loss of 1 gram of product. From an energy ratio standpoint, the equation is

$$Ratio = \frac{m * h_{fg}}{E_{H_2 production} + m * h_{300K-21K} + m * h_{fg} + E_{shipping} + E_{transferloss}} \qquad 1\text{-}14$$

It is difficult to estimate all the energy put into the entire process, especially the production process, but 88% of the enthalpy removed from the hydrogen during the liquefaction process occurs between ambient temperature and the saturated vapor state. However, when the liquid boils off and vents from the tank, this stored refrigeration is vented to atmosphere. This heat leak can be intercepted without creating boil off losses and the only energy cost to the system is the energy that goes into refrigeration. Assuming a refrigeration temperature of 20 K, an efficiency of 35% Carnot, and an electrical energy cost of $0.09 per kW-hr, a ZBO system equates to buying hydrogen for $0.50 per kg. There would be capital costs to be amortized over the life of the system, and these are not included in this simple analysis. Any additional operations (manpower) cost associated with this refrigeration will be offset by operational reductions in tanker offloads. There are safety benefits from the elimination of tank venting as well as reducing the number of transient operations.

Some estimates of the economic savings associated with ZBO ground systems are shown in Figure 1-11. There are a variety of cases analyzed, from current Shuttle launch operations to projected Crew Launch Vehicle and Heavy Launch Vehicle launch rates. The options include only recovery of boil off in the pad tanks, recovery of boil off and tanker losses, and finally recovery of boil off, tanker losses, and chill down losses. This figure shows the estimated payback time for the system is between 2 and 6 years.

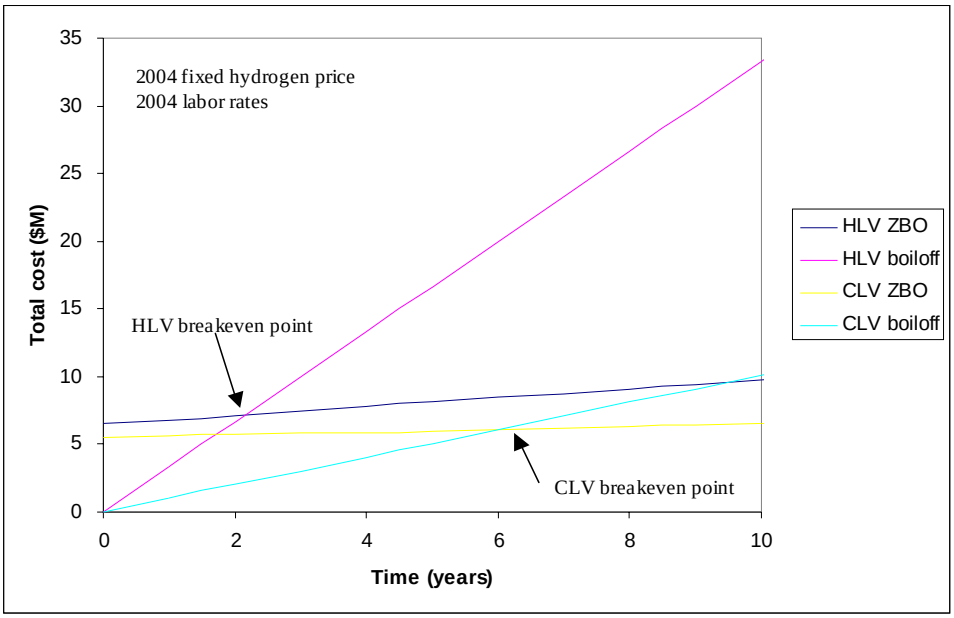

Figure 1-11 Zero loss storage economic analysis

Space Applications

In addition to developing ZBO systems for large-scale ground use, NASA has actively worked on developing a ZBO system for in space cryogenic storage. In this instance, the primary concern of product loss is magnified by the penalties imposed by the rocket equation. The cryogen in this case, fuel and oxidizer for a future propulsion stage, is considered payload for the launch vehicle and is subjected to the same small payload mass fraction as other payloads. As an example, consider an in space cryogenic depot situated in low Earth orbit (LEO). For every kilogram of product delivered, 6.5 kilograms of propellant are required for the launch vehicle to deliver it to LEO. The ratio becomes 12.9 to 1 for a depot at the L1 point, and 22 to 1 for hydrogen delivered to the surface of Mars.[19] Thus product loss from heat leak can make the use of cryogenic propellants prohibitive for many missions, unless zero boil off systems are developed.

Lockheed Missiles and Space first proposed the use of cryogenic refrigerators for long-term space missions in 1971[20], and the USAF investigated similar concepts in

1982[21]. At the time, cryocooler development was not at the required level of development in terms of low mass and flight quality reliability to warrant inclusion in systems at that time. Advances in flight quality cryocoolers in the 1980's and 1990's, especially using Stirling and pulse tube cycles, have made their use more attractive. Analysis of proposed hydrogen storage systems as feedstock for In Situ Resource Utilization (ISRU) systems for Mars exploration determined that ZBO made sense if the mission duration lasted longer than 45 days.[22] That is, less mass was added by the incorporation of a cryocooler and its associated power generation and heat rejections systems than was lost by boil off and the associated increase in tank size if the mission lasted longer than 45 days. Partially due to this analysis, NASA funded a series of experiments to determine the optimum integration methods of cryocoolers in microgravity cryogenic storage systems.

Initial testing at NASA Glenn Research Center (GRC) in 1999 was a proof of concept demonstration using an existing off the shelf cryocooler and a condensing heat exchanger in the vapor space of the tank. Test results were positive, showing constant or negative hydrogen vapor pressure slopes over the duration of 77 hours, but this configuration was not representative of actual space conditions, as there are no gravity forces that would separate the liquid and vapor phases.[23] Two phase flow handling in zero-g is the key technology that must be demonstrated. A more representative flight like test, performed at NASA Marshall Space Flight Center in 2001, used a circulatory system with a hydrogen pump drawing liquid from a liquid acquisition device and flowing it through a heat exchanger coupled with a cryocooler cold head. The cooled liquid then exited out a spray bar vent tube designed to provide destratification independent of ullage

and liquid positions in zero-g. The bulk hydrogen was maintained in the saturated liquid state, and refrigeration energy provided was exactly balanced by heat leak into the tank. Again, this cryocooler was not a flight quality unit but a commercial unit purchased off the shelf.[24] Testing ZBO concepts with a flight like cooler was accomplished in 2003 at NASA GRC. This test was performed with liquid nitrogen and a Northrop Grumman High Efficiency Cryocooler developed for the USAF. A submerged mixer pump was included to provide forced liquid nitrogen flow across a heat exchange surface, which was coupled to the cryocooler by a heat pipe and a flexible conductive link. Unfortunately, degradation in the system insulation performance over time led to larger than expected heat leak, and true ZBO conditions were never achieved. However, important information regarding integration of flight like cryocoolers with storage vessels was proven.[25]

In all the above cases, ZBO systems were proposed and tested that depended on the incorporation of a closed cycle refrigeration system to remove heat that had leaked into the tank. NASA Ames Research Center has proposed and performed a first order efficiency analysis on a system that uses the vapor from boil off as the working fluid in a refrigeration cycle.[26] This analysis shows it is advantageous from an efficiency point to directly perform work on the fluid to be maintained, primarily due to the fact that there is no temperature difference required to promote heat exchange at the low temperature end of the system. This concept, similar to ground based studies mentioned earlier, has not been proven in a test environment.

Hydrogen Densification

One performance enhancement under consideration for the next generation of space launch vehicles is densification of the cryogenic propellants. Propellant densification

refers to cooling the cryogens below their normal boiling point. Decreasing the temperature of liquid hydrogen from 20.3 K to 15 K increases the density from 70.8 kg/m3 to 76.0 kg/m3, an improvement of 7.3%. This density increase has a corresponding decrease in vehicle propellant tank volume and mass, reducing the overall dry mass of the vehicle. In addition to reduction in tank sizes, propellant densification has other performance benefits. Liquid hydrogen has a vapor pressure of 13 kPa at 15K, compared to 101 kPa at the normal boiling point. Lower vapor pressures mean lower tank operating pressures while still meeting the engine inlet net positive suction pressure required to prevent cavitation. This lower tank pressure can result in thinner tank walls, further reducing dry mass. Higher propellant density also results in smaller engine turbomachinery for a given mass flow rate, or increased safety margins by reducing the rotational speed on existing sized turbopumps. Finally, subcooled propellants can provide greater cooling power to the engine nozzles and combustion chambers due to the increased enthalpy gain prior to boil off, possibly making cooling passages smaller or minimizing chill down losses. All of the above reductions in vehicle dry mass have a cascading effect on the rest of the vehicle subsystems, resulting in mass reductions in airframes and aerodynamic surfaces, orbital maneuvering systems, thermal protection systems, landing gears and other systems. Studies by NASA contractors have estimated that propellant densification can result in the reduction of Gross Lift Off Weight by 12% to 20%, depending on the vehicle design and number of stages.[27] Figure 1-12 plots liquid hydrogen density, enthalpy, and vapor pressure as a function of temperature between the critical point and triple point.[6]

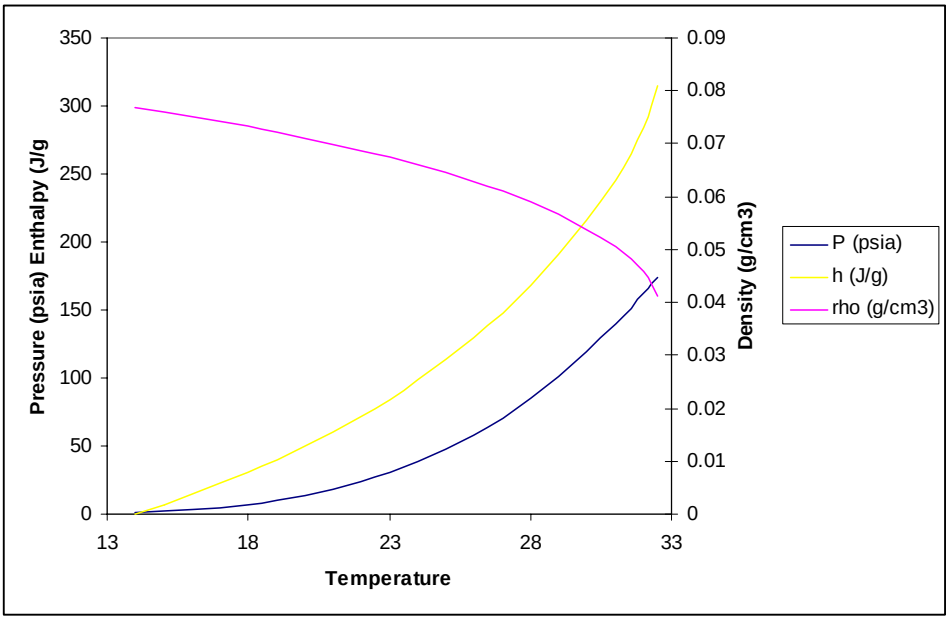

Figure 1-12 Saturated liquid hydrogen density, enthalpy, and vapor pressure

Because of the advantages that densified propellants offer, NASA and the Department of Defense have been interested in their potential use for many years. The National Bureau of Standards performed densified propellant property studies in the 1960's, usually producing the necessary refrigeration by evaporative cooling. Evaporative cooling refers to the technique of vacuum pumping the ullage space in a LH2 tank to reduce the vapor pressure, leading to evaporation of some of the liquid. The heat of vaporization needed for this evaporation is provided by the remaining liquid, creating a cooling effect. Union Carbide analytically investigated several slush hydrogen production techniques in the same timeframe. During the 1970's, Martin Marietta studied the concept of using a 50% slush LH2 mix with triple point oxygen in a single stage to orbit launch vehicle. Using slush hydrogen has increased benefits over subcooled liquids, primarily due to a density increase of almost 16% over normal boiling point hydrogen, and one of the recommendations from the report was to concentrate on hydrogen slush development only.[28] At this point, propellant densification was considered an immature

technology and NBP liquids were chosen as the propellants on the Space Shuttle. Further slush hydrogen work was accomplished during the National Aerospace Plane program in the late 1980's, with batch production of slush hydrogen being accomplished in 2000-liter quantities by the freeze-thaw method of evaporative cooling at NASA Glenn Research Center.[29] Operational and handling issues associated with pressurization, transfer, mixing and sloshing, and instrumentation was investigated. Although slush hydrogen offers significant performance benefits over subcooled liquids, technical issues with its use (including filtering, mixing to ensure homogeneous states, and mass gauging) has led NASA to primarily consider subcooled liquids above the triple point in most current studies.

More recently, NASA and aerospace contractors have considered using subcooled hydrogen on a modified Shuttle system, the X-33, and other 2nd Generation Reusable Launch Vehicles (RLV). Many of the funded programs in this area have concentrated on development of a densification production system. NASA GRC and Lockheed Martin have developed and tested subscale liquid hydrogen and liquid oxygen densification units based on the evaporative cooling method.[30] The largest hydrogen unit was capable of cooling 3.6 kg/sec of NBP hydrogen to 15 K, and the oxygen unit cools 13.6 kg/sec of NBP LOX to 66.6 K. In addition to production testing, tanking tests of the X-33 structural test article tank were completed. Tank loading procedures, including recirculation of warm propellants, were tested using subcooled LH2. However, safety and operational concerns with using subatmospheric boiling bath heat exchangers and cold compressors led NASA to solicit alternate technologies to producing subcooled propellants for the 2nd Gen RLV program. Refrigeration cycles that were chosen for

further development included orifice pulse tube refrigerators, a mixed gas J-T cycle refrigerators, and a packed column cooling tower design based on evaporation of liquid into a non-condensable gas. All three technologies were chosen based on the promise of simplicity and reliability of operation once development issues had been addressed.(31) After two years of development, these projects were not extended when the 2nd Gen RLV program transitioned into the Next Generation Launch Vehicle program and densified hydrogen fell out of favor compared to RP-1. However, operability assessments by NASA KSC during this program led to questions regarding the manner in which densified propellants would be implemented at the launch site.(32) This operability assessment is the basis of the proposed integrated refrigeration and storage system discussed in this dissertation. Other propellant studies have shown the mass savings associated with using densified oxygen and methane for ascent vehicles on the surface of Mars, coupled with an ISRU production facility.(33)

Launch Vehicle Operations

NASA has developed techniques for servicing spacecraft and launch vehicle cryogenic propulsion systems since the late 1950's. Techniques have evolved as hardware and software capability has developed, and each current program has some vehicle and pad specific systems and operations required. However, the basic approach remains similar, and servicing capabilities (in terms of quality of propellant loaded) are nearly identical. These systems, or derivatives of them, are capable of meeting the needs of an in space cryogenic depot, provided this depot uses propellant at or above the normal boiling point, and free venting of boil off in space is permitted. Conditioning of propellants via advanced ground storage systems has the potential to minimize cost and safety risks, while maximizing launch performance.

The current method of large-scale cryogenic storage and distribution is very similar across all programs at Kennedy Space Center and Cape Canaveral Air Station. Cryogens (Liquid Hydrogen and Liquid Oxygen) are produced off site, delivered via tanker trucks, and transferred to ground storage tanks days or weeks prior to launch. Cryogens in the tanks are stored as a saturated liquid, and boil off gas is not recovered. During launch countdown, as late as possible into the count, the cryogens are transferred to the flight tank, and in the event of a launch scrub, are drained back into the ground storage tanks. Details on how this is accomplished vary across programs.

Hydrogen for the Space Shuttle Program is purchased from Air Products New Orleans plant and delivered via 13000-gallon road tankers. Periodic sampling of tankers is done to ensure the propellant meets purity specifications. Waves of up to five tankers can be offloaded at a time, and two waves can be done in a day. Prior to offload, transfer lines are purged with gaseous helium and sampled. The tank is vented and valves are opened to start chill down. Product losses from tank venting and transfer line chill down are free vented at the top of the pad storage tank. After offload is complete, transfer lines are purged of hydrogen. The pad storage tank holds 850,000 gallons of liquid, with 10% ullage on top. The tank has a vacuum jacket and perlite bulk fill insulation. The cross-country lines 10” ID, 1500 feet long and are vacuum jacketed (VJ) with multi-layer insulation (MLI). The storage tank is pressurized using vaporizer heat exchangers.

Prior to launch, the tank must be filled to 700,000 gallons, which is enough for three launch attempts. Loading of the STS external tank (ET) begins at T-6 hours on the countdown clock. Purges to the various disconnect cavities is initiated and transfer line blanket pressure is vented. The ET vent valve is opened, chill down line valve is opened,

and chill down of cross-country lines begins. Then the storage tank is self-pressurized, and slow fill (1000 gpm) to the lower ET liquid level sensors is completed. The main transfer valve is then opened and fast fill to 98% initiated, with flow rate of 8500 gpm. When the ET ullage pressure rate reaches a limit, LH2 topping at 775 gpm is initiated until the upper liquid level sensor reads 100% wet. Then the replenish valve controls the flow to maintain 100%, usually less than 300 gpm. At T-1:57 minutes, replenish mode terminates. Overall, 383,400 gallons is loaded into the ET, with 48,000 gallons lost during chill down and 40,000 gallons lost during replenish. These vapor losses are burned in a flare stack. If the launch is scrubbed, drainback procedures are initiated.

Summary

The state of the art in ground processing of cryogenic propellants is considered mature, and KSC operators have over 50 years of experience in this type of operations. There are performance enhancements that can be made. Of these, local production and liquefaction of hydrogen offers benefits of eliminating tanker operations, and zero boil off storage can eliminate wasteful product losses. Hydrogen densification has performance benefits for the flight vehicle. NASA has invested significant funds to investigate these systems over the past 30+ years, but has never fielded an actual operating system. There are many reasons for this, but the most powerful of these has always been a lack of confidence that the benefits would outweigh the operational impacts, and conservative forces in management were unwilling to try something different. This work is an attempt to change some of these positions.

CHAPTER 2
PROPOSED INTEGRATED REFRIGERATION AND STORAGE SYSTEM

The current state of the art in hydrogen liquefaction, storage and distribution for space launch systems has successfully served its intended purpose for the past 50 years. However, there are possible improvements that can be made that will make liquid hydrogen use more economical, reliable, and safe than current systems. This chapter will describe the basic concept of such a system, will explain the significance of the development, and will qualitatively describe the thermodynamic behavior of the system. Later chapters will detail designs of an experimental system built to test these concepts, and data analysis of initial liquefaction, zero boil off and densification tests will be presented.

Integrated Refrigeration and Storage Concept

The optimum design of a liquid hydrogen storage and distribution system is highly dependent on the intended use of the product. For example, most industrial uses of liquid hydrogen are in a continuous or semi-continuous process, such as a steady flow of hydrogen to hydrogenate oils in the production of margarine or cooking oils or steady flow of hydrogen in an anhydrous ammonia plant. In these cases, hydrogen is liquefied only because of the transportation issues associated with supplying large quantities of gaseous hydrogen make the process impractical. The hydrogen is ultimately used as a gaseous product, although much of the cooling power is recuperated elsewhere in the process. Most of the time, there is not a large quantity of liquid transfer lines, the hydrogen is vaporized immediately downstream of the storage tank. In these cases, large

scale use of a continuous flow of gaseous hydrogen from a liquid storage system, heat leak into the tank that creates boil off is not considered an issue, there are not many issues associated with chill down and two phase flow in the supply lines, and there is no reason to increase the density of the liquid in the storage tank. Current state of the art in hydrogen storage and distribution is acceptable for these applications.

The typical usage scenario for a liquid hydrogen system in support of the space program is very different than that in industry. The hydrogen is used in a batch process, often with many months in between launches. During this time heat leak into the tank leads to significant product losses, in fact only 65% of the hydrogen delivered to Kennedy Space Center is ever actually launched aboard the Space Shuttle.[34] Another major difference is the hydrogen is required to be a liquid at the use point as opposed to a gas as in most major industrial operations. Not only is the hydrogen required to be a liquid, there are strict limits on the state of that liquid that are dictated by the design of the tank and the engine start box. For the Space Shuttle main engines, temperature measurements on the turbopump exit and recirculation lines as well as power limits on the recirculation pump (to detect cavitation) ensure there is liquid flowing through the engine passages prior to start.[35] In this manner, the usage requirements between industry and aerospace vary greatly, and current state of the art, while acceptable, is not optimized for space use. These usage requirements are even more strict when considering liquid hydrogen produced In Situ on the Moon or Mars. Therefore, liquid hydrogen systems designed to minimize or eliminate heat leak and boil off, operate in a number of batch processes with large thermal transients, and still deliver good quality

liquid when required at a use point many hundreds of meters away, are required for the next generation of space launch systems.

What is truly needed is a novel approach to ground processing of cryogenic propellants, as opposed to incremental improvements in existing philosophies. The new philosophy should conform to the KISS principle, by minimizing operations, especially ones that cause thermal transients or require opening the system to outside contamination. This new philosophy should take advantage of advances in cryogenic engineering over the past 20 years including efficient and reliable refrigeration systems, health monitoring of vital components, and advanced insulation systems. Most important, the system should offer economic and energy efficiency by minimizing boil off and chill down losses as well as venting of high cost purge gasses like helium. One possible approach to this issue is to integrate a closed cycle helium refrigeration system into the ground storage tank. This integrated refrigeration system would offer the advantage of exercising more control of the propellant thermodynamic state while still in ground storage. Such an advanced system could serve as a liquefier, a zero boil off storage system, and possibly a propellant densification system. Properly designed, this could provide cost, safety, reliability, and performance benefits over current state of the art.

This work proposes to integrate a cryogenic refrigerator into a liquid hydrogen dewar. Advantages to this proposal are numerous. First, the refrigerator can be used to remove the heat that leaks into the vessel from the ambient environment, so there is no pressure rise and associated boil off from the heat leak. This has obvious economic savings, however, there are safety benefits as well since the tank is not venting gaseous hydrogen most of the time. Second, if the refrigerator is sized properly, it can serve as a

local liquefaction system. This minimizes operations cost since fewer personnel are required for tanker offload operations. There are less purge and sampling operations as well since there are no tanker supply lines to inert. An added benefit is elimination of tanker offload losses from venting the tankers and chilling down the transfer lines. Again, there are safety and reliability benefits due to minimization of transient operations and venting operations. A third advantage of the integrated refrigeration and storage is the ability to control the state of the propellant. Currently, liquid hydrogen is created and stored as a saturated liquid, although some degree of subcooling is possible with pressurization of the liquid. This proposal allows for both subcooling for an extended period of time as well as densification of the liquid below the normal boiling point. This is a fundamental change in the way liquid hydrogen is stored. Currently, there is no true thermodynamic equilibrium in a cryogenic system as there is always some degree of heat leak between the ambient temperature and the liquid temperature. This proposal mechanically removes this heat leak, so the cryogen can be stored in a manner similar to thermodynamic equilibrium.

System Behavior

By integrating a cryogenic refrigerator into a storage vessel, thermodynamic control of the cryogenic propellants can be achieved. The control of the system will be based on the ability to change the enthalpy of the stored liquid, and depends on the design of the system. Specifically the difference between the amount of heat removed at the storage temperature by the refrigeration system compared to the energy entering the system from either heat leak into the system from the warm surroundings or energy entering the system from a mass input will determine the rate of change of the stored enthalpy. Mathematically this is expressed as

$$m * \frac{\delta h}{\delta t} = -Q_{ref} + Q_{HL} + \dot{m}\Delta h \qquad 2\text{-}1$$

There are three possible types of behaviors associated with such a system. If the first term on the right is less than the other two, there will be a net positive flow of energy into the system. This leads to a temperature increase, or if the fluid is saturated, an evaporation of some of the liquid combined with a pressure increase. Eventually the pressure will increase to the limit on the tank relief valve, and tank venting will lead to product loss. This type of system is what is currently used at KSC.

A second type of system behavior is to balance the energy entering the tank with the refrigeration produced, so there is no net energy input into the system. This quasi steady state behavior is characterized by constant system pressure and temperatures, despite the fact that the system is not truly in thermal equilibrium with the surroundings. NASA has been studying similar systems recently for the application of long term zero boil-off storage for space missions. Most of these studies are for closed systems with no mass input, but some proposals have sized the refrigerator to allow for liquefaction of some small amount of incoming propellant from an ISRU reactor.

The third type of behavior is exhibited when the refrigerator removes more energy from the system than enters via either mass input or heat leak. This results in a decrease in system pressure and temperature and a corresponding condensation of some of the ullage gas. Assuming a homogeneous system, the state will follow saturated liquid line to the triple point and then eventually the liquid completely freezes and the path follows the sublimation curve. For systems of interest to spaceport propellant servicing, the solid phase most probably will be avoided and refrigeration will be controlled to keep the state above the triple point. In addition, to avoid contamination the system pressure would

probably need to be kept above atmospheric pressure by using a non-condensable pressurization gas such as helium.

Combined with the fundamental change in behavior of the integrated refrigeration and storage system as described above, there are a number of operational enhancements to be considered. First and foremost, the system can be developed to be a zero loss storage system. Better than a zero boil off system, a true zero loss system would never have any product loss, including during chill down and transfer operations. While this idealized case will probably never be fully achieved, capture and recovery of 50% of current chill down losses during countdown will have substantial savings. This implies to less venting and flaring operations at the launch pad, which is a potential safety improvement, and requires a smaller storage vessel with less capital costs and heat leak than the current alternative. Another ambitious goal would be elimination of boil off from heat leak into the flight tank during loading operations. This would lead to a “storable” form of cryogenic propellant, which has great benefits from an operational standpoint. Storable cryogens will have extended countdown hold times, and can be useful as a rapid response type of launch vehicle. Since flight tanks are generally insulated with foam, the heat leak is an order of magnitude higher than what is found in the ground supply tank. This necessitates a refrigeration system with higher capacity, but this is a benefit in itself. Larger capacities imply greater efficiencies, and the added capacity can be used as a liquefaction system when not in launch countdown. If liquefaction capability is built in to the storage system, there is no need for tanker delivery of liquid, and the only supply connection can be a pure gaseous hydrogen input at the top of the tank. This leads to less ground support equipment (GSE), no tanker ports and transfer lines, less hazardous

operations, less thermal transients, and less potential for contamination from line connections. Finally, when the refrigeration system is not performing zero boil off or liquefaction operations, the capacity can be used to densify and subcool the propellant. Densification has advantages for launch vehicle performance, as will be discussed in later sections, however, even if launch vehicles use NBP propellants there are advantages in densifying and subcooling on the ground. Densified, subcooled propellant acts as a source of stored refrigeration energy that can be used as a thermal mass in liquefaction and zero boil off applications, may allow for faster chill down times, and are easier to transfer due to greater density and less tendency to exhibit two phase flow and cavitation. These three new operational capabilities, ZBO or zero loss, liquefaction, and densification/subcooling, will be discussed in greater detail below.

The added capability will come at some cost, mainly capital improvement of the pads by adding a cryogenic refrigeration system. This capital cost will be offset by savings in procurement by adding ZBO and liquefaction capability. If properly designed, there should be little added operations required as a result and should be offset by operational savings resulting from elimination of tanker operations. Close cycle helium refrigerators using the reverse turbo-Brayton cycle are current state of the art, and need no advanced development to be modified for this application. These systems are in use at many large-scale magnetic labs and particle accelerators and are proven to be efficient and reliable. Many components are also in use at open cycle liquefaction plants around the world. Helium screw compressors are at ambient temperatures and are oil lubricated. The only cold moving parts are the turbines, and at hydrogen temperature ranges these do not require expansion of helium into the two-phase region. The turbines are also

mounted outside the cold box and can be replaced LRU style with no interruption in service. The refrigerators are designed with modern controls systems are self-regulating to provide optimum operation at a range of output conditions.[36]

In a full scale Spaceport system, the refrigeration system may be sized to remove the heat leak in the flight tank. Flight tanks generally use Spray on Foam Insulation, so overall heat leak may be on the order of 200 kW. When the flight tank is not loaded, the refrigerator will be oversized. This excess capacity can either be turned down or the system can be used as a hydrogen liquefier. On site liquefaction has operational advantages. There are safety benefits, since there is no transportation across public highways, no transfers of cryogenic liquids from tankers to storage tanks, and less hazardous venting. Cost savings will occur due to less operations and transportation, especially if the hydrogen production facility can be sized to provide economy of scale for many sites. The entire spaceport can consist of one centralized hydrogen production facility supplying a number of modular, self-contained liquefaction and storage sites at each pad thru pipelines not unlike the natural gas lines in common use. There is possible synergy with the future hydrogen economy, and the need for localized hydrogen production and storage, and the system serves as a prototype of a future Lunar or Mars propellant production and storage facility.

The proposed testbed will have the capability to deliver hydrogen gas to the liquid system. After pressure reduction, the gas will be metered thru a mass flow controller. The regulated gas stream can be delivered in three possible ports. First, the gas can be added to the ullage space on top of the liquid, condensing at the liquid/vapor interface. Second, the gas can bubble up thru the bottom of the tank, with the bubbles exchanging heat with

the subcooled liquid. Finally, the gas can exchange heat directly with a condensing heat exchanger line at the cold head. For all three methods, the liquefaction rate must be measured. To increase efficiency of the liquefaction process, the gas may be pre-cooled with a liquid nitrogen HX or an intermediate stage of helium refrigeration, so the high temperature enthalpy changes can be removed with less expensive refrigeration. In addition, pre-cooling allows the addition of an ortho to para conversion catalyst to be added. This will help remove some of the heat of conversion before the hydrogen enters the dewar.

Behavior Issues

The proposed novel operational system will behave different than the NBP counterpart and there will be a learning curve associated with their use. Research into operational behavior must be addressed. The topics to be explored include pressurization and venting of stored subcooled liquids, integrated refrigeration systems controls to provide optimum performance during different operational phases of densification, zero boil-off and liquefaction, determination of heat and mass transfer coefficients, and methods of handling stratification layers. Advanced instrumentation should be developed to accurately determine the state of the propellant quality

The vapor pressure of liquid hydrogen stored at 14 K is only 7 kPa. Having a subatmospheric pressure inside the dewar may create safety concerns since any leak path in the tank will draw in outside air, which will immediately freeze. While the inner tank must be designed to hold a vacuum, that should not be the normal mode of operation. Another issue is the tendency of the tank pressure to decrease as heat is removed from the tank, as opposed to normal heat leak into a tank causing a pressure increase. The tank will operate at two pressure settings, normal (extended) operation with a small positive

pressure differential, and transfer operations pressure with a higher positive pressure to overcome line resistance and elevation changes.

Normal operational pressure will be approximately set at 140 kPa. The inside of the tank will not be in thermodynamic equilibrium, as the cold liquid will continuously condense the vapor at the top of the tank. To maintain positive pressure, three different sources of ullage pressure may be considered. First, gaseous helium, non condensable at 14 K, will be used. Testing will be performed to determine the rate of pressurization of the system using various flow rates of gaseous helium. This will depend on the heat transfer rate between the liquid/vapor interface and the convection heat transfer in the gaseous helium. Techniques to prevent the collapse of the ullage pressure will be investigated, including bubbling the helium up through the liquid hydrogen to increase heat exchange rate and pre-cool the helium. The other option for pressurization gas is hydrogen. Liquid hydrogen from the tank will be directed to a vaporizer consisting of a heat exchange coil, isolation valve, and pressurization regulator. The dynamics of the system heat exchange rates will be recorded, in an attempt to balance the rate of heat transfer between the liquid/vapor interface and the vaporizer and atmosphere. Again, gaseous hydrogen will also be bubbled up through the liquid, although this is not advantageous since the amount of heat entering the tank will increase using this method. Finally, a bottle of room temperature hydrogen will be used as a pressurization source. This gas will liquefy at the interface, so a continuous source of gas must be used to prevent ullage collapse. This pressurization method will be discussed more when hydrogen liquefaction is considered.

During operations that require transfer of liquid from one tank to another, tank pressure will need to be increased to overcome friction and elevation head losses. All three pressurization sources discussed above will also be evaluated for their suitability for this purpose. In this case, the ullage space in the tank will be increasing as the tank liquid level is decreasing, so the mass flow rate required will be greater than just tank pressure maintenance. This mass flow rate must equal the rate required to fill the extra volume plus the rate required to make up the contraction as the gas cools down. Depressurization without venting the tank will be achieved by terminating the flow rate of pressurization into the tank while maintaining the cooling of the hydrogen.

However, this approximation depends on perfect heat exchange between the cryocooler and the hydrogen, and it assumes there are no temperature gradients in the liquid (lumped capacitance method). In reality, the overall heat transfer coefficient of the free hydrogen convection must be determined. The tank will be instrumented to allow for monitoring of the temperature gradients in the liquid, so the total thermal energy in the system can be calculated. Knowing the performance capabilities of the cryocooler as a function of temperature, the rate of heat transfer from the liquid to the cold heat exchanger can be calculated, and the heat transfer coefficient can be determined. The cold head of the cryocooler will be designed to allow for a variety of heat exchangers to be used. The initial cold heat exchanger will be bundled of OHFC copper extending downward from the cold head. Future designs will include horizontal and vertical surfaces with a variety of extended fins. The vertical position of the heat exchanger will be variable by removing or replacing the heat pipe in the system. One enhancement under consideration will be the addition of a mixing or stirring device in the tank. This

could help the rate of heat transfer in two ways; ensuring a uniform temperature in the tank, and creating a forced convection current across the cold HX.

CHAPTER 3
ANALYSIS OF GOVERNING EQUATIONS

In Chapter 2, the concept of the integrated refrigeration and storage system was discussed, and the behavior of the system was addressed from a qualitative standpoint. This chapter will look at the thermodynamic behavior from a quantitative perspective. First, a thermodynamic model of the proposed liquefaction cycle will be developed. This model will integrate the closed cycle helium refrigerator into the hydrogen input stream. Details on the system operating characteristics will be presented, and a range of acceptable intermediate cycle temperatures will be found. Optimizing the cycle parameters, namely the hydrogen and helium compression ratios and the intermediate temperature, to minimize the total work input will be completed. Next, a simplified model of the storage system will be made using a two-dimensional transient mass and energy balance approach, starting with the integral form of the conservation equations. This model will then look at specific operational situations and predict system behavior. Where applicable, this behavior will be compared to experimental data obtained in Chapter 6. Corrective changes to this model will be proposed to more accurately predict the system behavior. These changes incorporate correction factors accounting for the variable liquid level in the system as well as non-isothermal temperature profiles in the ullage space that lead to variations in the system heat leak. Finally, since the bulk fluid mass and energy balance approach still falls short of a true physical model of the system, the full conservation equations will then be presented in differential form based on an analysis of expected flow and heat transfer regimes. Initial conditions and boundary

values will be presented to fully pose the problem. This problem formulation is an important first step in the generation of a full solution, as CFD experts may not have the requisite experience in understanding the behavior of the system to be modeled. These conservation equations will then be converted to dimensionless form, using the initial system energy and heat leak rate as dimensional constants. This will provide insight into the system behavior from the perspective of how much heat is entering the system with respect to how much energy was initially in the system.

Thermodynamic Analysis of Liquefaction Cycle

Cycle Description

A novel cycle for hydrogen liquefaction is presented in this section. This cycle takes advantage of the required helium refrigeration cycle needed for maintaining the hydrogen in the controlled storage state and uses excess refrigeration capacity to precool the incoming hydrogen stream as well as remove the latent heat of vaporization of any saturated hydrogen vapors downstream of the expansion valve. A schematic of this proposed cycle is show in Figure 3.1.

Pure hydrogen from a production plant enters the cycle at point 1 and is compressed to pressure P2 by a hydrogen compressor. HX3 removes the heat of compression and sends the ambient temperature, high-pressure hydrogen gas to the recuperative heat exchanger HX3. In HX3, a cold helium refrigeration system removes heat from the hydrogen and cools it down to the intermediate temperature T4. Then, the cold compressed hydrogen is expanded through a Joule-Thompson valve to the storage pressure P5. At this point, depending on the storage pressure P5 and the unexpanded hydrogen state (T4, P4) the hydrogen is either a cold vapor or a two-phase flow. The integrated heat exchanger HX4 inside the storage tank removes the remainder of the heat

to convert the hydrogen to 100% liquid that can be stored or drained from the tank at location 6.

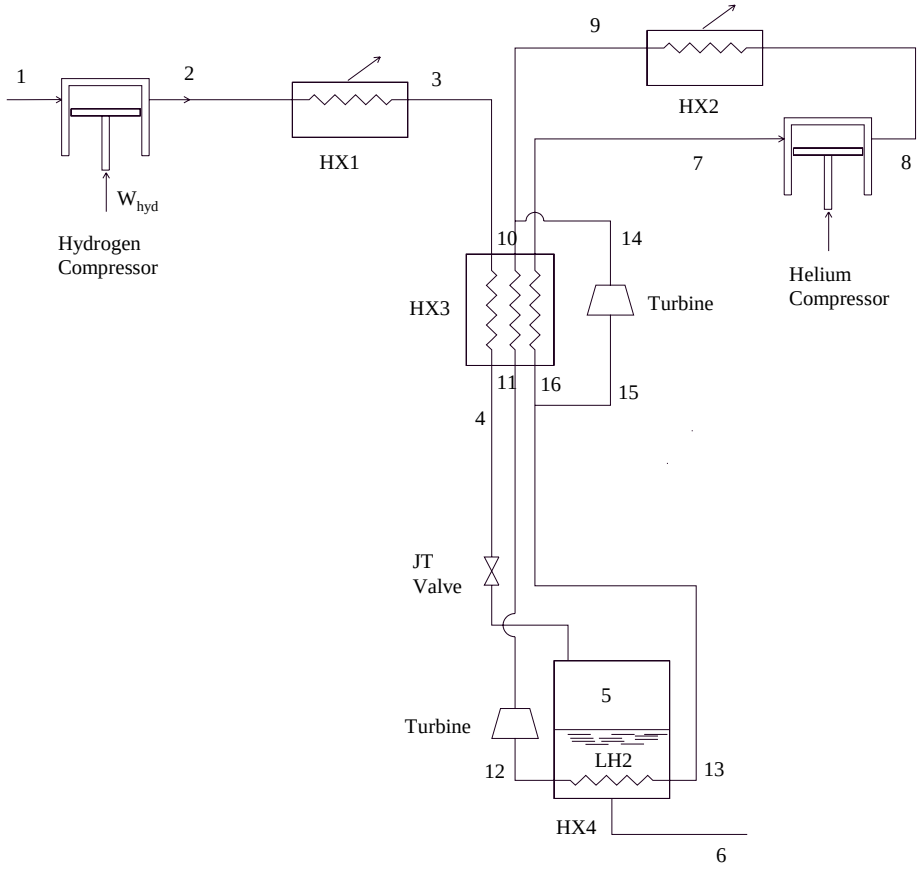

Figure 3-1 Proposed Liquefaction Cycle Schematic

The closed cycle helium refrigerator in this model is a two-stage Brayton cycle with external heat loads at HX3 and HX4. The helium is compressed from the low pressure to an undefined high pressure P8. Heat of compression, as well as external heat loads, is removed in HX2. The helium flow is split downstream of this heat exchanger, and some mass flow ($\dot{m}_{14}$) is split off to be expanded through the first (high temperature) turbine. The remainder of the flow ($\dot{m}_{10}$) is pre-cooled in HX3 and then expanded in the

second (low temperature) turbine to a temperature required to remove the leftover heat of the hydrogen vapors in the tank for that particular mass flow rate. Both expansion turbines operate at the same pressure inlets and outlets and it is not a dual pressure cycle. The two turbine flow streams recombine immediately downstream of HX3 and flow together to pre-cool the high pressure helium stream and incoming hydrogen stream.

Some of the unique features that differentiate this cycle from other hydrogen liquefaction cycles are now discussed. Note how the hydrogen input stream is not a continuous cycle with cold vapors returning to the hydrogen compressor. The hydrogen flow is in one direction only, from the compressor to the tank, and the ultimate liquid yield is 100%. This is due to the presence of HX4, which removes the remaining heat of vaporization from hydrogen downstream of the JT valve. In fact, in some cases the JT expansion may not even be needed and no cooling of hydrogen comes internally from expansion. The final pressure of the JT expansion is not fixed, but variable depending on the mass flow rate of the hydrogen and the amount of cooling provided by the helium refrigerator at HX4. In some cases this may be subatmospheric pressure if the desired storage state is densified hydrogen.

The recuperative heat exchanger HX3 is a key component in this cycle. It is a counterflow heat exchanger with two warm inlet streams and one cold inlet stream. There is a net heat load on the helium cycle that is determined by the hydrogen mass flow rate multiplied by the enthalpy difference between state 3 and state 4. The final hydrogen temperature T4 prior to expansion is a variable to be optimized in the model. This optimization is done in a later section with HX3 assumed to be a perfect heat exchanger with no pressure drop. The advantages to using HX3 to precool the hydrogen are

obvious. The greater the amount of energy removed from the input stream at high temperatures, the more efficient the cycle efficiency will be. This is the purpose for many of the LN2 pre-cooled systems in use today, except this cycle does not use consumable nitrogen as a pre-cooling source but relies on closed cycle helium refrigeration instead. An additional feature is the incorporation of an ortho-para catalyst in the inner passages of the hydrogen stream, which allows for the heat of conversion to be removed continuously at every temperature in the most efficient manner possible.

The depiction of the compression step is shown for simplicity only and in most cases multiple stages of compression will be used with interstage cooling. The helium compressor is most probably an oil flooded screw compressor, and extra equipment will be needed downstream of the compressor to remove oil and other contaminants prior to flowing into the coldbox. These compressors are used successfully in large-scale helium liquefiers at major particle accelerator facilities. The hydrogen can be compressed either by a mechanical compressor or as a high pressure output of a hydrogen production system, such as a steam methane reformer or an electrolysis unit. If the hydrogen is already compressed by the production system, this will save energy by taking advantage of the prior compression, and in these cases the work input for compression of hydrogen will not be factored into the liquefaction work input. In some cases the hydrogen may not even be compressed, if the JT expansion process is not needed. This is the situation presented in the Chapter 6 experimentation section, with room temperature hydrogen being cooled and liquefied entirely by the heat exchanger in the storage tank.

Model Development

A thermodynamic model based on the conservation of mass and conservation of energy principles has been developed to predict cycle behavior and optimize the

operating conditions. The model uses P1, T1, P7, T7, and $\dot{m}_{hyd}$ as input parameters. The heat exchanger delta pressure and temperature can be specified as well, but in most cases the heat exchange process was approximated as perfect. In the model, an isentropic compression in one stage is used, but multiple stages and intercooling more closely approximates an isothermal compression stage and would reduce the overall work input. An isentropic expansion efficiency of 80% is used for the calculations for both the compressors and expansion turbines. The desired liquefaction storage temperature is also required as an input, and has a great effect on the outcome.

The compression ratios of the hydrogen and helium streams are variables to be optimized. Work required for compression is calculated, then the heat exchange required to reject the heat of compression is performed prior to flowing through the recuperative heat exchanger. Knowing the desired storage pressure and the heat exchanger pressure drops, the system pressures are known at all points in the cycle. The high temperature turbine exit pressure is set by the low-pressure requirements of the compressor, and a dual pressure system is not approximated. The unknown parameters at the recuperative heat exchanger are the outlet temperatures (T4, T11, and T16) and the required helium mass flow rates through both the high temperature and low temperature turbines. Assuming an intermediate hydrogen temperature at T4, the other heat exchanger temperatures can be calculated. The helium mass flow rates are then computed using the energy balance on the tee and the energy balance across the whole heat exchanger by the relations

$$\dot{m}_{13}h_{13} + \dot{m}_{15}h_{15} = \dot{m}_{16}h_{16} = (\dot{m}_{13} + \dot{m}_{15})h_{16} \qquad 3\text{-}1$$

$$\dot{m}_{3}(h_{4} - h_{3}) + \dot{m}_{10}(h_{11} - h_{10}) = \dot{m}_{16}(h_{16} - h_{7}) \qquad 3\text{-}2$$

From there, an isenthalpic expansion is calculated across the JT valve to the desired storage pressure. The heat required to fully liquefy the JT product stream is calculated, and that determines the sizing of the helium at heat exchanger 4. If the hydrogen is not saturated at the exit of the JT valve (a condition that can occur if T4 is not low enough or P2 is not high enough), then the helium in HX4 must remove the remaining sensible heat prior to hydrogen liquefaction. The low temperature expansion turbine pressure ratio is already determined by the cycle parameters, so the turbine exit temperature is known. The required mass flow rate is calculated using an energy balance across HX4. The model optimizes the cycle in terms of minimum mass flow rate required for the desired cooling in HX3 and HX4. Several constraints are placed on the optimization subroutine. A minimum temperature at the outlet of the low temperature turbine is set at 14K to eliminate the potential for freezing hydrogen in the vessel. The mass flow rates for all points on the helium cycle must be positive or zero. The low-pressure helium stream into the recuperator is constrained to be lower than the hydrogen exit intermediate temperature and the high-pressure helium exit temperature.

Analysis

From the development of the model, it becomes apparent the independent variables to be used in the optimization process are the hydrogen compression pressure P2, the intermediate temperature downstream of the recuperative heat exchanger T4, and the helium compression pressure P8. The combined work of the hydrogen and helium compressors are the dependent variables to be minimized. This process can be repeated for a range of inlet conditions and final storage pressures for hydrogen, variations in compressor and turbine efficiencies, and inefficiencies in the recuperative heat exchange process.

For a given pair of hydrogen and helium high pressures, there is a range of intermediate temperatures that can be used to give a satisfactory solution to the equations 3-1 and 3-2. The family of curves shown in Figure 3.2 displays this relation. For this figure, the hydrogen cycle was assumed to have no hydrogen compression and the stream is isobaric at 120 kPa. This means no isenthalpic cooling of the hydrogen and the liquefaction is completely performed by the heat exchange with the helium in HX3 and HX4. Using a range of different helium pressures (ranging from 360 kPa to 7200 kPa), the temperatures that give a non-trivial solution are plotted. If the intermediate temperature is colder than the left hand curve in the figure, the system will not work because the high temperature turbine will be limited to the temperatures it can achieve, and T16 will not be less than T4. Similarly, using T4 higher than the right hand curve requires a greater amount of cooling has to be performed at the low temperature turbine, and the turbine exit temperature decreases. In order to get the required cooling inside the storage tank, the mass flow rate increases. The recuperative heat exchanger becomes unbalanced and eventually the required mass flow rate through the high temperature turbine becomes zero. Notice the range of temperatures increase as the helium compression ratio increases, which allows for greater cycle flexibility during operation. Similar behavior was observed in the cycle when the hydrogen was compressed and expanded in the JT valve. The dependence of the cycle feasibility on a small range of acceptable intermediate temperatures places many constraints on the actual system, and care must be taken to ensure the cycle does not operate outside these limits. It is also shown later that the overall work increases as the intermediate temperature increases, so operating on the left hand side of the curve is desired.

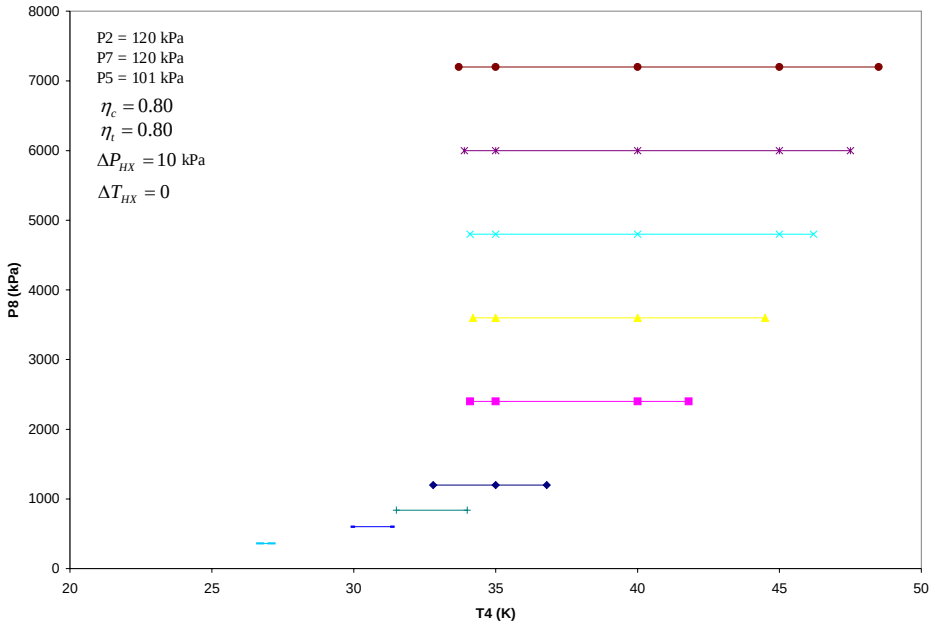

Figure 3-2 Acceptable Intermediate Temperatures as a Function of Helium Compression

The figure above gives no information on the work input requirements, only operating conditions that are acceptable for the cycle at those temperatures and pressures. Since the cost of liquefaction is directly related to the energy input rate, regards for the dependence of work input on the system operating points should be considered. Below, Figure 3-3 plots the work input for liquefaction of 1 gram per second of gaseous hydrogen against the intermediate cycle temperature, for a range of compression ratios in the helium cycle. All other cycle parameters are constant and defined below. No work input was done on the incoming hydrogen gas stream and all cooling was done through a heat exchange process in HX3 and HX4. Notice there is a range of acceptable solutions for certain intermediate temperatures, and points past the endpoints of the isobaric lines do not have solutions that converge in the model. For a given helium compression ratio, the work input is reduced as the intermediate temperature is decreased. This dependence is more pronounced as the helium compression is reduced, as small increases in T4 lead

too much larger increases in work input. In addition, the required work actually increases for these smaller pressure ratios, due to the increase in required mass flow rate. Subsequent analysis therefore concentrates on helium compression ratios of 10 or greater.

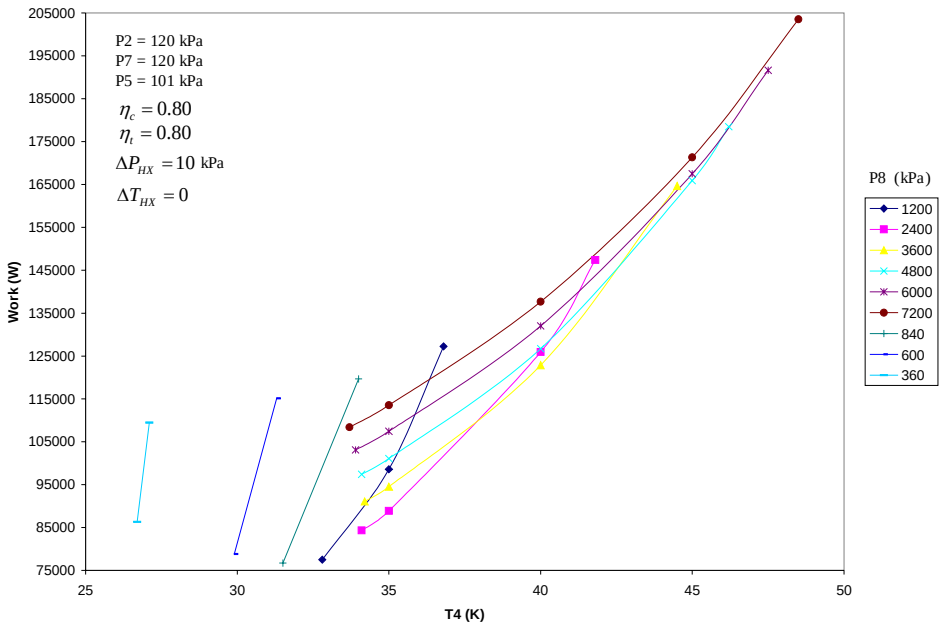

Figure 3-3 Compression Work vs Intermediate Temperature (P2=120 kPa)

Figure 3.4 shows a similar plot of work vs T4 for a cycle that has some compression work in the hydrogen side. The hydrogen compression ratio is 10, and some isenthalpic cooling is occurring at the JT valve. Note the lower helium compression ratios are not included in the figure. The plots look very similar to the case where there is no hydrogen compression (Figure 3-3), but there are some slight differences in values of total work. These differences will be explored a little later in Figure 3.8, when the work is plotted as a function of the hydrogen compression ratio. Again, for the low helium pressures, there is a steep increase in work for very small increases in intermediate temperature, and these cycles should be avoided if possible. The higher helium compression cycles also exhibit greatly increased work input requirements.

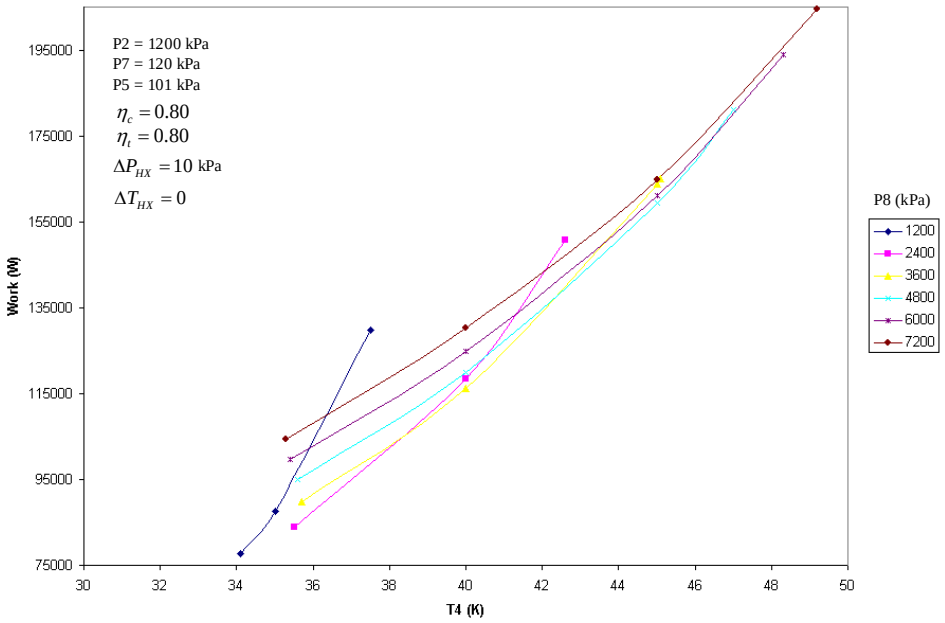

Figure 3-4 Compression Work vs Intermediate Temperature (P2=1200 kPa)

Meanwhile, it is informative to look at some of the cycle parameters in this case to see how the cycle functions. Figure 3-5 plots the required helium mass flow rate through each turbine as a function of intermediate temperature for a cycle with both the hydrogen and helium compression ratios set at 10 to 1. Note how the overall mass flow rate increases as the intermediate temperature increases, and the high temperature turbine flow rate decreases from approximately 10% of the flow at the lower T4 to zero at the upper end of the T4 curve. The secondary y-axis plots the work input for both the hydrogen and helium. The hydrogen work is constant since the compression ratio and mass flow rate are fixed. The helium work input increases due to the increase in requires mass flow rate, even though the compression ratio is fixed.

Another way to evaluate the efficiency of each cycle is to look at the heat rejected by the hydrogen in each heat exchanger. Figure 3-6 shows the heat rejection in HX3 and HX4 for a range of intermediate temperatures and helium compression ratios, with the

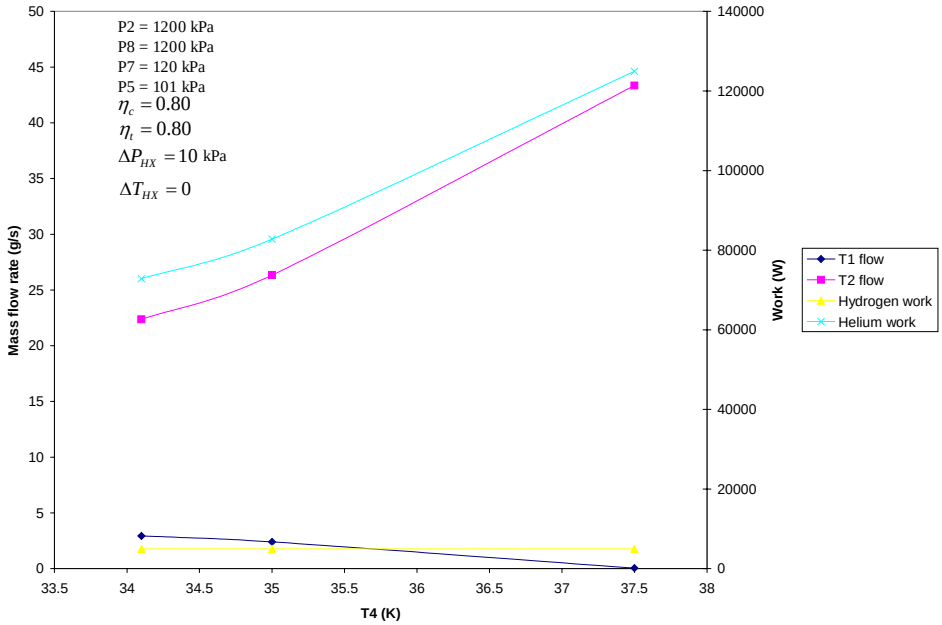

Figure 3-5 Turbine Mass Flow Rates and Cycle Work

hydrogen pressure fixed at 1200 kPa. The upper curve shows the majority of the heat being rejected in HX3, which is the higher temperature heat exchange. However, for warmer intermediate temperatures, the amount of heat rejected is decreased in HX3 and increased in HX4. This fact does not change with increases in helium cycle pressure, as is evidenced by the different P8 curves plotting on top of each other. Another way of looking at this plot is to think the cycle that rejects the greatest amount of heat at the highest temperatures will be the most efficient, and the work curves plotted in Figures 3-3 and 3-4 provide more evidence of this.

In the preceeding paragraphs, it is demonstrated that the optimum intermediate temperature to have in the cycle is the lowest temperature allowed for the given hydrogen and helium pressures. The next step is determining the work required as a function of hydrogen pressure. The total amount of hydrogen work is much less than the helium

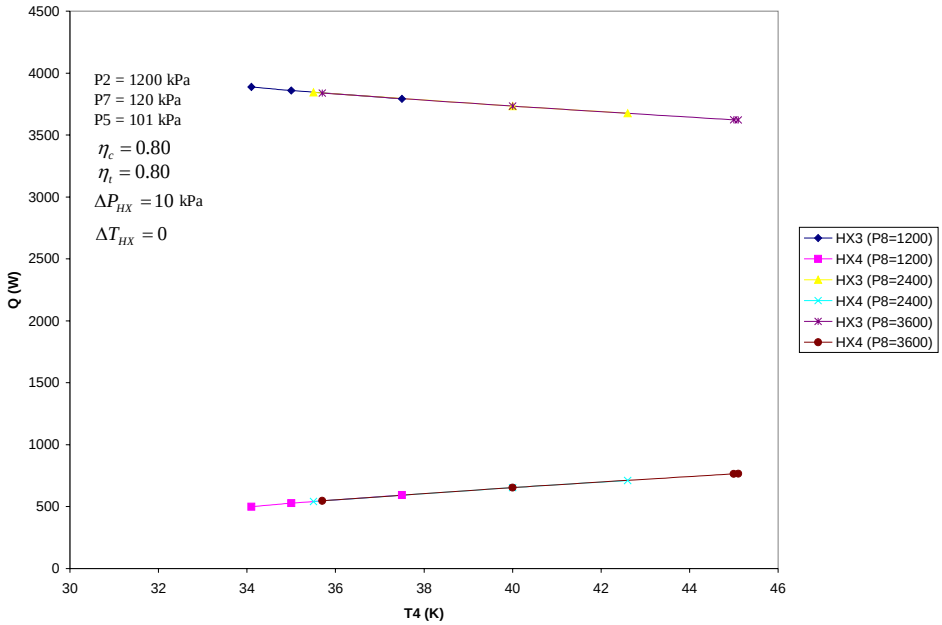

Figure 3-6 Heat Rejection at HX3 and HX4

work due to the flowrates involve, but an overall advantage can occur if some level of cooling can be achieved by hydrogen expansion. Again, work input may not matter if the work is from the hydrogen production process. Figure 3-7 shows the work required as a function of T4 for a range of hydrogen pressures. The helium cycle is working at a pressure of 2400 kPa. There is little movement in the curves for the pressure ratios less than 10 to 1, then gradually the curve shifts to the higher temperature areas. Then the curves start clustering again above P2=3000 and no further advantage can be gained by higher compression.

Choosing the lowest temperature point in the curves in Figure 3-7 obtains a plot of lowest allowed work input for each specific helium compression ratio as a function of hydrogen pressure. Figure 3-8 shows there is an initial small spike in compression work, followed by a decrease to a local minimum, followed by a gradual increase as systems reach very high hydrogen pressures. This shows there exists an optimum hydrogen

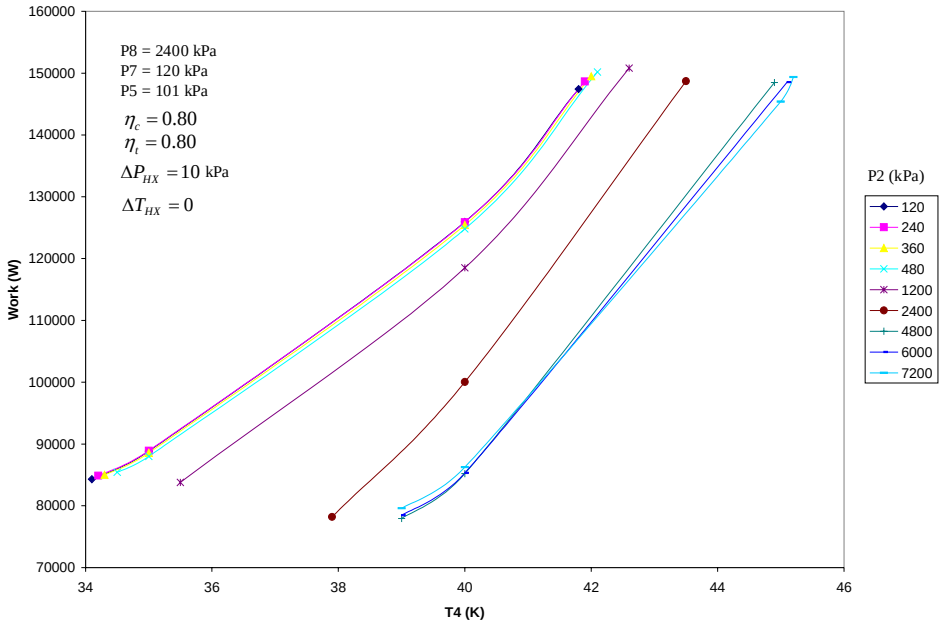

Figure 3-7 Cycle Work vs Temperature for a Range of Hydrogen Pressures

pressure, for each helium pressure and intermediate temperature, for which the liquefaction cycle operates at maximum thermodynamic efficiency. This hydrogen pressure occurs at 2400 kPa. Similarly, Figure 3-9 shows the cycle work for a range of helium pressure ratios. It is evident there exists a helium pressure that leads to a minimization of work for each set of hydrogen pressures, and this pressure is below 1200 kPa. This figure also shows the curve with a hydrogen pressure of 2400 kPa provides the lowest work total.

Based on the above analysis, it is concluded that the proposed combined hydrogen and helium liquefaction cycle is feasible, and a range of operating conditions exist. There is a minimum and a maximum intermediate temperature that can be used downstream of the recuperative heat exchanger. Temperatures higher than this range will not work due to HX3 becoming unbalanced as the mass flow rate through the high temperature turbine

goes to zero. Temperatures lower than the acceptable range will not work due to the high temperature turbine not being able to provide a low enough temperature to

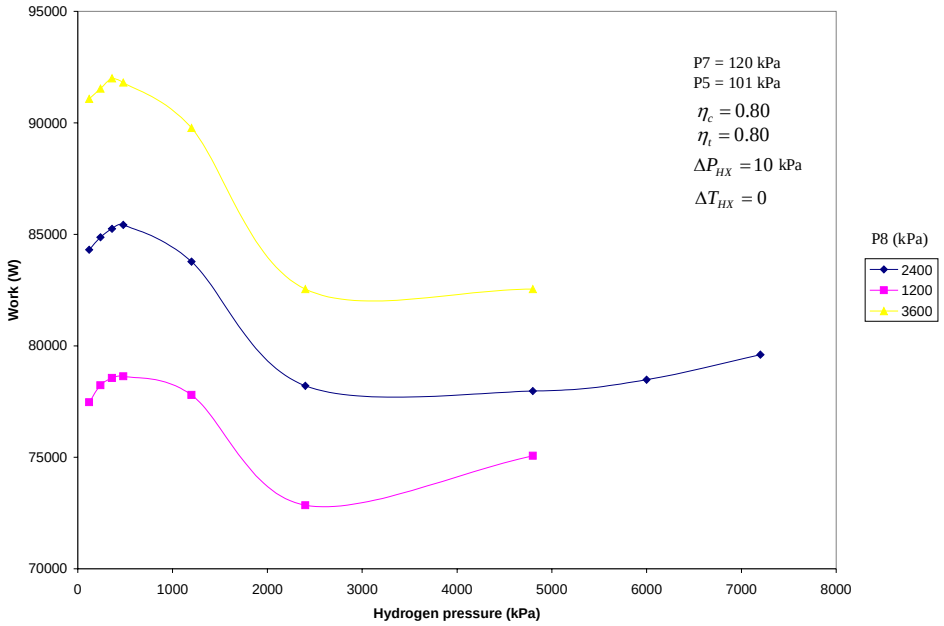

Figure 3-8 Cycle Work vs Hydrogen Pressure

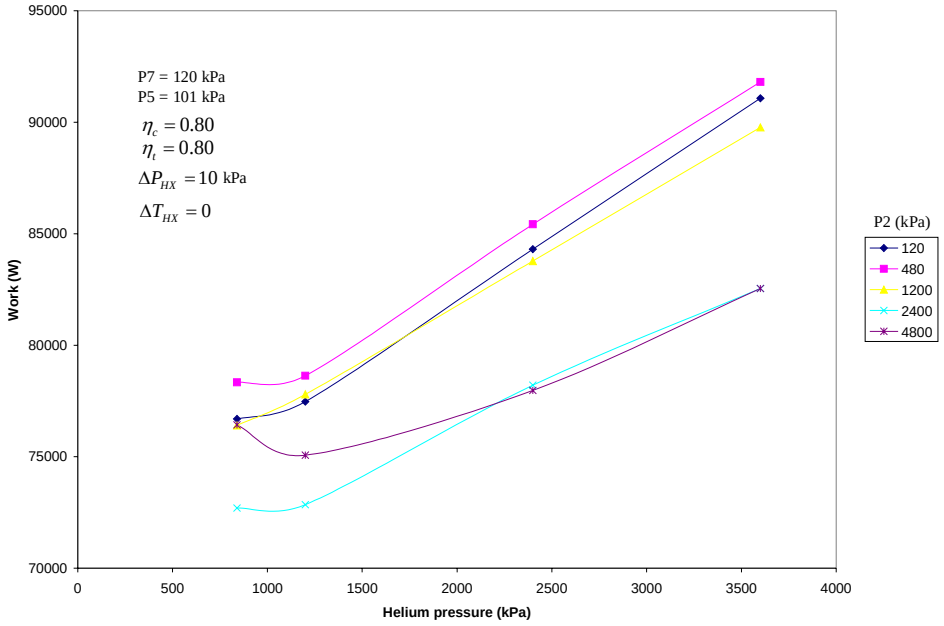

Figure 3-9 Cycle Work vs Helium Pressure

ensure T16 is less than T4. The most efficient intermediate temperature to use for a given set of hydrogen and helium pressures is the lowest temperature possible. This maximized the amount of heat rejected at higher temperatures. The analysis in this section also shows the functional relationship between hydrogen and helium pressures and work. It is shown the most efficient cycle will operate with the hydrogen pressure at 2400 kPa, and a helium pressure at 1200 kPa. The efficiency of the liquefaction system is 17%, which is respectable for a small scale LH2 system with only 1 intermediate stage.

Thermodynamic Analysis of Storage System

An effort will now be made to model the thermodynamic behavior of the liquid hydrogen in the storage tank for a variety of operating conditions. In many practical applications, simplifications to the full conservation equations can be made to provide great insight into the physical characteristics of a system without sacrificing too much accuracy. Such simplifications allow for closed form analytical solutions that do not require sophisticated numerical techniques to solve. This section will focus on applying these simplifications over a control volume to obtain general expressions for the mass and energy balance of the system. These control volume mass and energy balances will then be tailored for the specific operational constraints found during the zero boil off, liquefaction, and densification processes, and these specific expressions will be compared to results of the experimental testing discussed in Chapter 6.

Definitions and Assumptions

The control volume to be analyzed is presented in Figure 3-10. A cylindrical double walled tank of volume 150 liters, with a diameter of 50.8 cm and length of 74 cm, is initially partially full of liquid hydrogen in the saturated condition. The temperature of the tank is well below the ambient temperature and there is a flow of heat into the tank

from the surroundings through the insulation into the system. This heat transfer can be assumed to be of two forms, the radiation heat transfer from the outer vessel to the inner vessel, and conduction heat transfer down the length of the neck of the vessel and other solid supports. In addition, there is a cold heat exchanger integrated into the vessel that can remove heat from the liquid. There are three ports connecting the inner vessel to the surroundings. The liquid fill and withdraw port is present to allow for the flow of the hydrogen from the storage vessel to the use point, in this case the flight tank of a rocket. The vent port is designed to vent vapor from the top of the tank to the ambient pressure surroundings, either in a controlled vent or as an emergency relief when the system pressure reaches the maximum operating pressure. The gas supply port is necessary to allow for pressurization of the fluid as well as to introduce hydrogen gas for liquefaction operations. The inner tank holds only hydrogen in gaseous or liquid form. The system thus defined constitutes an open, transient, homogeneous, multiphase system with heat and work interactions.

Despite the apparent complexity of the system as defined above, numerous simplifications can be made to allow for fairly accurate analysis. First, it can be assumed that the time constant associated with defining an equilibrium state between the liquid and vapor phases is much less than the time constant associated with any system interactions with the surroundings. This assumption is valid as long as the heat transfer into or out of the system is low, as it typically is in well insulated cryogenic vessels, or the mass flow rate into and out of the system is small compared to the total system mass.[37] This defines the system as being in thermodynamic equilibrium with respect to the liquid and vapor phases, and requires the liquid and vapor phases to have equal

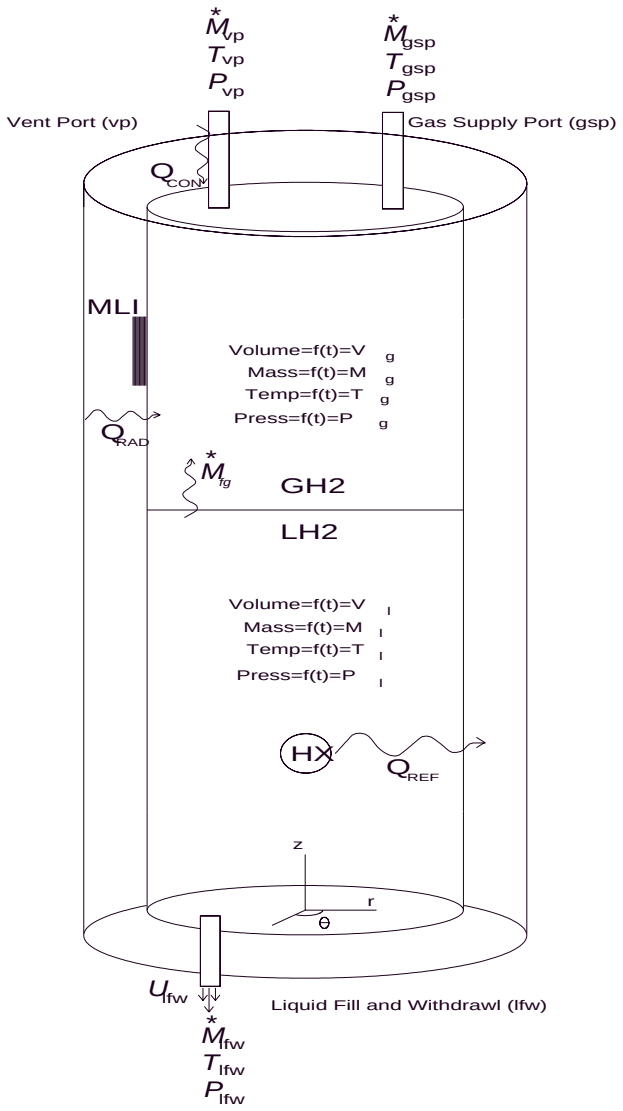

Figure 3-10 Simplified system representation

temperature and pressure. It is important to keep in mind that the definition of thermodynamic equilibrium does not imply there is no time dependence in the system, and in this case the model is a still a transient system.

A second assumption is the liquid and vapor phase have a defined, impenetrable boundary. It is assumed there are no bubbles in the liquid and no mist in the vapor. This allows for modeling the system as a combination of two separate single-phase control

volumes, with heat and mass transfer between them at the liquid to vapor interface. The overall volume of these control volumes will vary with time, depending on the level of evaporation or condensation at the interface as well as the temperature and pressure of the liquid and vapor.

Next, assumptions about the properties of the fluids must be made. The fluid velocities are considered small. Effects of heat addition or removal and mass addition or removal are considered over the entire control volume instantaneously, and there are no boundary layer effects. The fluid can therefore be assumed inviscid. Since interactions with the surroundings are assumed to act instantaneously, the fluid properties are assumed to be constant with respect to spatial dimensions in the control volume.

Conservation of Mass

The general form of the conservation of mass equation for a fixed control volume can be expressed in integral form as[38]

$$\frac{\partial}{\partial t}\iiint_{v} \rho dV = -\oiint_{S} \rho \bar{V} \bullet d\bar{S} \qquad 3\text{-}3$$

For the system described in Figure 3-10, with uniform, one-dimensional flow across one inlet and two outlet locations, the conservation of mass reduces to

$$\frac{\partial}{\partial t}\iiint_{v} \rho dV = \rho_{gsp} u_{gsp} A_{gsp} - \rho_{lfw} u_{lfw} A_{lfw} - \rho_{vp} u_{vp} A_{vp} \qquad 3\text{-}4$$

While the total control volume is fixed, there are actually two volumes of interest inside the tank that are variable, the total liquid volume and the total gas volume. Breaking these up into separate volumes, and assuming the density is constant in that particular volume, the conservation of mass equation becomes

$$\frac{\partial}{\partial t}\rho_l V_l + \frac{\partial}{\partial t}\rho_g V_g = \rho_{gsp} u_{gsp} A_{gsp} - \rho_{lfw} u_{lfw} A_{lfw} - \rho_{vp} u_{vp} A_{vp} \qquad 3\text{-}5$$

For this model, it is assumed that the thermodynamic state and the total mass flow rate of the gas entering the gas supply port is known. The density of the vapor venting out of the tank is assumed to be equal to the density of the vapor in the ullage, and the density of the liquid leaving the tank out the liquid withdraw port is assumed to be equal to the density of the bulk liquid in the control volume. Using the assumption that the system can be treated as a bulk fluid, the mass addition is immediately distributed over the entire control volume and the effects of the fluid velocity at the inlets are outlets are neglected. Breaking up the system into two control volumes at the liquid to vapor interface the following expressions for the conservation of mass are obtained

$$\rho_{g2} V_{g2} - \rho_{g1} V_{g1} = (\dot{m}_{gsp} - \dot{m}_{vp} + \dot{m}_{fg})\Delta t \qquad 3\text{-}6$$

$$\rho_{l2} V_{l2} - \rho_{l1} V_{l1} = (-\dot{m}_{lfw} - \dot{m}_{fg})\Delta t \qquad 3\text{-}7$$

Conservation of Energy

The general form of the conservation of energy equation for a fixed control volume, assuming inviscid flow and neglecting gravitational potential energy and assuming there are no internal reactions that are exothermic or endothermic, can be expressed in integral form as[38]

$$\iiint_v \dot{q}\rho dV - \iint_S P\bar{V} \bullet d\bar{S} + \iiint_v \rho(\bar{F} \cdot \bar{V}) dV = \qquad 3\text{-}8$$

$$\iiint_v \frac{\partial}{\partial t}[\rho(u + \frac{V^2}{2})]dV + \iint_S \rho(u + \frac{V^2}{2})\bar{V} \cdot d\bar{S}$$

where the first term is the rate of heat added to the fluid inside the control volume from the surroundings,[38] the second term is the rate of work done on the fluid by surface (pressure) forces, the third term is the rate of work done on the control volume by body forces, the fourth term is the time rate of change of energy inside the control volume due to transient effects, and the fifth term is the net rate of flow of energy across the control surface.

Breaking down the first term, $\dot{q}$ is defined as the rate of heat added per unit mass. Physically accurate modeling of this heat transfer would account for the heat flux across a narrow thermal boundary layer near the surface of the tank, however this control volume model assumes bulk fluid properties and no boundary layer effects. Furthermore, the nature of the integrated refrigeration and storage system includes two heat transfer mechanisms, the heat leak into the tank from the ambient surroundings as well as the heat removed from the system from the refrigerator. Integrating the first term over the entire volume therefore gives the following simplified expression for heat transfer to the system as

$$\iiint_{v} \dot{q}\rho dV = Q_{HL} - Q_{REF} \qquad 3\text{-}9$$

Body forces, namely the gravitational effects required for natural convection, are an important physical effect that must be taken into account to accurately predict the heat transfer rates across the system boundaries. However, for this simple control volume mass and energy balance where bulk fluid properties and inviscid flow are assumed, the work done by body forces can be neglected, and the third term in Equation 3-8 can be dropped.

Assuming the fluid velocities are negligible, the effect of kinetic energy of the fluid can be neglected. Again assuming bulk fluid properties, the density and internal energy of the fluid are constant in the control volume and can be taken out of the volume integral in the fourth term. After integrating over the control volume, the transient term the right hand side becomes

$$\iiint_{v} \frac{\partial}{\partial t}[\rho(u + \frac{V^2}{2})]dV = \frac{\partial}{\partial t} mu \qquad 3\text{-}10$$

The two surface integrals can be evaluated together. This integral is evaluated only over the inlet and outlet locations since $\overline{V} \cdot d\overline{S}$ equals zero at all other locations. Assuming bulk fluid properties, the evaluation of these integrals yields

$$\iint_{S} P\overline{V} \cdot d\overline{S} + \iint_{S} \rho u\overline{V} \cdot d\overline{S} = \qquad 3\text{-}11$$

$$(P_1 + \rho_1 u_1)V_1 A_1 - (P_2 + \rho_2 u_2)V_2 A_2 + (P_3 + \rho_3 u_3)V_3 A_3$$

Rearranging Equations 3-9, 3-10, and 3-11, substituting in the definitions for mass flow rate and enthalpy, breaking up this expression for separate control volumes in the liquid and vapor space, and integrating over time reduces the general conservation of energy equation to[39,40]

$$\rho_{g2} v_{g2} h_{g2} - \rho_{g1} v_{g1} h_{g1} = \dot{m}_{gsp} h_{gsp} \Delta t - \dot{m}_{vp} h_{vp} \Delta t + \dot{m}_{fg} h_g \Delta t \qquad 3\text{-}12$$

$$\rho_{l2} v_{l2} h_{l2} - \rho_{l1} v_{l1} h_{l1} = Q_{HL} - Q_{REF} - \dot{m}_{lfw} h_{lfw} \Delta t - \dot{m}_{fg} h_g \Delta t \qquad 3\text{-}13$$

where the mass flow rate between the liquid and vapor phases is found by assuming all heat leak into the tank enters the liquid control volume and creates an equivalent amount of boil off to the vapor control volume. The heat leak term is the summation of the individual heat transfer components of conduction down the solid supports and

convection and radiation thru the MLI. The selection of the vapor enthalpy as the amount of energy leaving the liquid control volume is somewhat arbitrary, and reflects the true control volume boundary as being drawn macroscopically in the vapor space above the liquid level.

Equation of State

At these low temperatures, the ideal gas model cannot be assumed. To relate the thermodynamic properties of pressure, temperature, and specific volume, the National Institute of Standards and Technology (NIST) Thermophysical Properties Database RefProp was used. This database incorporates the Modified Benedict-Webb-Rubin (MBWR) equation of state for hydrogen, using eight empirical constants derived from testing at the NIST laboratory.[41] Once the state of the fluid is determined, Maxwell's relations can be used to find the other thermodynamic variables.

Operational Simplifications

Although the above equations can be used for analysis of operations with multiple simultaneous mass influx and outflows, such scenarios are rare. In the vast majority of operations, there will be mass influx or outflow through only one of the ports at a time, if any at all. The operations can be classified depending on whether the system is open or closed to mass transfer from the surroundings, and the direction of heat transfer in the system. Table 3-1 shows the different operating characteristics of the system. If the refrigerator is operating and greater the capacity is greater than the heat leak, the heat transfer is out of the system, and if the refrigeration capacity is less than the heat leak the net heat transfer is into the system. This leads to the following simplifications of the conservation equations, depending on the operational scenario.

Table 3-1 Operational scenarios

	HEAT IN	ADIABATIC	HEAT OUT
MASS IN	Gas Pressurization		Liquefaction
CLOSED	Self Pressurization	ZBO	Densification
MASS OUT	Boil Off or Transfer	Liquid Transfer	Liquid Transfer

Closed Storage With Heat Transfer To the System (Self Pressurization)

Current storage systems often have periods of time where they are vented and then closed from the surroundings. During these periods, the valves remain closed and the heat leak into the tank creates an evaporation of liquid that causes a pressurization of the system. The pressure will rise until the maximum operating pressure is reached and the relief valve opens. During this time, the mass inside the entire tank is constant, but the relative amounts of liquid mass and vapor mass will change. The conservation of mass equations for the vapor and liquid space can be expressed as

$$\rho_{g2}V_{g2} - \rho_{g1}V_{g1} = \dot{m}_{fg}\Delta t \qquad 3\text{-}14$$

$$\rho_{l2}V_{l2} - \rho_{l1}V_{l1} = -\dot{m}_{fg}\Delta t \qquad 3\text{-}15$$

During this period it is assumed the refrigerator is off and the only heat transfer in the model is the heat leak. The conservation of energy equations for the vapor and liquid space can be written as

$$\rho_{g2}V_{g2}h_{g2} - \rho_{g1}V_{g1}h_{g1} = \dot{m}_{fg}h_g\Delta t \qquad 3\text{-}16$$

$$\rho_{l2}V_{l2}h_{l2} - \rho_{l1}V_{l1}h_{l1} = Q_{HL} - \dot{m}_{fg}h_g\Delta t \qquad 3\text{-}17$$

The above equations have seven unknowns ($\rho_{g2}, V_{g2}, h_{g2}, \rho_{l2}, V_{l2}, h_{l2}, and\ \_\dot{m}_{fg}$). The initial temperature and pressure in the tank are known giving the rest of the initial

thermodynamic state variables, and the heat leak is assumed known by either design data on the insulation system effectiveness or by experimentation. However the liquid and vapor volume are related by the following expression,

$$V_{system} = V_l + V_g \tag{3-18}$$

and the mass flow between the liquid and vapor depends on the heat transfer by

$$Q_{HL} = \dot{m}_{fg} h_{fg} \tag{3-19}$$

Combing equations 3-14 thru 3-19 with the equation of state, the system of seven equations and seven unknowns can then be solved.

A Microsoft Excel based program has been written to model this behavior. First, the heat leak into the system is estimated for the given initial conditions. This heat leak model includes the effects of radiation and convection thru the multi layer insulation as well as the effect of conduction down the solid wall of the neck and various interface tubing. The radiation and convection across the tank surface area follows the modified Lockheed correlation for multi layer insulation.[42] This takes into account the number of layers of insulation, the density of the layers, and the boundary conditions of temperature. This also assumes a vacuum in the annulus of less than 10^{-3} Torr. The conduction heat leak down the length of the neck or tube can be found by the Fourier equation, except the thermal conductivity will not be constant over that wide range of temperatures. The thermal conductivity can be integrated over a range of temperatures if the governing equation is known, and the thermal conductivity integral has been calculated for a range of materials and temperatures by McMordie.[43] These relations are then added into the model to create an estimate for heat leak into the tank as a function of geometry and thermal boundary conditions. For this model, it is assumed the upper boundary

temperature is constant at 300K, while the lower boundary temperature is variable and equal to the fluid temperature at that instant.

Once the heat leak is known, the total interactions with the surroundings are known since this is a closed system. Next, the initial temperature, pressure, and mass are set, and the rest of the initial conditions are determined. Then, the equation of state is used to find the liquid and vapor densities. Then the total volume of liquid and gas are found using the conservation of mass and the volume relation expressed in Equation 3-18. The liquid and vapor specific enthalpies are found using the RefProp program, and the total liquid and vapor enthalpy is then computed. At this point all state properties of the liquid and vapor phases are known for the initial condition. The total amount of energy transferred into the system is then calculated by multiplying the heat leak rate by the chosen timestep. Ideally, knowing the new enthalpy in the tank, RefProp should be able to calculate the new pressure since the specific enthalpy and the density of the system are known. Unfortunately, there are some thermodynamic states for certain fluids where convergence of the enthalpy/density specifications cannot be met by the RefProp program, and this proved to be the case in this situation. An alternate procedure was developed, where a new pressure is assumed, then new liquid and vapor enthalpies and total quality are calculated, and the total system enthalpy is compared to the previous timestep plus the known heat leak. The Excel add in Solver was used to eliminate the differences in these system enthalpies by varying the pressure, and a new system pressure was determined.

This model was used to predict system pressure and temperature increases over a period of time for a liquid hydrogen system with a known heat leak. Figure 3-11 shows

the temperature and pressure for a 150-liter hydrogen dewar initially filled with liquid hydrogen at the 50% mark. Notice the system temperature rate

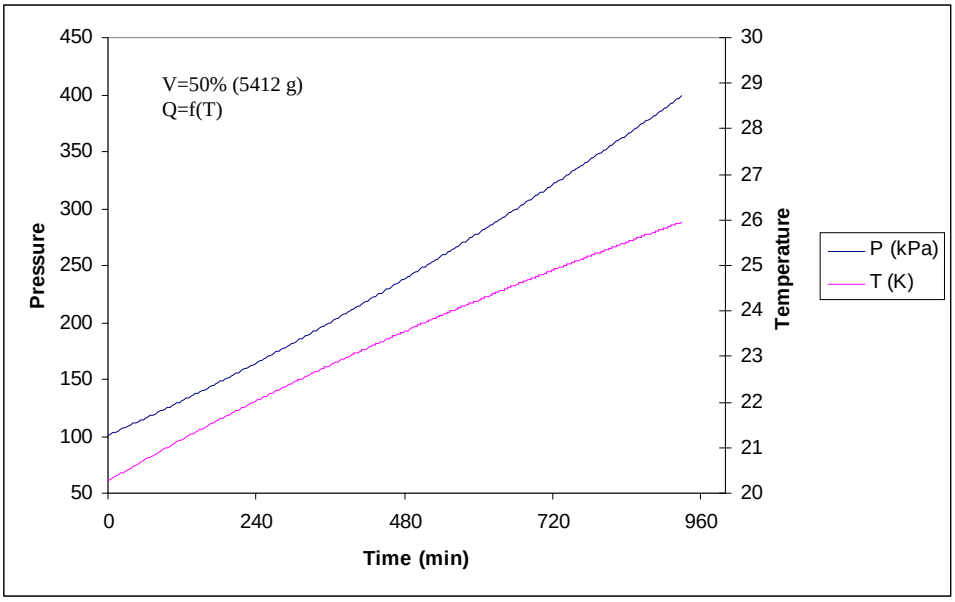

Figure 3-11 Self pressurization temperature and pressure vs. time

of increase begins to fall while the pressurization rate of increase gets larger as time progresses. As the time continues, the system temperature increases so the heat of vaporization decreases, and more of the heat leak is contributing to latent heating of the hydrogen as opposed to sensible heating.

Although liquid hydrogen is being converted into a vapor, the overall liquid level continues to rise over time. Figure 3-12 shows the system quality and the liquid and vapor volumes respectively. Notice the fraction of the vapor in the system increases in a similar manner to the pressure, again this is due to the decrease in the heat of vaporization. But due to a decrease in density in the warmer liquid, the overall liquid volume is increasing. The corresponding decrease in vapor volume also plays a role in the pressurization rate increase, although the vapor density is also increasing. This increase in liquid volume is critical to the design of dewars especially when they are near

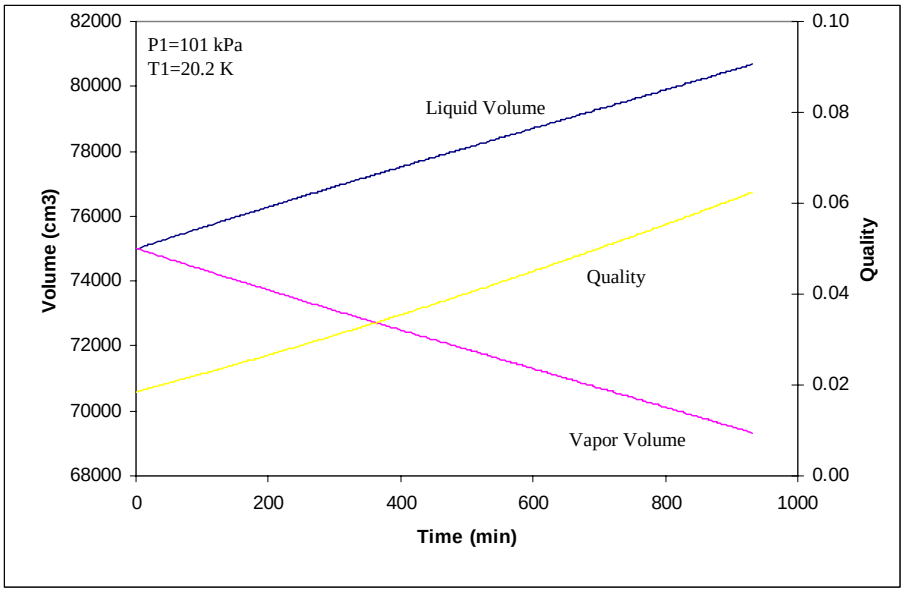

Figure 3-12 Self pressurization tank quality and phase volume vs. time

their 100% full level, since further increases in temperature will lead to thermal expansion of the incompressible liquid, and a rapid overpressurization may occur.

A comparison of system pressurization rates is shown in Figure 3-13 for three different liquid levels. It seems intuitive that the system that is most full will pressurize more quickly since there is less vapor space to fill. However, this proves not to be the case. This is explained by the fact that the greater the liquid quantity in the tank, the more of the heat leak is absorbed by sensible heat of the liquid and less goes to vaporization. For example, the liquid absorbed 97% of the heat leak into the system as sensible energy for the tank that was 75% full, but only 78% of the heat leak for the 25% full case.

Figure 3-14 shows the behavior of the system as predicted by the model compared to the experimental data. The data is from a zero boil off test conducted overnight with the cryocooler turned off, after liquefaction operations introduced 1.25 kg of hydrogen into the tank. The initial pressure was measured at 33 kPa. As is evident in the graph,

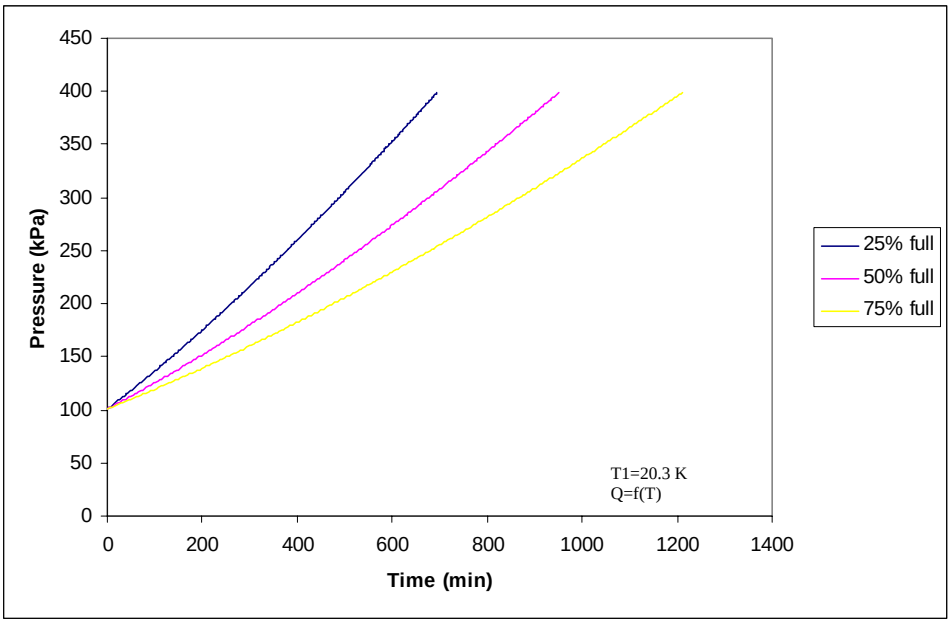

Figure 3-13 Self pressurization rates for variable liquid level

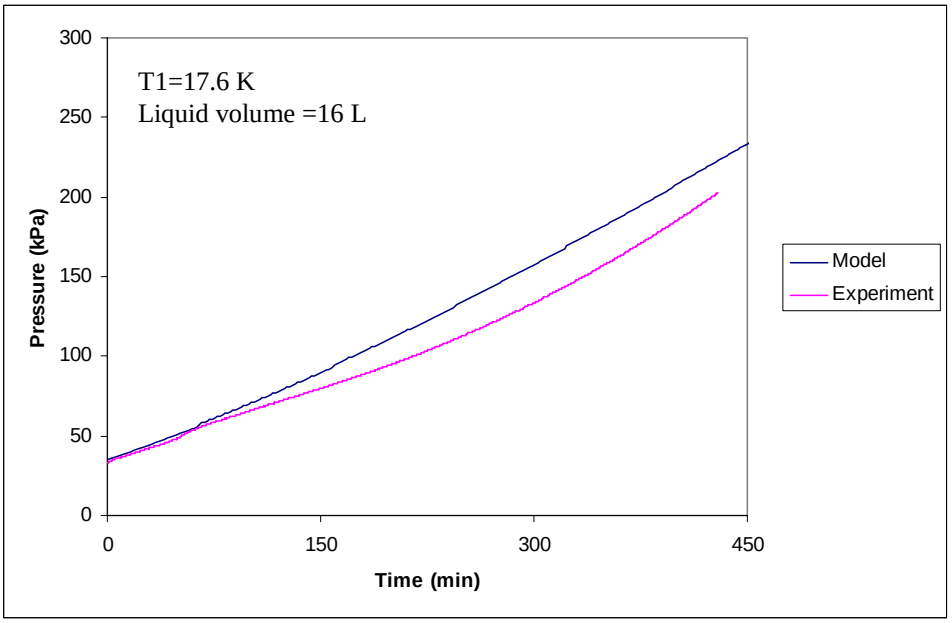

Figure 3-14 Self pressurization (model vs. data)

the predicted system pressurization rate is within 15% of the actual test data. This discrepancy is explained by the assumptions that the tank is modeled as an isothermal system, with the temperature at the top of the tank being equal to the temperature at the bottom (liquid temperature). The heat leak estimate assumes the tank is nearly full, so it

gives the heat leak rate for tanks in this condition. In this instance, 1.25 kg of hydrogen only had a liquid level of 16 liters, and there was a large temperature gradient down the length of the tank, reducing the heat leak compared to the model prediction. Corrections to this model will be made in later sections to account for variable liquid levels.

Open Storage With Heat Transfer To The System (Boil off)

There may be periods of time when the heat leak into the tank created a pressure rise that causes the tank relief valve to open, creating a boil off loss. During these times, it is assumed the system is closed to gaseous mass input or from liquid mass output. Typically during boil off situations, the tank pressure will remain constant, at the set pressure of the relief valve. Some systems with no backpressure vent directly to atmospheric pressure. This implies the liquid temperature inside the tank will also remain constant, at the saturation temperature corresponding to the tank pressure, and so the liquid density is also constant. Likewise, the vapor temperature and density can assume to be constant, although there will be some small increase in density as the liquid boil off creates a forced convection current that cools the upper part of the vapor volume. The conservation of mass equations then reduce to

$$\rho_g (V_{g2} - V_{g1}) = (-\dot{m}_{vp} + \dot{m}_{fg})\Delta t \qquad 3\text{-}20$$

$$\rho_l (V_{l2} - V_{l1}) = -\dot{m}_{fg}\Delta t \qquad 3\text{-}21$$

and the conservation of energy equations reduce to

$$\rho_g h_g (V_{g2} - V_{g1}) = -\dot{m}_{vp} h_{vp}\Delta t + \dot{m}_{fg} h_g \Delta t \qquad 3\text{-}22$$

$$\rho_l h_l (V_{l2} - V_{l1}) = Q_{HL} - \dot{m}_{fg} h_g \Delta t \qquad 3\text{-}23$$

The above equations have four unknowns and can be solved easily. Note the equation of state is not necessary since the state of the fluid is assumed constant with the isobaric venting process.

A Microsoft Excel spreadsheet has been developed to model this boil off process. Initial conditions and system constraints are first determined. For this example, the initial system mass must be input, and the relief valve set pressure is determined. Using these parameters with the system volume, the initial temperature, liquid and vapor mass, density and volumes, and heat of vaporization are calculated. The system heat leak is calculated for this tank temperature. Then, the mass of the liquid boil off is calculated, and the new liquid mass and volumes are found. Next, the new vapor volume is calculated and using the constant vapor density, a new vapor mass is found. Knowing the initial and final vapor and liquid masses, the mass of the vent loss is calculated. This mass will always be slightly less than the mass of the liquid boil off, since some boil off vapor must fill in the additional volume lost by the liquid.

Figure 3-15 shows the values of liquid and vapor mass in a 150 liter dewar filled halfway with liquid hydrogen at atmospheric pressure. Notice the liquid mass drops at an approximately linear rate, since the heat leak is a function of the constant liquid temperature. The vapor mass increases slightly over the boil off process. Figure 3-16 compares the time it takes to completely evaporate a given volume of liquid depending on the boil off pressure. Hydrogen storage losses occur more quickly when the vapor pressure is elevated, mainly due to the decrease in heat of vaporization, but also partly due to the greater mass fraction of hydrogen that is in the vapor phase initially.

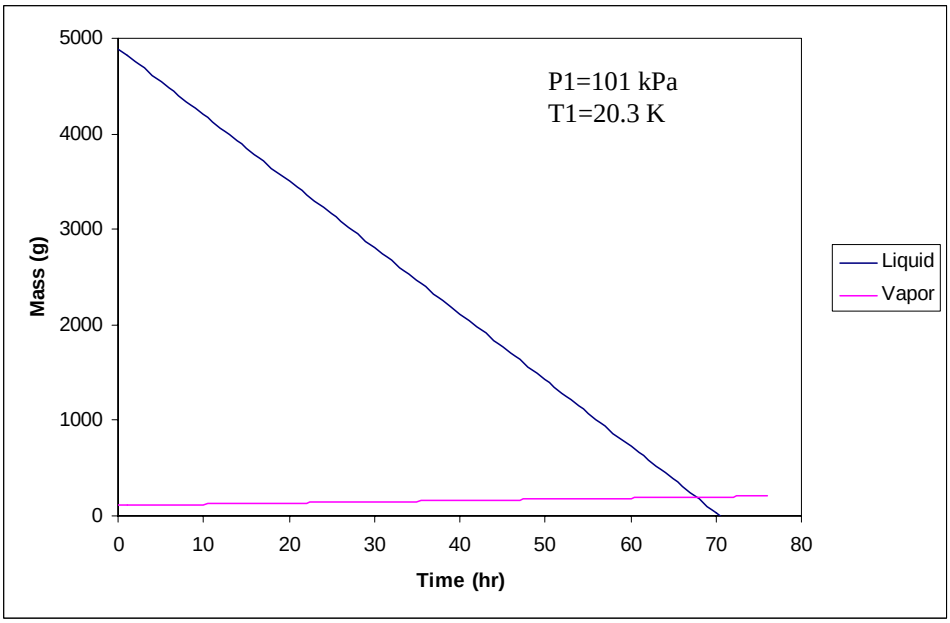

Figure 3-15 Liquid and vapor mass during boil off

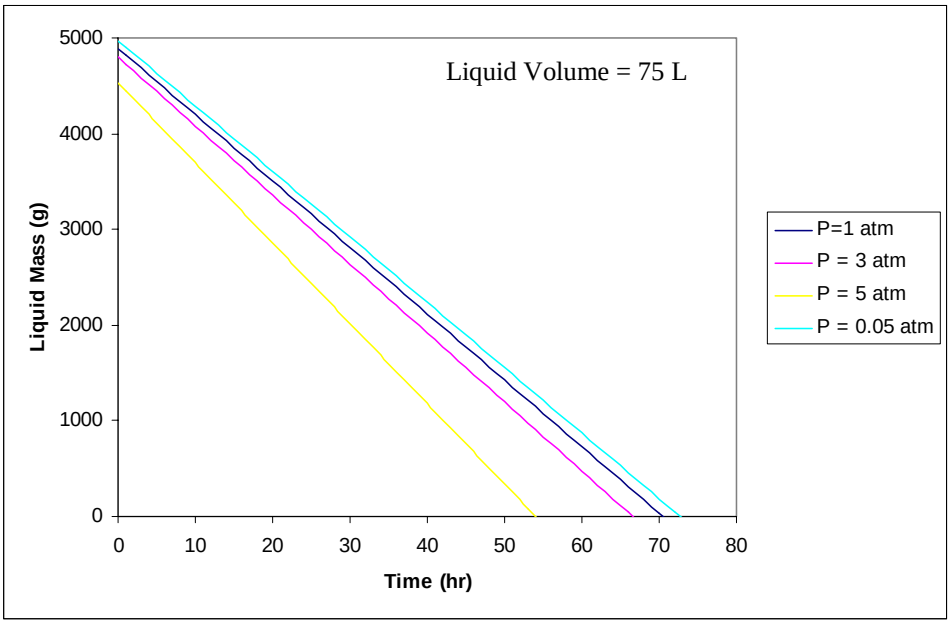

Figure 3-16 Boil off time dependence on pressure

The simplification made that the liquid and vapor temperature and pressure were uniform throughout the volume makes this boil off model less precise, in actuality there will be temperature gradients in the ullage space and down the tank walls that will decrease the total heat transfer to the liquid as the liquid volume drops. There is no experimental data

in this work to compare this model to, since no boil off occurred during the liquid hydrogen experimentation portion discussed in Chapter 6.

Closed Storage With Zero Net Heat Transfer (Zero Boil Off)

The ZBO operation is a closed storage system with refrigeration provided to remove heat leak into the tank. The state of the fluid will depend on the capacity of the refrigeration system. There exists a point on the refrigerator capacity vs. temperature curve where the capacity is exactly equal to the heat leak into the tank. As such the system can be modeled as steady state and the conservation equations can be reduced to

$$V_{g2} = V_{g1} \tag{3-24}$$

$$V_{l2} = V_{l1} \tag{3-25}$$

$$Q_{HL} = Q_{REF} \tag{3-26}$$

As given by Cryomech, the AL330 performance curve is plotted with the heat leak vs. temperature curve below in Figure 3-17. After curve fitting the performance curve,

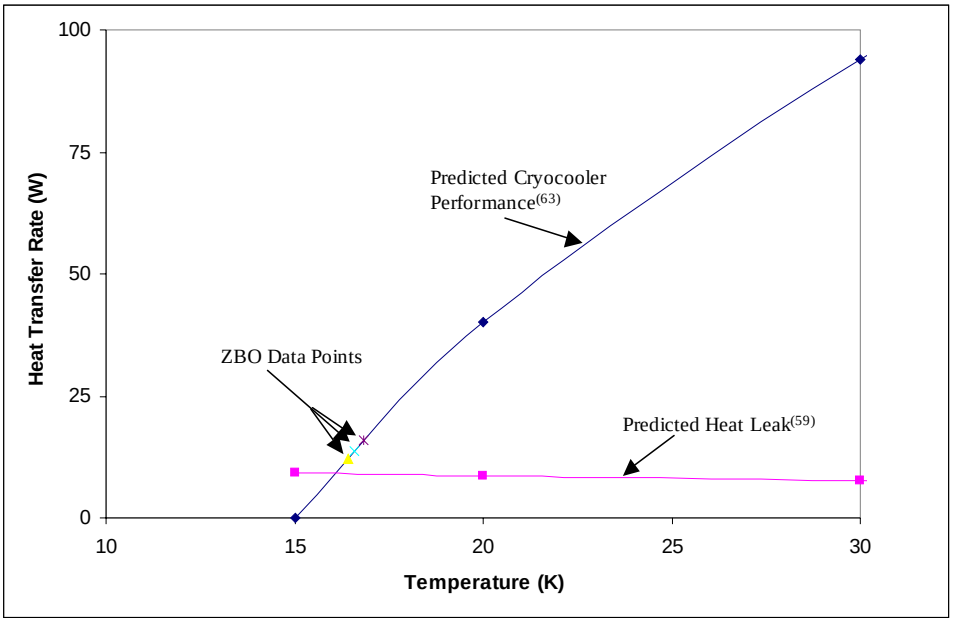

Figure 3-17 Cryocooler performance and heat leak vs. temperature

the equations can be set equal to each other and solved for the intersection, which is 16.25 K. This system temperature can be considered analogous to a cryocooler no-load temperature. The results of this closed system energy balance derived in this section agrees very well with the experimentation value of no load system temperature, ranging from 16.42 K to 16.85 K, obtained during several densification tests. These data points are plotted on the cryocooler curve and are labeled below

Open System With Heat Transfer Out Of The System (Liquefaction)

During liquefaction operations it is preferable there is no mass outflow from the tank, so there is always an increase in overall system mass. The refrigeration system must be operating (except when stored refrigeration energy in a subcooled liquid can temporarily liquefy a small quantity of gas) to remove the enthalpy flowing into the gas supply port. The conservation equations can be simplified as follows;

$$\rho_{g2}V_{g2} - \rho_{g1}V_{g1} = (\dot{m}_{gsp} + \dot{m}_{fg})\Delta t \qquad 3\text{-}27$$

$$\rho_{l2}V_{l2} - \rho_{l1}V_{l1} = -\dot{m}_{fg}\Delta t \qquad 3\text{-}28$$

$$\rho_{g2}V_{g2}h_{g2} - \rho_{g1}V_{g1}h_{g1} = \dot{m}_{gsp}h_{gsp}\Delta t + \dot{m}_{fg}h_{g}\Delta t \qquad 3\text{-}29$$

$$\rho_{l2}V_{l2}h_{l2} - \rho_{l1}V_{l1}h_{l1} = Q_{HL} - Q_{REF} - \dot{m}_{fg}h_{g}\Delta t \qquad 3\text{-}30$$

At first it is tempting to consider the liquefaction model to be equivalent to the boil off model as they both are open systems with net heat exchange, but instead of heat transfer into the tank and mass transfer out of the tank, the liquefaction system operates in the opposite direction. However this is not accurate, as there are additional simplifications in the boil off model imposed by the relief valve, namely that the pressure in the tank is constant. Depending on the gas supply port mass flow rate and the net amount of refrigeration, the tank pressure may increase, decrease, or remain constant. But

during operations where the ullage pressure is increasing, gas is entering the tank at a faster rate than the cryocooler capability to remove its energy, and a non-saturated vapor condition occurs. This phenomenon is not described accurately by this model, which assumes thermodynamic equilibrium between the liquid and vapor phases.

The model has been modified to accept these conditions and predict the system liquefaction rate to maintain thermal equilibrium for a given set of initial conditions. The net heat transfer out of the system from the combination of heat leak and cryogenic refrigeration is then calculated for that given temperature condition. To maintain equilibrium this must match the increase in system enthalpy from the gas supply port. Knowing the conditions of the inlet stream and the final liquid state, the change in enthalpy required for liquefaction is calculated. The appropriate mass and vapor volumes are then found. Figure 3-18 shows predicted liquefaction rates for a range of storage states. This chart shows the liquefaction rate increases as expected, when the storage pressure is higher. This is due to the saturation temperature corresponding to this pressure being higher, which has three effects. First, the cryocooler operates more efficiently at higher temperatures and there is greater cooling power available. Second, the amount of enthalpy required to be removed from the incoming gas is less. Finally, the net heat transfer from the surroundings is slightly less since there is a smaller thermal gradient.

Figure 3-18 also shows the experimental data for three periods where the mass flow rate was constant and sufficient to maintain a constant pressure in the tank. This comparison shows a general correlation in the shape of the profile, but the results vary by as much as +/- 28%. The discrepancies between the predicted vs. actual liquefaction

rates can be partially explained by the experiment not taking into account the heat of conversion between ortho and para hydrogen. The model assumes equilibrium hydrogen but there is a finite time required to change the normal hydrogen to equilibrium hydrogen. Other factors include the actual experiment was not an isothermal system and there were temperature stratifications that the model did not include. An additional cause of the discrepancy is the uncertainty in the measurements, since the exact state of the incoming gas was not known and there was no experimental method to control the

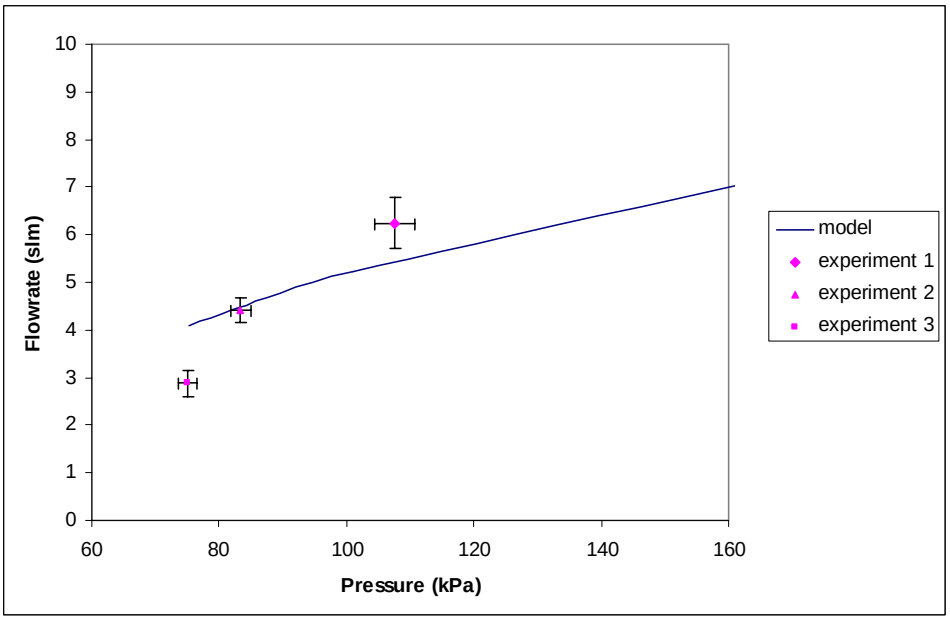

Figure 3-18 Comparison of predicted vs. actual liquefaction rate

pressure and mass flow rate. In these cases it can be seen that while the pressure and mass flow rate was relatively constant, there were variations in the measurements that implied the system was not truly in thermodynamic equilibrium. These uncertainties are plotted as x and y error bars in the individual liquefaction experiment data points. In some cases, variations in the "constant" mass flow rate were as high as 8.7%, and pressure fluctuations were up to 2.2%. Clearly, more data needs to be collected, and with better control and fidelity.

Closed Storage With Heat Transfer Out Of The System (Densification)

A closed system with heat transfer out of the system by refrigeration is similar to the closed self-pressurization case with the exception the pressure and temperature will decrease until the system reaches steady state and the refrigeration capacity balances out the heat leak into the tank. In the meantime, the mass of the liquid and vapor will change as some vapor is condensed out of the ullage space. The conservation equations can be written as

$$\rho_{g2}V_{g2} - \rho_{g1}V_{g1} = \dot{m}_{fg}\Delta t \qquad 3\text{-}31$$

$$\rho_{l2}V_{l2} - \rho_{l1}V_{l1} = -\dot{m}_{fg}\Delta t \qquad 3\text{-}32$$

$$\rho_{g2}V_{g2}h_{g2} - \rho_{g1}V_{g1}h_{g1} = \dot{m}_{fg}h_g\Delta t \qquad 3\text{-}33$$

$$\rho_{l2}V_{l2}h_{l2} - \rho_{l1}V_{l1}h_{l1} = Q_{HL} - Q_{REF} - \dot{m}_{fg}h_g\Delta t \qquad 3\text{-}34$$

Again this is a system of seven unknowns and seven equations (including the volume relation, the mass transfer between the vapor and liquid relation, and the equation of state), and can be solved in a similar manner. The same Excel program was used to estimate densification rates as the self pressurization rates, with the exception that the heat transfer rate previously given by the heat leak estimation is now the difference between the heat leak and the refrigeration capacity of the cryocooler at the system temperature. Results of this model are shown below.

Figure 3-19 shows the temperature and pressure of the system with a tank initially 50% full of LH2 at the normal boiling point. The pressure and temperature decrease more rapidly at first since the cryocooler is producing more refrigeration at higher temperatures. Eventually the pressure and temperature reach the steady state condition

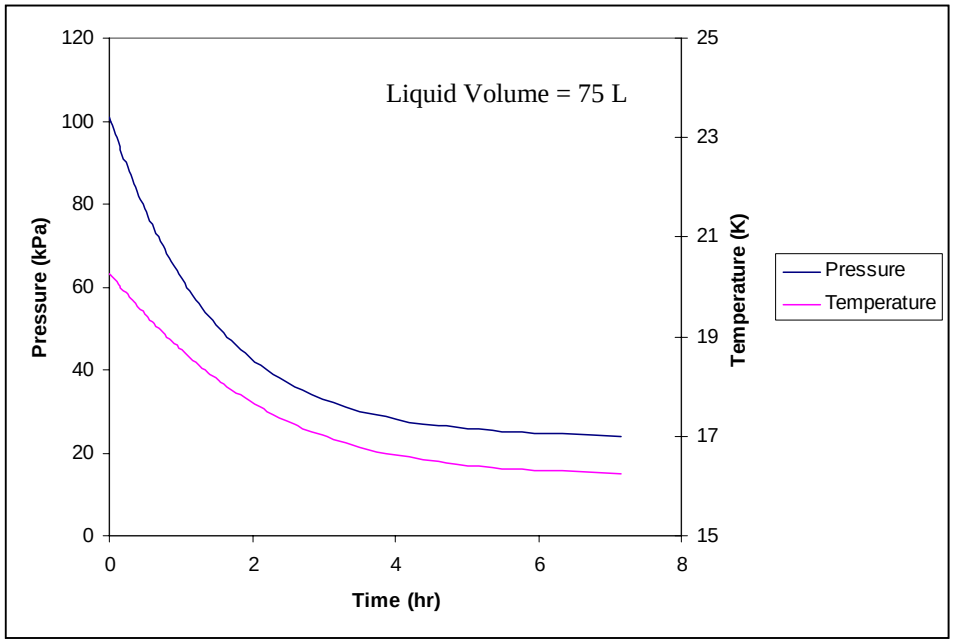

Figure 3-19 Predicted densification temperature and pressure

defined by the zero boil off model. Figure 3-20 demonstrated the predicted densification times for three different initial liquid levels ranging from 25% to 75% full. As expected the smaller the mass in the tank, the less time it takes for densification. Some launch

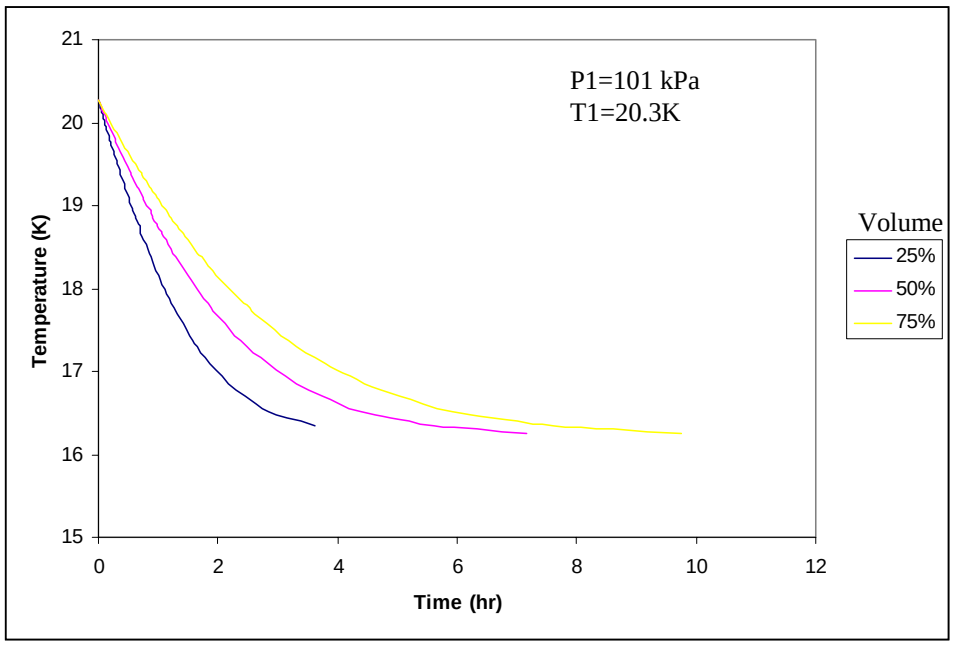

Figure 3-20 Densification rates for variable liquid levels

scenarios may depend on on-board densification, and predictive models will need to be developed to estimate countdown hold times for densification

Figure 3-21 compares temperature data obtained during experimentation with the simplified model. Note the predicted densification time profiles vary widely; this is explained by two factors. First, non-equilibrium processes are occurring in the tank where the ullage space is developing significant temperature stratifications. Some cryocooler capacity must be used to chill this vapor back to the saturated state. Refer to Figure 6-14 on page 149 for details on the thermal profiles in the tank during this densification process. Second, similar to the pressurization model, heat transfer processes are modeled using a uniform temperature in the tank and the heat leak and cryocooler performance will vary in those conditions.

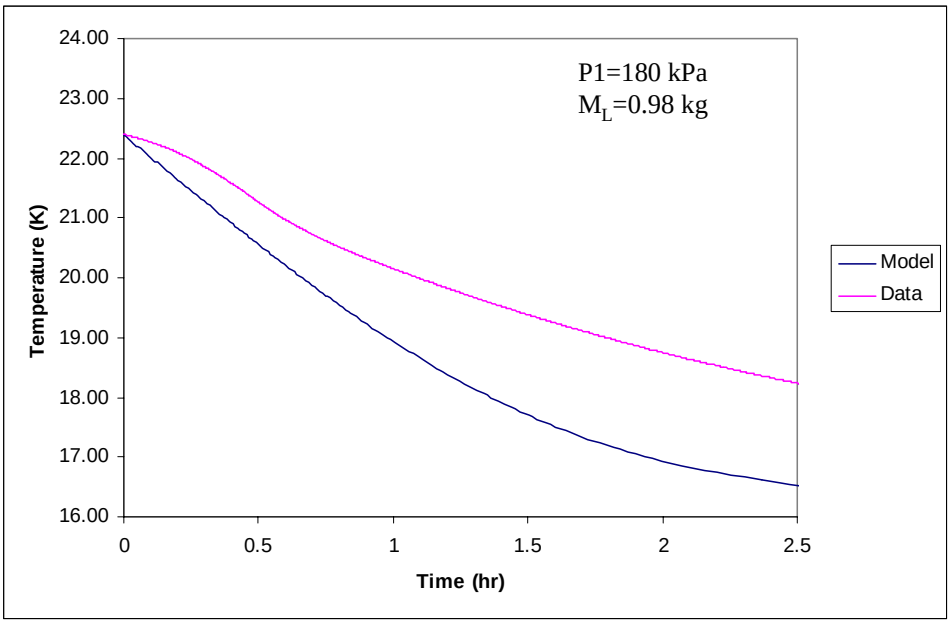

Figure 3-21 Predicted vs. actual densification rates

Based on the above discussions, it appears the model has two major components of error. First, the isothermal model is not entirely accurate as thermal stratification in the tank will cause variations in heat leak. Second, there are non-equilibrium processes

happening during many operational scenarios, especially when the liquid and vapor states are not fully saturated. An attempt to create a correction factor for these two situations will be made in the following section.

Corrected model

Variations in the predicted heat leak will occur since the model used assumes an isothermal tank and the physical system has temperature stratifications inside the vapor region. These stratifications will cause warmer temperatures at the top of the tank, minimizing the temperature gradient and reducing heat leak from the outside. A correction to the isothermal model developed above will be proposed to account for this variation. The correction factor will consist of two components. First, an adjustment must be made to account for variations in the tank liquid level. The modified Lockheed Martin correlation for MLI performance depends on the tank being at 100% full and at a constant temperature. Actual tanks will have a temperature gradient up the vertical walls of the tank between the liquid level and the top of the tank. This means the delta T between the hot and cold temperatures will be less than 100% for a portion of the tank, especially any warm supports and tubes that connect to the top of the tank. Boil off testing at KSC has shown heat leak is approximately a linear relationship with liquid level, so the first component of the heat leak correction will be of this form.

The second component of the correction factor must take into account transient effects associated with the generation or destruction of thermal stratification layers inside the system. This correction will be applied during operational models when the state of the liquid and vapor in the tank is changing. For the cases above, this includes pressurization and densification operations. During boil off venting, steady state zero boil off, and steady liquefaction the thermodynamic variables exhibit no time

dependence, since there is no net heat transfer to or from the fluid at these times. During the steady boil off or liquefaction the enthalpy flow into or out of the tank cancels the heat leak or refrigeration, and during zero boil off the refrigerator is balanced by the heat leak. During the pressurization case, a net heat leak into the system creates a temperature change is the fluid, while during densification the net refrigeration power has the opposite effect.

Looking at an energy balance in the system during this transient operation shows a general relationship for the heat leak into the tank and a temperature change according to the relation

$$\rho \frac{\partial h}{\partial t} = \nabla \cdot k \nabla T \qquad 3\text{-}35$$

Integrating this equation with respect to time gives a function for heat leak that is dependent on the time and the initial volume. To determine exact true function of this relationship, this differential equation can be solved. The boundary conditions for this case would be a variable temperature at z=0 (liquid level), variable temperature along the walls of the tank and a variable temperature at the top of the tank. This would also need to be modeled with a variable thermal conductivity and specific heat, and enthalpy would need to be expressed in terms of the temperature and pressure in the tank. This exercise is beyond the scope of this simplified model correction. To determine a general form of this correction term, it is useful to examine the profiles of ullage temperatures in Figure 6-22. Data taken during self pressurization tests that show thermal stratifications in the liquid level give an indication a logarithmic relationship of heat leak with respect to time.

Adding a time dependent logarithmic correction in combination with the linear dependence on liquid level gives a corrected heat leak of the form

$$Q_{corrected} = (A + (Q_{LM} + Q_{CON} - A) * B) * C * Ln(D * t) \quad 3\text{-}36$$

where A is the heat leak in the tank as the liquid level approaches zero, Q_{LM} is the predicted heat leak from the MLI correlation, Q_{CON} is estimated conduction heat leak, B is the liquid level (%), and C and D are constants used to fit the model data to the experimental curve.

The corrected model (model B) shown below uses the following values; A=5, B=10% (based on conditions used in experiment), C=0.019, and D= 10,500. Figures 3-22 and 3-23 below show the results of this corrected model for the densification and self-pressurization processes as compared to the experimental data. An additional day of data was added to each figure, and this data is compared to the model as well. The added pressurization data has the same initial conditions as the first, and the curves plot on top of each other very neatly. The added densification data was from testing several days after the previous data curve, and the initial mass and temperature change. In this case, the corrected model was run again and the curve is plotted against the data. In both the pressurization operation and the densification operation, the corrected model is a better prediction tool than the original isothermal model. However, in order to get a true model of the system behavior the full conservation equations must be discretized and solved numerically.

Storage Fluid Analysis

In order to more accurately model the behavior of the hydrogen in the system, the full conservation of mass, momentum and energy equations must be considered. The system described by Figure 3-24 is an unsteady, open system that will be approximated in

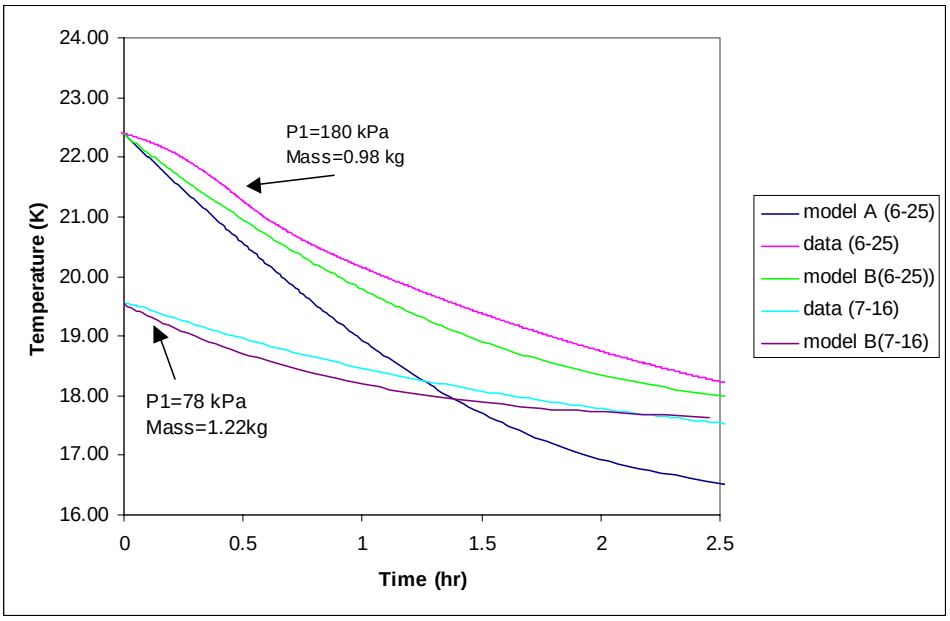

Figure 3-22 Corrected model vs. densification data

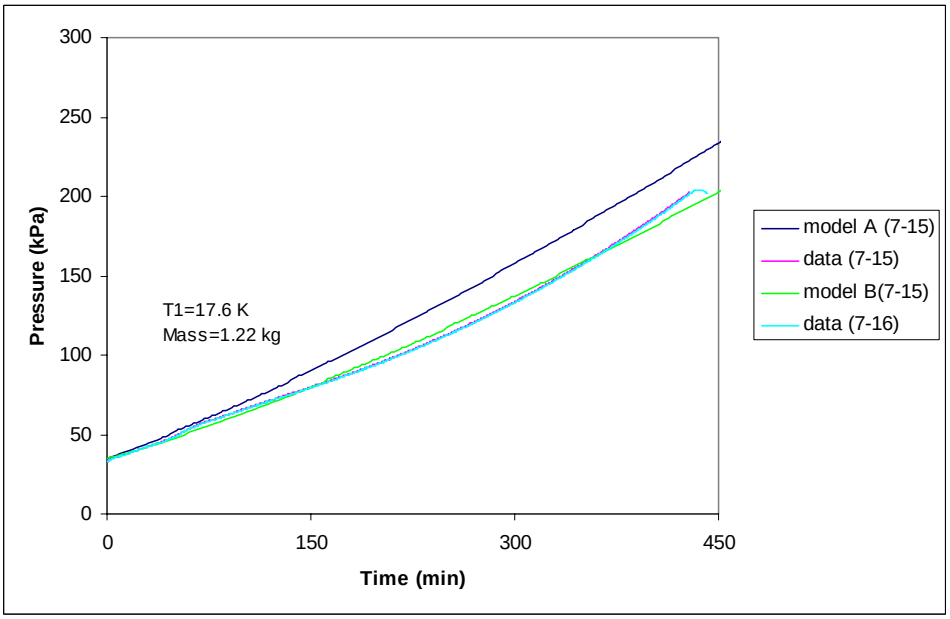

Figure 3-23 Corrected model vs. pressurization data

three-dimensional space using cylindrical coordinates. Due to symmetry about the axis, dependence in the θ direction can be neglected. Gravitational effects must be taken into account. The overall system boundary is set as the inside wall of the inner tank, defined as r=R. The upper height of the tank is at the coordinate z=Z. There are three modes of

heat exchange between the system and the surroundings, radiation on the outer surfaces through the MLI, conduction down the length of any pipe or tube support between the inner and outer vessel, and refrigeration by the cold heat exchanger of the cryocooler. There is mass transfer in and out of the tank from the gas supply line and the vent line. The velocity profiles at the tank inlet and outlet will depend on the geometry, and for now a fully developed laminar flow profile driven by the pressure gradient can be assumed at the interface. There is a longitudinal and radial velocity component in both the liquid and vapor space. The liquid velocity is driven by the free convection currents at the heat exchange surfaces, with a circulation pattern of warm updrafts along the walls and a cold downdraft in the center at the cold HX. This differs from conventional cryogenic dewars that only have the warm upward velocity with a layer of warm fluid at the top of the liquid. Therefore the liquid velocity will have a superimposed freestream velocity from the circulation currents as well as the free convection velocity. One important result of a full numeric analysis is to determine whether this freestream velocity will drive the heat transfer coefficient higher than otherwise, and hence increase the amount of heat transfer from the surroundings. If so, anti convection baffles may be added. The vapor velocity will be driven by warm convection currents as well as the velocity in and out of the supply and vent line. The thermodynamic state of the liquid and gas is variable, dependent on both time and location inside the tank. The total mass of the liquid and vapor will depend on the initial conditions as well as mass flow into and out of the tank and evaporation or condensation at the liquid to vapor interface. The liquid to vapor interface is assumed to be a free liquid surface, with homogenous phases above and below, and the location of the interface in the z direction and the profile will

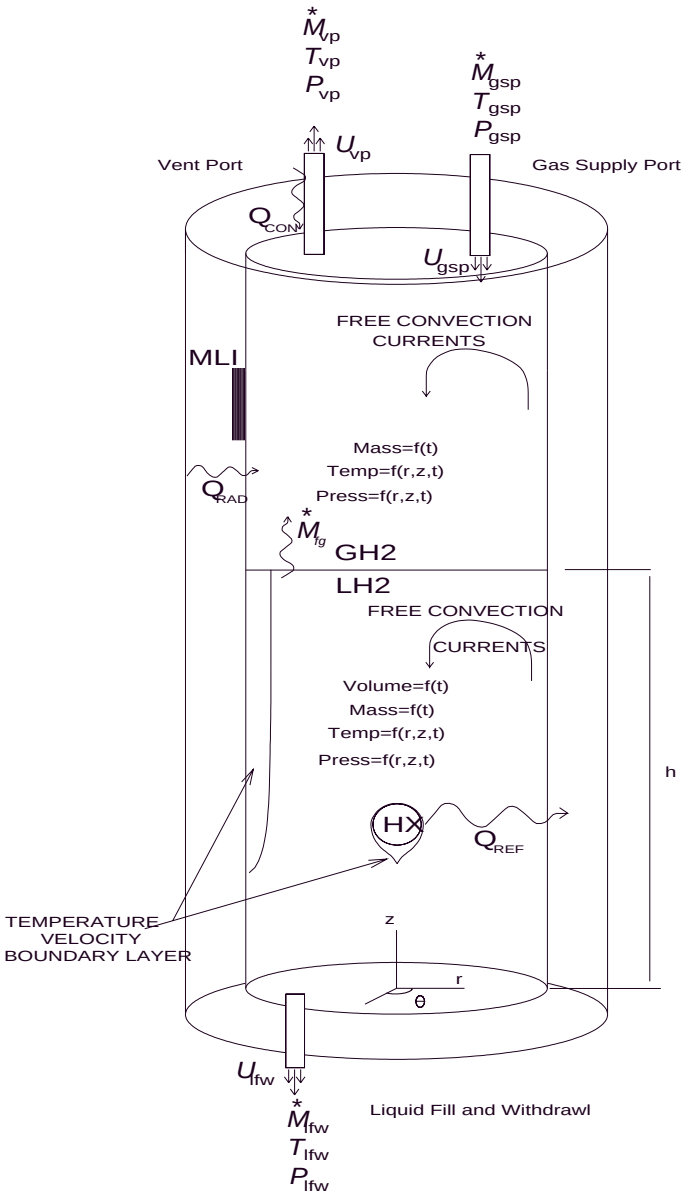

Figure 3-24 Proposed system representation

vary. This location will be denoted as z=h. More details on this interface will be given when the boundary conditions are discussed.

To understand the fluid behavior in order to model it, a consideration of the flow regime must be taken into account. While the exact flow velocity is unknown, order of magnitude estimates can be made to find a representative Reynolds number. A potential

and kinetic energy balance of the fluid gives a velocity of the magnitude[44]

$$\bar{V} \approx \{gL\frac{\Delta\rho}{\rho}\}^{1/2} \qquad 3\text{-}37$$

The velocity depends on the characteristic length of the system and the relative change in density, which depends on the temperature gradient. An energy balance between the heat leak thru the insulation compared to the heat transfer to the liquid allows for a rough calculation of the temperature difference between the wall and the bulk fluid. Using the heat transfer coefficient found in Chapter 6, for steady state conditions this delta T will be between .01 and .04 K. This estimate compares well to the experimental data found during boil off tests conducted with liquid nitrogen at KSC.[45] During some transient operations this temperature gradient will be greater. Varying the length scale of the heat transfer and the delta T, the liquid vertical velocity ranges between 2.5 and 35 cm/sec. The vapor velocities are slightly higher. The dependency of the characteristic velocity as a function of temperature difference is shown in Figure 3-25. The liquid velocities are plotted for cooling of the hydrogen by the cold heat exchanger, while the vapor velocities are for the warming of the vapor by the tank walls. The length scale is 35 cm, which is approximately with the tank half full. At first, this free convective velocity seems very high, but an examination of the fluid properties shows this is feasible. The volumetric coefficient of thermal expansion, β ,for liquid hydrogen at 20 K is 0.0164 K^{-1}. This is two orders of magnitude higher than β of water, which is 2.15 x 10^{-4} K^{-1} . Similarly, the bulk coefficient of gaseous hydrogen is 17 times greater than that of steam. Small temperature differences in hydrogen systems cause large displacements and hence, high velocities.

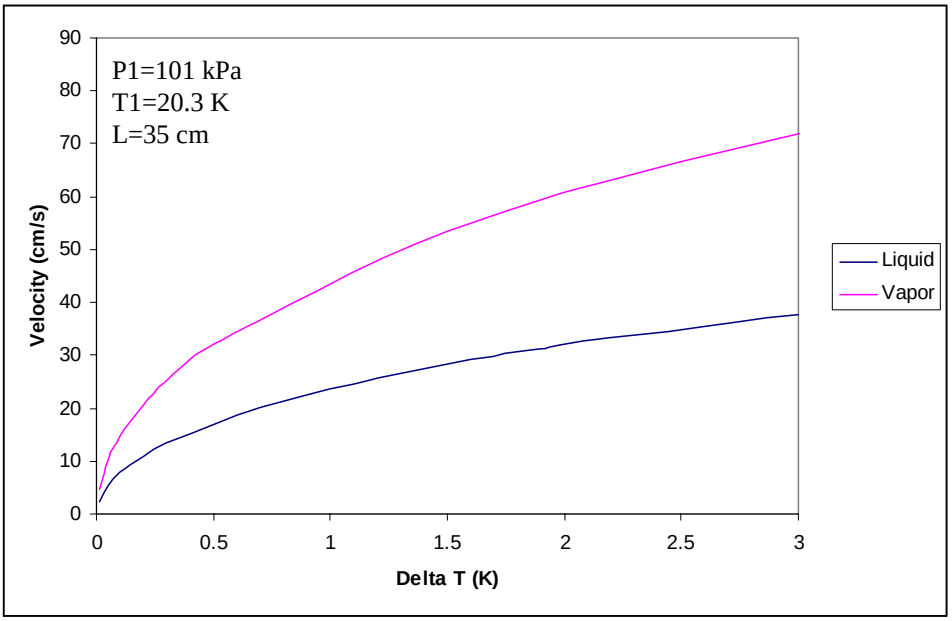

Figure 3-25 Predicted Free Convection Velocity

Using the density and viscosity of both triple point and NBP liquid hydrogen, a range of estimates for Re can be computed. The characteristic length used is the height of the liquid and for the figure below is set at 50% full. Figure 3-26 plots this estimate of Reynolds number for a range of temperature gradients. From this figure, it appears the Reynolds numbers may be quite high at times, like when the temperature gradients are higher during transient operations. After the system has had time to approach steady state conditions, the delta T will be less and the liquid and vapor Reynolds number will approach $8x10^4$ and $4x10^4$, respectively. In this case the flow inertia is more moderate, and viscous forces play a greater factor in the flow. However the Reynolds number is still high enough that the flow can be modeled with a viscous boundary layer and an inviscid core. This premise will be revisited in a few sections when an order of magnitude analysis on the conservation of momentum equation is addressed.

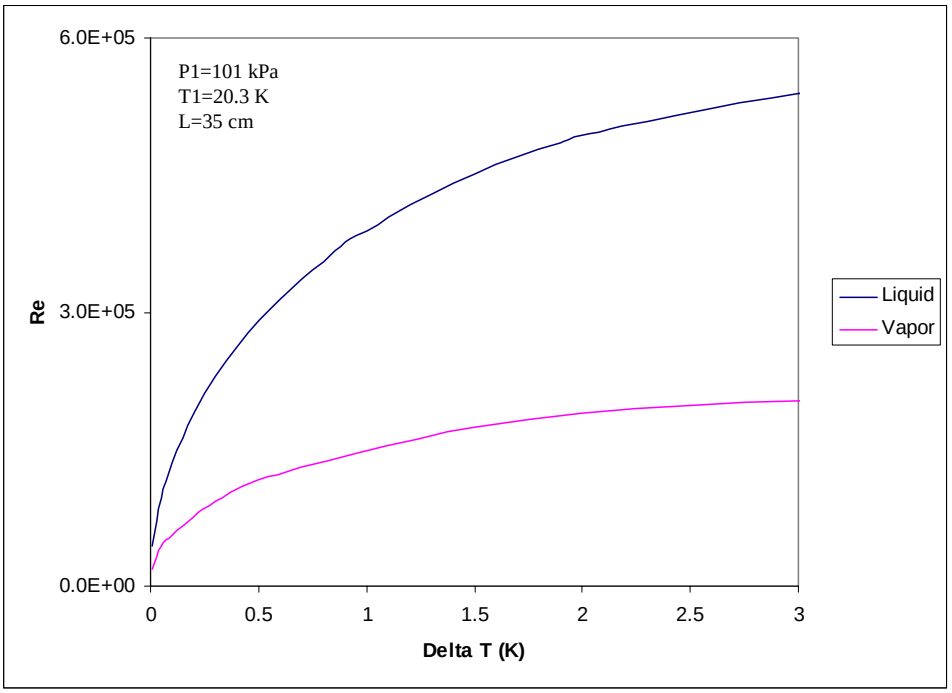

Figure 3-26 Predicted Free Convection Reynolds Number

Perhaps a better representation of the flow regime is given by the Grashof number. This non-dimensional number is defined as

$$Gr_x = \frac{g\beta(T - T_\infty)x^3}{\upsilon^2} = \mathrm{Re}_x^2 \qquad 3\text{-}38$$

And is a measure of the free convective buoyancy effects vs. the viscous effects. Again, this value will depend on the exact conditions, but a representative value at 20K for the liquid and vapor space for a range of temperature gradients has been plotted in Figure 3-29. Again, during transient operations with higher gradients, the flow is more turbulent, but normal operations with smaller delta T the flow regime is laminar, especially in the vapor region. The high value of the bulk coefficient accounts for the high Gr. Typically the transition to turbulent flow occurs around $Gr=10^9$.

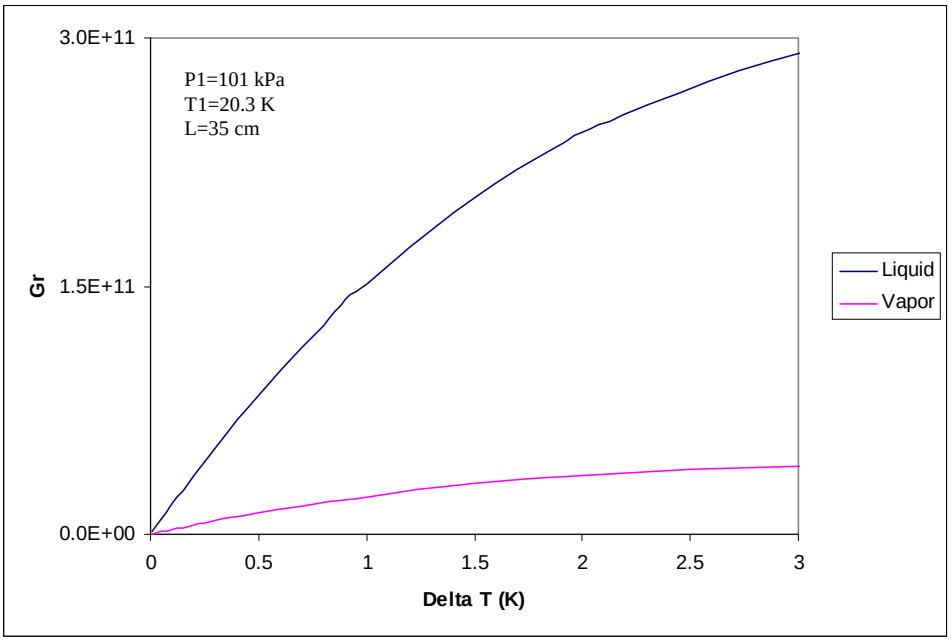

Figure 3-27 Predicted Grashof Number

The above analysis is a rough scaling analysis of the type of flow regime expected to occur, and is useful for later analytical solutions based on heat transfer correlations. However, to truly model the system behavior, an exact numerical solution to the full Navier Stokes equations is required. Fortunately the availability of modern fast computer processing makes this endeavor more feasible than in the past. The following section derives the equations that must be solved.

The following conservation equations will be considered in differential form. There are numerous texts that derive the full conservation equations starting from an infinitesimal, fixed control volume,[46-49] and this effort will not be repeated here. The full two dimensional conservation equations for unsteady flow of a Newtonian fluid in cylindrical are stated below, followed by addition of some simplifying assumptions. The variations in the θ direction are neglected due to symmetry about the axis.

Conservation of Mass

The Conservation of Mass can be expressed in differential form as

$$\frac{\partial \rho}{\partial t} + \frac{1}{r}\frac{\partial}{\partial r}(r\rho v_r) + \frac{\partial}{\partial z}(\rho v_z) = 0 \qquad 3\text{-}39$$

where the first term is the rate of change of mass inside the element and the next two terms are the net mass flow into or out of the element from the r and z directions respectively. This equation is applicable for all fluids and assumes the density is variable. Typically for cryogenic applications, a large range of temperatures does not allow for system analysis using constant properties. In this case, liquid densities can vary 18.8% between the triple point and 25 K, and vapor densities vary 460% between the NBP and the ambient temperature. Therefore this system will not be modeled with a constant density as the density will vary with respect to time, dependent on the temperature and pressure variations. Temperature gradients will be present in the radial direction driven by heat flux from the wall and convection currents and the axial direction due to buoyancy effects. The local velocity field will be driven primarily by natural convection, although during periods of filling or draining the tank the local velocity will be driven by pressure gradients. It is anticipated the velocity will be dependent on both spatial coordinates inside the system. Rearranging the equation to do an order of magnitude analysis gives

$$\frac{\partial \rho}{\partial t} = \frac{\rho v_r}{r} + v_r\frac{\partial \rho}{\partial r} + \rho\frac{\partial v_r}{\partial r} + \rho\frac{\partial v_z}{\partial z} + v_z\frac{\partial \rho}{\partial z} \qquad 3\text{-}40$$

In order for this equation to be valid, the right hand side must be the same order of magnitude as the left hand side, so the LHS order of magnitude is relevant. For this enclosed system, the order of magnitude of the radial velocity must be the same as the

axial velocity (order of V), and knowing the geometry of the tank determines the order of magnitude of the radial and axial directions are the same (order of L). Breaking down the equation and dividing by V/L, the order of magnitude of the terms on the RHS become

$$O(\rho) + O(\Delta\rho) + O(\rho) + O(\rho) + O(\Delta\rho) \qquad 3\text{-}41$$

For the vapor region, a review of thermodynamic variables as a function of temperature shows the order of magnitude of the density change is the same as for the total density. For the liquid region, the density changes are an order of magnitude less than the total density, and for a simple model with less accuracy required, the $\frac{\partial\rho}{\partial r}$ and $\frac{\partial\rho}{\partial z}$ terms could be neglected. However, if an accuracy greater than 90% is desired, these terms must be included.

Assuming boundary layer scaling ($V_r << V_z$, $r << z$), the second term on the RHS can be neglected. In this case even though $\partial\rho/\partial r \approx \partial\rho/\partial z$, the inequality $V_r << V_z$ still applies and the term is not the same order of magnitude as the others. In this case (if boundary layer approximations are used), the conservation of mass reduces to

$$\frac{\partial\rho}{\partial t} = \frac{\rho v_r}{r} + \rho\frac{\partial v_r}{\partial r} + \rho\frac{\partial v_z}{\partial z} + v_z\frac{\partial\rho}{\partial z} \qquad 3\text{-}42$$

Conservation of Momentum

The general conservation of momentum of a 2 dimensional viscous, unsteady flow for the r and z directions can be expressed in differential scalar form as

$$\begin{aligned}&\rho\left(\frac{\partial v_r}{\partial t} + v_r\frac{\partial v_r}{\partial r} + v_z\frac{\partial v_r}{\partial z}\right) = \rho g_r - \frac{\partial P}{\partial r}\\ &+\frac{1}{r}\frac{\partial}{\partial r}\left\{2\mu r\left(\frac{\partial v_r}{\partial r} - \frac{1}{3}\left(\frac{v_r}{r} + \frac{\partial v_r}{\partial r} + \frac{\partial v_z}{\partial z}\right)\right)\right\} + \frac{\partial}{\partial z}\left\{\mu\left(\frac{\partial v_z}{\partial r} + \frac{\partial v_r}{\partial z}\right)\right\}\end{aligned} \qquad 3\text{-}43$$

$$\rho\left(\frac{\partial v_z}{\partial t} + v_r \frac{\partial v_z}{\partial r} + v_z \frac{\partial v_z}{\partial z}\right) = \rho g_z - \frac{\partial P}{\partial z}$$
$$+ \frac{1}{r}\frac{\partial}{\partial r}\left\{r\mu\left(\frac{\partial v_z}{\partial r} + \frac{\partial v_r}{\partial z}\right)\right\} + \frac{\partial}{\partial z}\left\{2\mu\left(\frac{\partial v_z}{\partial z} - \frac{1}{3}\left(\frac{v_r}{r} + \frac{\partial v_r}{\partial r} + \frac{\partial v_z}{\partial z}\right)\right)\right\} \qquad 3\text{-}44$$

where the first term on the left hand side is the time rate of change of momentum inside the fluid element and the next two terms are the momentum flow into the element from the r and z directions. The right hand side of the equation is the summation of forces on the element, with the first term being the gravitational force (other body forces such as electromagnetic are neglected), the second term is the pressure acting on the normal surface, and the third and fourth terms are the viscous dissipation forces.

At this point it is tempting to simplify this equation by assuming constant fluid properties, reducing the viscous terms to a much simpler expression of $\mu\nabla^2\overline{V}$. In many cases this could be a poor assumption, since the liquid hydrogen viscosity is highly temperature dependent. Indeed, the viscosity of liquid hydrogen will vary 67% between the normal boiling point and the triple point. Changes in the fluid properties will occur over time, as the temperature of the fluid increases or decreases depending on the level of heat flow into or out of the tank. The vapor density and viscosity exhibit similar dependency on temperature. This dependency is known from thermodynamic relations and experimental data, and the function $\mu = f(P,T)$ can be numerically differentiated in the solution procedure. The previous section discussing the conservation of mass also determined the system couldn't be assumed to have constant density. Another common assumption, the Boussinesq approximation, cannot be used since density changes are important in all terms and the viscosity variations are of the same order of magnitude as the density variations. The fact that the density and viscosity are variable makes these

Navier Stokes equations much more complicated, and requires a solution to the energy equation that is coupled to the momentum equation.

An order of magnitude analysis, similar to the one done for the conservation of mass, will help validate the assumption that the viscosity cannot be considered constant. Again assuming O(r)~O(z)~L and O(v_z)~O(v_r)~V, the order of magnitudes of the viscous terms in the LHS can be expressed as

$$\frac{1}{L}\{\frac{\Delta\mu}{L}L\frac{V}{L}+\mu\frac{V}{L}+\mu L\frac{V}{L^2}-\frac{\Delta\mu}{L}L\frac{V}{L}-\mu\frac{V}{L}-\mu L\frac{V}{L^2}\}+\frac{\Delta\mu}{L}\frac{V}{L}+\mu\frac{V}{L^2}+\frac{\Delta\mu}{L}\frac{V}{L}+\mu\frac{V}{L^2}$$

From this it is apparent that all the viscous terms in this equation are of the order $\mu\frac{V}{L^2}$ or $\Delta\mu\frac{V}{L^2}$. Looking at the thermodynamic and transport properties of hydrogen vapor, the $\Delta\mu$ between the NBP at ambient is 7.68 $\mu Pa-\sec$ while the actual viscosity is 1.07 $\mu Pa-\sec$. Similarly, $\Delta\mu$ =12 $\mu Pa-\sec$ and μ =13.3 $\mu Pa-\sec$ for liquid hydrogen between the NBP and 14 K. This means O(μ)~O($\Delta\mu$) and the assumption of constant viscosity cannot be used to simplify the momentum equation.

Another simplification that is frequently taken into account are boundary layer approximations, where an order of magnitude analysis of different terms in the conservation equations reveals some terms that are so small they can be considered negligible in that thin region. The thickness of a boundary layer in free convection flows can be scaled[50] on the order of

$$\delta/x = 3.93*(\frac{0.952+\mathrm{Pr}}{\mathrm{Pr}^2})^{\frac{1}{4}}Gr_x^{-1/4} \qquad 3\text{-}45$$

The predicted Grashof number for liquid hydrogen was previously plotted in Figure 3-29 for a range of conditions. From this plot it is apparent the Grashof number is

between the order of Gr =10^9 and 10^{11}, depending on the temperature difference between the wall and the bulk fluid. The liquid Prandtl number at the NBP is 1.22 while the vapor Prandtl number is 0.77, implying the relative magnitude of the viscous and thermal boundary layers are of the same order. A quick estimate shows that the scale of the boundary layer thickness is $\delta = .022x$, two orders of magnitude less than the length scale of the system.

Knowing the boundary layer approximations are acceptable for the thin viscous region near the tank surfaces, the conservation of momentum equations for this region can be expressed as

$$\frac{\partial P}{\partial r} = 0 \qquad 3\text{-}46$$

$$\rho\left(\frac{\partial v_z}{\partial t} + v_r \frac{\partial v_z}{\partial r} + v_z \frac{\partial v_z}{\partial z}\right) = \rho g_z - \frac{\partial P}{\partial z} + \frac{\partial}{\partial z}\left(\mu \frac{\partial v_z}{\partial z}\right) \qquad 3\text{-}47$$

Now that viscous effects are accounted for in the thin boundary layer region, an order of magnitude analysis should be done to determine if viscosity is important in the rest of the flow. The balance of forces in the momentum equation shows the inertial forces scale on the order of $F_I \sim \frac{\overline{V}^2}{L}$, the pressure forces scale to $F_P \sim \frac{P}{\rho L}$, and the viscous forces scale to $F_V \sim \upsilon \frac{\overline{V}}{L^2}$. Knowing estimates for the characteristic length, velocity, kinematic viscosity and density, an order of magnitude analysis can be performed. This results in the approximation, in the freestream outside the boundary layer, that the $O(F_v) << O(F_I)$. Of course, this reveals the same thing as the calculation of the Reynolds number performed previously. Neglecting viscous effects in the freestream gives the following equations for conservation of momentum.

$$\rho\left(\frac{\partial v_r}{\partial t} + v_r \frac{\partial v_r}{\partial r} + v_z \frac{\partial v_r}{\partial z}\right) = -\frac{\partial P}{\partial r} \tag{3-48}$$

$$\rho\left(\frac{\partial v_z}{\partial t} + v_r \frac{\partial v_z}{\partial r} + v_z \frac{\partial v_z}{\partial z}\right) = \rho g_z - \frac{\partial P}{\partial z} \tag{3-49}$$

Conservation of Energy

The first Law of thermodynamics applied to a differential fluid element can written as

$$\begin{aligned}\rho\left(\frac{\partial h}{\partial t} + v_r \frac{\partial h}{\partial r} + v_z \frac{\partial h}{\partial z}\right) &= \frac{\partial P}{\partial t} + v_r \frac{\partial P}{\partial r} + v_z \frac{\partial P}{\partial z} + \frac{\partial}{\partial r} k \frac{\partial T}{\partial r} + \frac{k}{r}\frac{\partial T}{\partial r} + \frac{\partial}{\partial z} k \frac{\partial T}{\partial z} \\ &+ 2\mu\left\{\left(\frac{\partial v_r}{\partial r}\right)^2 + \left(\frac{v_r}{r}\right)^2 + \left(\frac{\partial v_z}{\partial z}\right)^2 + \frac{1}{2}\left(\frac{\partial v_r}{\partial z} + \frac{\partial v_z}{\partial r}\right)^2 - \frac{1}{3}\left(\frac{\partial v_r}{\partial r} + \frac{v_r}{r} + \frac{\partial v_z}{\partial z}\right)^2\right.\end{aligned} \tag{3-50}$$

where the first term on the left hand side represents the rate of change of energy in the element over time, and the next two terms are the convective flow of energy into or out of the element. The first three terms on the right hand side is the work done on the system by the pressure forces, and the next three terms is the rate of heat transferred into the system through the control surface via conduction. The final terms on the right hand side are the rate of energy dissipation via viscosity.

Previous analysis has shown that the viscous terms cannot be neglected, or even simplified by assuming constant viscosity, in the boundary layer region. However, an order of magnitude analysis can reduce the complexity of the equation in the boundary layer. Knowing $v_r << v_z$ and $\frac{\partial}{\partial z} << \frac{\partial}{\partial r}$, and from the r momentum equation $\frac{\partial P}{\partial r} = 0$, the conservation of energy can be reduced to

$$\rho\left(\frac{\partial h}{\partial t} + v_r \frac{\partial h}{\partial r} + v_z \frac{\partial h}{\partial z}\right) = \frac{\partial P}{\partial t} + v_z \frac{\partial P}{\partial z} - \frac{\partial}{\partial r} k \frac{\partial T}{\partial r} + \frac{k}{r}\frac{\partial T}{\partial r} + \mu\left(\frac{\partial v_z}{\partial r}\right)^2 \tag{3-51}$$

In many applications, if Fourier's law is assumed, and the thermal conductivity is assumed to be constant, the heat transfer term can be reduced to $k\nabla^2 T$. However, like the density and viscosity, the thermal conductivity is too dependent on temperature to be assumed constant. There is no way to simplify this term, but if the nature of the thermal conductivity dependence is known, it can be numerically differentiated.

This equation adds another thermodynamic variable, namely the enthalpy, to the list of unknowns. However, enthalpy can be expressed as a function of the other thermodynamic variables in a number of ways. Most often, the ideal gas approximation is used, but obviously that cannot work in this instance. However, for all substances, enthalpy can be expressed as

$$dh = c_p dT + (1 - \beta T) dP \qquad 3\text{-}52$$

Outside the boundary layer, inviscid flow can be assumed, based on the same assumptions discussed above for the momentum equations. However, the boundary layer approximations cannot be used. In this case, the conservation of energy reduces to

$$\rho\left(\frac{\partial h}{\partial t} + v_r \frac{\partial h}{\partial r} + v_z \frac{\partial h}{\partial z}\right) = \frac{\partial P}{\partial t} + v_r \frac{\partial P}{\partial r} + v_z \frac{\partial P}{\partial z} + \frac{\partial}{\partial r} k \frac{\partial T}{\partial r} + \frac{k}{r} \frac{\partial T}{\partial r} + \frac{\partial}{\partial z} k \frac{\partial T}{\partial z} \qquad 3\text{-}53$$

Summary

The preceeding section presented the conservation equations for unsteady, viscous, compressible flow with variable transport properties for cylindrical coordinates in the r and z direction. The flow is considered axisymmetric and there is no dependence in the angular direction. It has been shown through order of magnitude analysis of individual terms and scaling of competing forces that this system can be modeled as a whole by considering four separate regions. First, the liquid and vapor regions must be considered separately. Then, in each of these regions, there is a thin boundary layer where viscous

dissipation must be considered but many terms will be negligible due to the normal boundary layer approximations. Inside this boundary layer region, for both the liquid and vapor flow, the following equations must be solved;

Conservation of Mass – Eqn 3-41

Conservation of Momentum in r direction – Enq. 3-46

Conservation of Momentum in z direction – Enq. 3-47

Conservation of Energy – Eqn. 3-51

Outside the thin boundary layer, the flow can be modeled as inviscid. No boundary layer approximations are used. The following equations apply in this region;

Conservation of Mass – Eqn 3-40

Conservation of Momentum in r direction – Enq. 3-48

Conservation of Momentum in z direction – Enq. 3-49

Conservation of Energy – Eqn. 3-53

Solution Procedure

In general the above four conservation equations contain 6 unknowns in each region (P, T, ρ, h, v_r, v_z). This is assuming the transport properties (thermal conductivity, viscosity) are known from experimental data as a function of temperature and pressure. Two additional relations are needed to solve this system of equations. First, the equation of state can be used to relate the thermodynamic variables P, T, and ρ. The ideal gas equation of state will not be accurate in this region. NIST has developed a hydrogen thermodynamic property datatbase using the Modified Benedict-Webb-Rubin (MBWR) equation of state for hydrogen, and this can be used for the current analysis. Indeed, in the first part of this chapter, this NIST database is used to

help close the system of simplified equations. A second thermodynamic relation relating the enthalpy of a fluid to the temperature and specific heat can also be used, but care must be taken to incorporate variations in the specific heat as a function of temperature. This relation was presented by equation 3-52 when the conservation of energy was discussed.

More specific, this system is described by a set of six partial differential equations. This system of equations must be solved simultaneously. Variations in fluid properties are significant and the continuity and momentum equations are coupled to the energy equation. In addition, these coupled equations probably need to be solved separately but simultaneously over liquid and vapor regions in the system. The overall geometry of these spaces are time dependent as well since the liquid level and boundary layer thickness will change as mass is added to the system and the temperature of the system will change. The appropriate boundary conditions between these fluid regions must then be equalized.

The transport properties will vary over time and with respect to location, and the assumption that these properties are variable will add to the complexity of the conservation equations discussed above. However, these properties are assumed only dependent on temperature and the nature of this dependence is known. Therefore, a function relating this dependence must be found and input into the solution procedure, and the derivatives can easily be calculated.

Boundary Conditions

First, since the storage system to be analyzed is unsteady, there must be initial conditions prescribed for all the variables at all locations inside the system. These initial conditions will depend on the flow situation to be analyzed. Most likely, there will be an initial liquid level required, and the liquid will be assumed to be at a saturated condition

with no mass flow in or out of the tank. The initial pressure will be constant in the vapor space, and will have a hydrostatic distribution in the liquid space. The initial temperature, density and enthalpy will be constant in the vapor space and will vary slightly with pressure in the liquid. All velocities will be assumed zero for an initial condition. The initial conditions can be expressed mathematically as

Vapor region $P(r,z,0)=P_{sat}$ $T(r,z,0)=T_{sat}$ $v_z(r,z,0)=0$ $v_r(r,z,0)=0$

Liquid region $P(r,z,0)=P_{sat}+\rho\, g(h-z)$ $T(r,z,0)=T_{sat}$ $v_z(r,z,0)=0$ $v_r(r,z,0)=0$

Boundary conditions must be prescribed for the four independent variables P, T, v_r, and v_z. The density and enthalpy initial and boundary conditions can be calculated knowing the pressure and temperature at that location. For both the liquid and vapor boundary conditions, fluid velocity components will be assumed zero at the tank wall. This no-slip boundary condition will apply around the entire geometry, with the exception of the gas supply and vent ports, where a complete profile for the velocity, temperature and pressure distribution will have to be assumed. Against the wall the thermal boundary condition is given from a calculated heat flux through the insulation. The pressure boundary condition can be specified by considering the fluid at the liquid to vapor interface. There will be a thin layer of liquid at the top of the tank that will be at the saturated condition, and here there is only one independent thermodynamic variable. The boundary pressure in the liquid below the interface will be equal to this saturation pressure plus the hydrostatic head pressure. The pressure around the boundary in the vapor space is assumed to be constant.

The most complicated boundary condition in this system is at the liquid to vapor interface[37]. At this infinitesimal interface, the total velocity, shear stress and

temperature must be continuous across the surface. The normal and tangential velocities must match, and can be expressed in terms of the interface motion. The temperatures also match. Pressure equilibrium is satisfied by factoring in the surface tension forces. Heat flux is equal across the interface, although the temperature gradient will differ due to different thermal conductivity. The boundary conditions are expressed mathematically as

Vapor boundary layer

$P(\delta,z,t)= P_{\infty}$ $P(r,h,t)=P_{liq}$

$T(\delta,z,t)= T_{\infty}$ $\frac{\partial T}{\partial r}(R,z,t)= Q''/k$ $\frac{\partial T}{\partial z}(r,Z,t)= Q''/k$ $k_{gas}\frac{\partial T}{\partial z}(r,h,t)= k_{liq}\frac{\partial T}{\partial z}$

$v_z(R,z,t)=0$ $v_z(\delta,z,t)= v_{z\infty}$ $v_z(r,0,t)=0$ $v_z(r,h,t)=v_{zliquid}$

$v_r(R,z,t)=0$ $v_r(\delta,z,t)=v_{r\infty}$ $v_r(r,0,t)=0$ $v_r(r,h,t)=0$

Vapor free stream

$P(\delta,z,t)= P_{BL}$ $P(r,h,t)=P_{liq}$

$T(\delta,z,t)= T_{BL}$ $\frac{\partial T}{\partial r}(0,z,t)= 0$ $\frac{\partial T}{\partial z}(r,Z,t)= Q''/k$ $k_{gas}\frac{\partial T}{\partial z}(r,h,t)= k_{liq}\frac{\partial T}{\partial z}$

$\frac{\partial v_z}{\partial r}(0,z,t)=0$ $v_z(r,Z,t)=0$

$v_r(0,z,t)=0$ $v_r(r,Z,t)=0$

The liquid boundary layer and freestream boundary conditions are similar. Using the conservation equations shown above combined with the initial conditions and boundary conditions expressed in this section, the solution to the fluid behavior in this system can be modeled numerically. This would be a difficult modeling exercise, well beyond the scope of this dissertation, which is intended to focus on thermodynamic issues of this system.

Dimensionless analysis

The overall usefulness of these governing equations can be made greater if the equations are presented in non-dimensional form. This result can be obtained when the variables in the equations are changed by dividing them by a constant reference property. The choice of reference constants is arbitrary, but should have some physical significance to the system being analyzed. The following non-dimensional variables are proposed for this system.

$$r^* = \frac{r}{L} \qquad z^* = \frac{z}{L} \qquad V_r^* = \frac{V_r}{V_0} \qquad V_z^* = \frac{V_z}{V_0}$$

$$\rho^* = \frac{\rho}{\rho_0} \qquad P^* = \frac{P}{P_0} \qquad h^* = \frac{h}{h_0} \qquad T^* = \frac{T}{T_0}$$

$$t^* = \frac{t}{t_0} \qquad \mu^* = \frac{\mu}{\mu_0} \qquad k^* = \frac{k}{k_0}$$

The dimensional length constant L is taken to be the length of the diagonal of the R-Z right triangle. This gives a measure of the size of the system without having to use the both the tank radius and tank height as dimensional constants, and takes into account a variety of aspect ratios. The choice for dimensional constants for all the thermodynamic variables is just the initial value of the variable, most probably the saturated conditions at the normal boiling point. Similarly, the thermal conductivity and viscosity constants are also the initial values. The choice of dimensional time constant is unique to this analysis and is taken to be the amount of heat required to vaporize the total amount of liquid inside the system divided by the rate of heat transfer to the system. This is simply the time required to vaporize the contents of the vessel. The dimensional velocity constant V_0 then is defined as the system length divided by this time constant.

Plugging the new variables into the conservation of mass in the boundary layer yields

$$\frac{\rho_0}{t_0}\frac{\partial \rho^*}{\partial t^*} = \frac{\rho_0 V_0}{L}\frac{\rho^* v_r^*}{r^*} + \frac{\rho_0 V_0}{L}\rho^*\frac{\partial v_r^*}{\partial r^*} + \frac{\rho_0 V_0}{L}\rho^*\frac{\partial v_z^*}{\partial z^*} + \frac{\rho_0 V_0}{L}v_z^*\frac{\partial \rho^*}{\partial z^*} \qquad 3\text{-}54$$

Substituting the relation $t_0 = L/V_0$ leaves the equation of mass conservation unchanged when converting to dimensionless variables. This is expected and is a general result for all conservation of mass equations. The final dimensionless equations for the boundary layer region and the inviscid region are expressed below.

$$\frac{\partial \rho^*}{\partial t^*} = \frac{\rho^* v_r^*}{r^*} + \rho^*\frac{\partial v_r^*}{\partial r^*} + \rho^*\frac{\partial v_z^*}{\partial z^*} + v_z^*\frac{\partial \rho^*}{\partial z^*} \qquad 3\text{-}55$$

$$\frac{\partial \rho^*}{\partial t^*} = \frac{\rho^* v_r^*}{r^*} + v_r^*\frac{\partial \rho^*}{\partial r^*} + \rho^*\frac{\partial v_r^*}{\partial r^*} + \rho^*\frac{\partial v_z^*}{\partial z^*} + v_z^*\frac{\partial \rho^*}{\partial z^*} \qquad 3\text{-}56$$

Using the same dimensional constants as above, and rearranging terms, the conservation of momentum can be derived in dimensionless terms. The equation for the boundary layer region expressed by equations 3-46 and 3-47 can be rewritten as

$$\frac{\partial P^*}{\partial r^*} = 0 \qquad 3\text{-}57$$

$$\rho^*\left(\frac{\partial v_z^*}{\partial t^*} + v_r^*\frac{\partial v_z^*}{\partial r^*} + v_z^*\frac{\partial v_z^*}{\partial z^*}\right) = \left(\frac{t_0^2 g_z}{L}\right)\rho^* - \left(\frac{P_0 t_0^2}{\rho_0 L^2}\right)\frac{\partial P^*}{\partial z^*} + \left(\frac{\mu_0 t_0}{\rho_0 L^2}\right)\frac{\partial}{\partial z^*}\mu^*\frac{\partial v_z^*}{\partial z^*} \qquad 3\text{-}58$$

For the inviscid core region, the non-dimensional momentum equations can be simplified to

$$\rho\left(\frac{\partial v_r}{\partial t} + v_r\frac{\partial v_r}{\partial r} + v_z\frac{\partial v_r}{\partial z}\right) = -\left(\frac{P_0 t_0^2}{\rho_0 L^2}\right)\frac{\partial P^*}{\partial r^*} \qquad 3\text{-}59$$

$$\rho^*\left(\frac{\partial v_z^*}{\partial t^*} + v_r^*\frac{\partial v_z^*}{\partial r^*} + v_z^*\frac{\partial v_z^*}{\partial z^*}\right) = \left(\frac{t_0^2 g_z}{L}\right)\rho^* - \left(\frac{P_0 t_0^2}{\rho_0 L^2}\right)\frac{\partial P^*}{\partial z^*} \qquad 3\text{-}60$$

There are three dimensionless parameters contained in the above equations, shown in parenthesis on the right hand side of equation 3-58. These dimensionless parameters show the relative strength of the buoyancy, pressure, and viscous forces with respect to the inertial forces, but in a different manner than the classic dimensionless equations. The choice of dimensionless constants emphasizes the relation of the latent heat of vaporization in the system to the rate of heat leak as a dimensional time constant. For small time constants, the heat leak is very high with respect to the latent heat, and the liquid boils off more rapidly. This implies the heat transfer to the liquid is greater, leading to higher convection velocities. This makes the dimensionless parameters smaller, and the viscous, buoyancy, and pressure forces are respectively lesser than the inertial forces. Large time constants imply a well-insulated system with small heat leak and smaller convection velocities. The dimensionless parameters are larger, implying the inertial forces become less significant. It is worth noting the buoyancy and pressure forces scale with respect to t_0^2, demonstrating a greater sensitivity to the time constant than the viscous terms.

Performing the same dimensional analysis on the conservation of energy for the viscous region and the inviscid region respectively yields

$$\rho^*\left(\frac{\partial h^*}{\partial t^*}+v_r^*\frac{\partial h^*}{\partial r^*}+v_z^*\frac{\partial h^*}{\partial z^*}\right)= \left(\frac{P_0}{h_0\rho_0}\right)\left\{\frac{\partial P^*}{\partial t^*}+v_z^*\frac{\partial P^*}{\partial z^*}\right\}-\left(\frac{k_0T_0t_0}{h_0\rho_0L^2}\right)\left\{\frac{\partial}{\partial r^*}k^*\frac{\partial T^*}{\partial r^*}+\frac{k^*}{r^*}\frac{\partial T^*}{\partial r^*}\right\}+\left(\frac{\mu_0}{h_0\rho_0t_0}\right)\mu^*\left(\frac{\partial v_z^*}{\partial r^*}\right)^2 \quad 3\text{-}61$$

$$\rho^*\left(\frac{\partial h^*}{\partial t^*}+v_r^*\frac{\partial h^*}{\partial r^*}+v_z^*\frac{\partial h^*}{\partial z^*}\right)= \left(\frac{P_0}{h_0\rho_0}\right)\left\{\frac{\partial P^*}{\partial t^*}+v_r^*\frac{\partial P^*}{\partial r^*}+v_z^*\frac{\partial P^*}{\partial z*}\right\}+\left(\frac{k_0T_0t_0}{h_0\rho_0L^2}\right)\left\{\frac{\partial}{\partial r^*}k^*\frac{\partial T^*}{\partial r^*}+\frac{k^*}{r^*}\frac{\partial T^*}{\partial r^*}+\frac{\partial}{\partial z^*}k^*\frac{\partial T^*}{\partial z^*}\right\} \quad 3\text{-}62$$

Again, three dimensionless parameters show up. They can be interpreted as showing the relative importance of the flow work, the heat transfer, and the viscous dissipation. The term $h_0\rho_0$ is a measure of the initial energy in the system, and shows up in the denominator of all three dimensionless parameters. It is interesting to note the flow work parameter appears independent of the time constant, while the heat transfer parameter has a direct relation with the time constant and the viscous term is inversely proportional to the time constant. For smaller time constants, the viscous terms are relatively more important than the heat transfer terms. However, if the time constant increases, the convection velocities decrease and the thermal conductivity terms increase in relative value.

To fully pose the problem in dimensionless terms, the boundary conditions and initial conditions must also be non-dimensionalized. Looking at the vapor region, the initial conditions are expressed as

$P^*(r^*,z^*,0)=1 \qquad T^*(r^*,z^*,0)=1 \quad v_z^*(r^*,z^*,0)=0 \quad v_r^*(r^*,z^*,0)=0$

The boundary conditions in the vapor boundary layer become

$$P^*(\delta^*,z^*,t^*)=P_\infty^* \qquad P^*(r^*,h^*,t^*)=P_{liq}^*$$

$$T^*(\delta^*,z^*,t^*)=T_\infty^* \qquad \frac{\partial T^*}{\partial r^*}(R^*,z^*,t^*)=\frac{\rho_0 h_0 L^2}{k_0 T_0 t_0}\frac{Q^{"*}}{k^*} \quad \frac{\partial T^*}{\partial r^*}(r^*,Z^*,t^*)=\frac{\rho_0 h_0 L^2}{k_0 T_0 t_0}\frac{Q^{"*}}{k^*}$$

$$k_{gas}^*\frac{\partial T^*}{\partial z^*}(r^*,h^*,t^*)=\frac{k_{0-liq}}{k_{0-gas}}k_{liq}^*\frac{\partial T^*}{\partial z^*}$$

$$v_z^*(R^*,z^*,t^*)=0 \qquad v_z^*(\delta^*,z^*,t^*)=v_{z-\infty}^*$$

$$v_z^*(r^*,0,t^*)=0 \qquad v_z^*(r^*,h^*,t^*)=v_{z-liq}^*$$

$$v_r^*(R^*,z^*,t^*)=0 \qquad v_r^*(\delta^*,z^*,t^*)=v_{r-\infty}^*$$

$$v_r^*(r^*,0,t^*)=0 \qquad v_r^*(r^*,h^*,t^*)=0$$

Boundary conditions in the freestream are

$$P^*(\partial^*,z^*,t^*)=P_{BL}^* \qquad P^*(r^*,h^*,t^*)=P_{liq}^*$$

$$T^*(\delta^*,z^*,t^*)=T_{BL}^* \qquad \frac{\partial T^*}{\partial r^*}(0^*,z^*,t^*)=0$$

$$\frac{\partial T^*}{\partial z^*}(r^*,Z^*,t^*)=\frac{\rho_0 h_0 L^2}{k_0 T_0 t_0}\frac{Q^{"*}}{k^*} \qquad k_{gas}^*\frac{\partial T^*}{\partial z^*}(r^*,h^*,t^*)=\frac{k_{0-liq}}{k_{0-gas}}k_{liq}^*\frac{\partial T^*}{\partial z^*}$$

$$\frac{\partial v_z^*}{\partial r^*}(0,z^*,t^*)=0 \qquad v_z^*(r^*,Z^*,t^*)=0$$

$$v_r^*(0,Z^*,t^*)=0 \qquad v_r^*(r^*,Z^*,t^*)=0$$

Two other dimensionless parameters appear in the boundary conditions. The first is simply the ratio of the dimensionless thermal conductivity between the liquid and vapor space. Choosing the same dimensionless constant could have eliminated the parameter. The second relates the heat flux to the temperature gradient at the Neumann boundary condition. In this case, the dimensionless parameter can be simplified by remembering the dimensional time constant is the initial energy in the system divided by the heat flux.

CHAPTER 4
HYDROGEN SAFETY

To validate the analysis conducted in Chapter 3, a liquid hydrogen test program was initiated. Any serious discussions regarding use of hydrogen, either as a liquid or a gas, must include factors pertaining to its safe use. For this dissertation, such considerations are taken within two separate contexts; first, safety of liquid hydrogen specifically as it relates to the experimental system designed for data gathering for this work, and second, general hydrogen safety principles that must be followed for the evolution to a hydrogen energy based economy to take place. This chapter will focus primarily on safety principles necessary for the specific experimental set-up, with general safety concerns included as applicable. NASA KSC has historically been one of the world's largest consumers of liquid hydrogen, and aerospace use of hydrogen has helped lead to the development of many of today's systems in use in industrial applications. NASA's hydrogen safety specification[51] is the primary reference for this chapter, although the National Fire Protection Association[52] (NFPA) and Department of Transportation[53,54] (DoT) codes were considered as well. There is also an aerospace industry standard that is in development (AIAA), but this work draws heavily on the NASA standard and was not referenced in this chapter.

Hydrogen Properties

Hydrogen is a nontoxic, non-corrosive gas that is colorless, odorless, and tasteless, and is therefore difficult to detect with human senses. It forms a diatomic molecule with a molecular weight of 2.06. In nature, hydrogen has two isotopes; hydrogen with an

atomic mass of 1, and deuterium, with an atomic mass of 2. The ratio of ordinary hydrogen to deuterium is 3200/1. Due to the small molecular size, gaseous hydrogen is difficult to contain in a leak free manner, and liquid storage is even more difficult due to the low temperatures required. The NBP of hydrogen is 20.3 K, with a triple point of 13.9 K and a critical temperature of 33.2 K. A T-s diagram for liquid hydrogen[(9)] is shown in Figure 4-1. The NBP of hydrogen is the second lowest of any element, only liquid helium is lower. Hence, NBP hydrogen will freeze out any contaminants except helium, so care must be taken in LH2 systems to eliminate any contaminants, especially air.

Hydrogen is unique in that it exists in two separate molecular forms, depending on the direction of spin of the individual atoms. In ortho-hydrogen, the atoms spin in the same direction, whereas para-hydrogen atoms spin in opposite directions. Normal hydrogen, or hydrogen gas at room temperature is a mixture of 75% ortho and 25% para. However, this mixture varies with temperature, so one refers to equilibrium hydrogen as the equilibrium mixture percentage at a given temperature. At the NBP, equilibrium hydrogen is 99.8% para-hydrogen. This conversion from ortho to para is significant since there is a heat of conversion associate with the change. This heat of conversion is due to the momentum change required as one atomic nucleus reverses spin direction, and this is an exothermic process. The heat released is significant, greater than the heat of vaporization at the NBP. Energy efficient handling of liquid hydrogen requires accounting for this heat of conversion, and catalysts are usually used to speed up the conversion process so the heat can be removed at a higher temperature. During hydrogen system design processes, care must be taken to account for other changes in thermal and transport properties, depending on the equilibrium mixture.

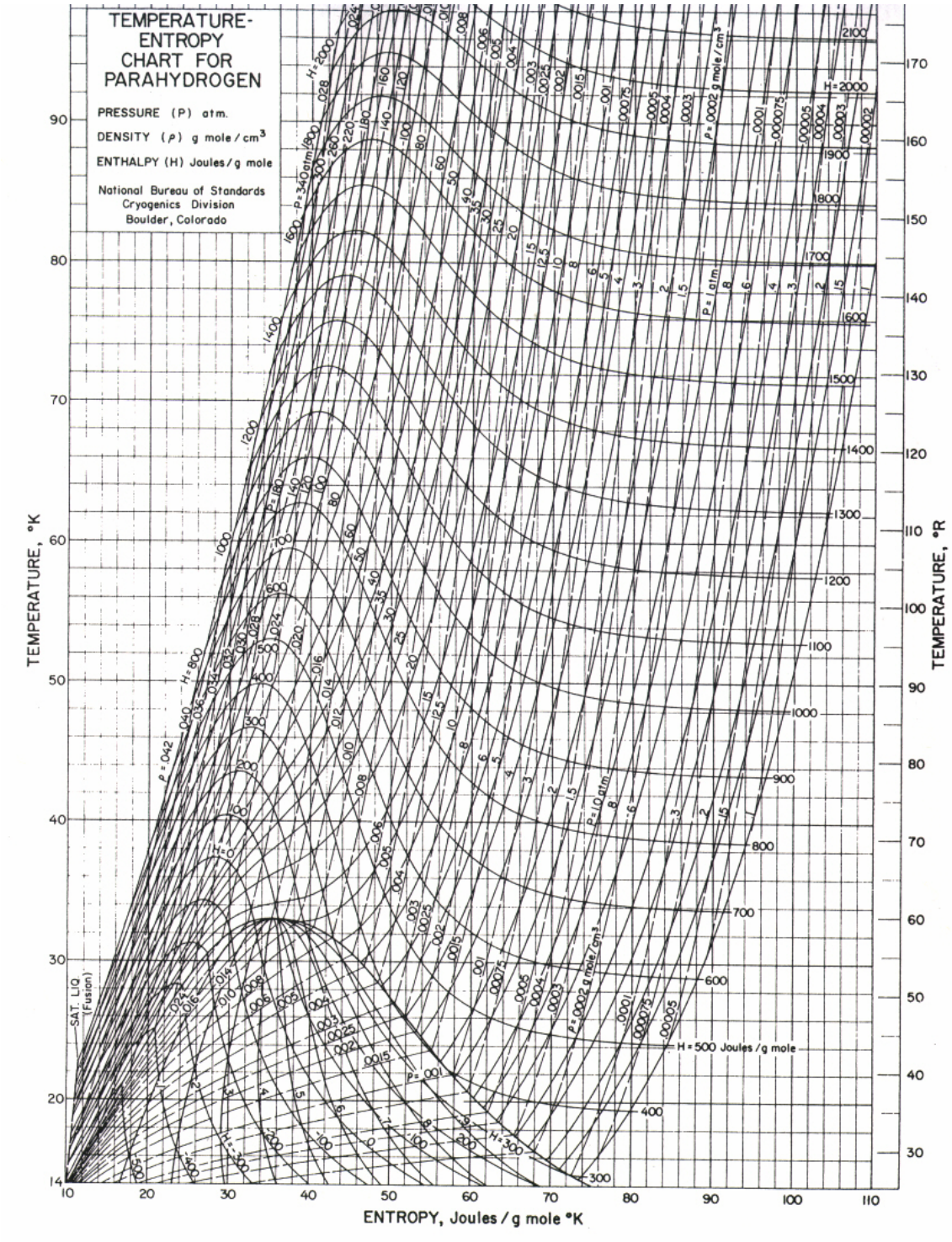

Figure 4-1 Hydrogen T-s diagram (Flynn)

Hydrogen possesses a very low mass density; its vapor is buoyant in air even at a temperature of 23K. Combined with a high diffusion coefficient, hydrogen leaks disperse readily in the atmosphere. Knowledge of hydrogen convection and diffusion patterns is helpful in designing hydrogen storage facilities, in order to minimize chances of a detonable mixture forming. Another interesting property of hydrogen is the low Joule-Thompson inversion temperature of 193 K. Hydrogen is one of three gasses with a JT temperature this low, helium and neon being the others. This requires precooling of a high-pressure gas stream to below this temperature before an isenthalpic expansion will produce a refrigeration effect. Room temperature hydrogen heats up during an isenthalpic expansion process.

Combustion Hazards

Combustion theory describes a “fire triangle” consisting of three sides necessary for combustion; fuel, oxidizer, and an ignition source. Obviously in the case of hydrogen systems, the presence of hydrogen indicates the presence of a fuel. One characteristic of hydrogen fuels is they need very little ignition energy to initiate a reaction. The minimum ignition energy usually described is 0.017 mJ, or 1000 times less than a spark generated by static electricity. An ignition source should always be assumed, and common ignition sources include static electricity, lightning, particle impacts, metal rupture/fracture, friction, hot surfaces, adiabatic compression, shock waves, and heat from smoking, open flames and welding. The best practice for eliminating hydrogen fires is therefore to minimize mixing with an oxidizer. However, another characteristic of hydrogen fires is the large range of flammability limits in air. The lower flammability limit (LFL) of hydrogen in air is 3.9% and the upper flammability limit (UFL) is 75%. A small hydrogen leak has the potential to build up the concentration to a flammable limit, so care

should be taken to design the storage system to allow for any leaks to disperse quickly. This is best accomplished by minimizing confinement of the hydrogen, for instance to allow for a vent path out of a facility at a high point or to create a forced flow into and out of a facility.

In order to safely address concerns associated with hydrogen combustion, knowledge of the combustion process is necessary. Once a spot in a fuel/oxidizer mixture is raised to its ignition temperature, combustion begins. This reaction then heats the adjacent mixture above the ignition temperature and the combustion can proceed thru the entire mixture that is in the combustible range. The speed of the combustion is a function of several variables and generally depends on the rate of heat transfer in the mixture. Usually this flame speed is of the order of magnitude of a few meters per second, and this is referred to as deflagration. However, mixtures in the range of 18% to 59% hydrogen can undergo a detonation. In this case, combustion occurs without the limitation of heat transfer because a shock wave forms that is strong enough to heat the mixture above the ignition temperature. The combustion speed then becomes supersonic, the speed of the shock wave. Detonations are caused by sufficiently strong ignition sources within a detonable mixture range, or if there is sufficient confinement or turbulence in an existing flame. While deflagrations have pressure ratios of the order of magnitude of 8, detonations have pressure ratios that can exceed 100. Normal pressure relief devices can usually handle the overpressure resulting from deflagration, but not detonation. In addition, the pressurization rate is so much faster in detonations that vent paths cannot keep up with the pressure wave. Therefore detonations are much more destructive than deflagrations and systems should be designed to minimize detonation hazards. This is

accomplished by minimizing confinement, such as internal rooms with four walls or internal pipes with smaller diameters, as well as reducing turbulence in internal flows like that caused by flow restrictions and flow path changes. Diluents should be used, especially in vent lines, to reduce the possibility of detonable mixtures from forming.

In the event of a hydrogen fire, personnel responding must be trained in the best practice for fighting hydrogen fires. A hydrogen flame is invisible and has a low thermal emissivity, so personnel cannot see or feel the fire until they enter the actual combustion zone. There is no smoke present, and all combustion products rise in the atmosphere. Proper training can ensure personnel are aware of this danger and do not enter into a hydrogen combustion area. While there have been instances of small hydrogen fires being extinguished with chemical suppressants, these methods are unreliable, and may actually allow the hydrogen leak to build up to a detonable mixture. The best practice is to isolate the leak from the hydrogen supply, and spray water on surrounding surfaces to prevent the fire from spreading. Eventually the fire will self extinguish once the fuel source has been isolated.

All the existing explosive hazards testing for liquid hydrogen has been completed with liquid hydrogen at its normal boiling point, so special consideration must be given for densified hydrogen. This is primarily due to increased mass of hydrogen in a given storage volume, however the reaction dynamics will also change when the additional sensible heat of the subcooled liquid is considered. A small-scale simulation was modeled using subcooled LOX and LH2 and the results indicated an explosive yield of 2-3 % should be expected, which is well below the yield normally used for normal boiling point propellants. However, there always exists the possibility the subcooled propellants

could warm up to the saturation state, so the study recommended no change in the safety standards.[55]

Hydrogen Embrittlement

Hydrogen can attack metals in a number of ways. Generally, what occurs is a diffusion of hydrogen atoms in the lattice of the metal, and the result of this attack is the mechanical properties of the materials are significantly altered. Collectively this phenomenon is referred to as hydrogen embrittlement, although physically there are three different types of embrittlement. First, environmental hydrogen embrittlement occurs when metals and alloys are plastically deformed in a hydrogen environment, such as compression on springs. The effect is magnified in high-pressure systems. Next, internal hydrogen embrittlement occurs when hydrogen is absorbed during some manufacturing process, such as welding, electroplating, or acid treating. Finally, hydrogen reaction embrittlement occurs when absorbed hydrogen chemically reacts with the parent metal, forming a weaker hydride. This reaction is increased during high temperature processes. No matter what the physical process, hydrogen embrittlement reduces the tensile strength, ductility, and fracture toughness of materials. Crack propagation occurs more readily, and brittle failures occur more frequently.

Knowledge of the system environment and material properties is essential in designing for reduced hydrogen embrittlement hazards. High-pressure processes increase the hazards, and high temperatures increase reaction embrittlement hazards. The embrittlement hazard is increased with prolonged exposure time and the concentration of hydrogen present has a great effect. Reducing stress on components reduces the hazard, and a highly polished surface will permit less hydrogen intrusion than a rough surface. Microcracks or stress fractures are to be avoided since these are embrittlement entry

points. To design for minimum hazard, hydrogen components should be manufactured for a hydrogen environment. Thicker overall parts reduce stress and surfaces should be polished. If possible, oxide layers that restrict hydrogen absorption can be used. EDM processes should be minimized, since dielectric fluids used contain hydrogen that is released during ionization. Proper welding techniques to reduce the exposure to hydrogen should be followed. Certain alloys should be avoided, including cast iron, nickel and nickel alloys, and some stainless steels such as 410 SS and17-7 pH SS. Aluminum alloys in the 1100, 6000, and 7000 series are not susceptible to embrittlement and 300 series stainless, oxygen free copper, and titanium are generally considered safe as well. For our application, we used 304 stainless steel in every wetted part, plus our pressures and tensile stresses were so low that embrittlement was not a concern.

Cryogenic Hazards

Not specifically hydrogen related, general safety principles during use of cryogenic systems must be maintained. Cryogenic liquids are stored far below atmospheric temperature, so nature requires heat transfer to occur from ambient to the inside of the storage vessel. Such heat leak is unavoidable but proper insulation can minimize the total amount. This heat leak also leads to boil-off of the hydrogen, creating a pressure rise in the system. This pressurization rate is generally small if the vessel is properly insulated and can be accommodated by two means. First, the quantity of heat leaking into the tank can be removed by mechanical refrigeration before boil-off of the hydrogen occurs. Such zero-boil-off systems may be desirable in many cases and have been discussed at length earlier in this work. The other method is to allow for a small pressure rise before boil off gasses are vented thru a relief valve. This has been the method typically preferred in the past. In this case, sizing of the relief valve is critical. The capacity for flow in the relief

valve must be matched to the maximum possible boil-off rate, otherwise pressurization above the maximum operating pressure (MOP) may occur. NASA safety standards[56] require the relief valve to be sized to accommodate flow resulting in complete loss of insulation of the vessel, plus any internal heat generation from ortho to para conversion. Typically this means assuming the vacuum internal to the annulus of a dewar has failed, and convection heat transfer now occurs between the inner and outer vessel. As an added precaution, redundancy is required in this function, preferably using non-mechanical relief. Icing or other freezing constituents may cause blockage of relief valves, and burst disks may be less susceptible. A primary relief valve set at 100% of maximum operating pressure coupled with a burst disk set at 116% MOP satisfies this intent. In addition, single relief valves must be installed in every flow passage that has the possibility of being isolated from the vessel relief system. Finally, at the component level, internal wetted parts must be designed to preclude the possibility of trapping liquid or cold vapor in an internal space, such as passages of closed ball valves or lobed pumps.

Low temperatures can create physical hazards to the human body. Cryogenic burns, similar to heat burns, damage tissues. This can occur either from direct contact with a liquid or contact with surfaces exposed to liquid hydrogen. Proper equipment for protection, such as cryogenic gloves and aprons, are essential. In most cases, vacuum jacketed insulation, or other high quality insulation, eliminates the potential for accidentally touching cold surfaces. Asphyxiation can occur when personnel enter areas where oxygen has been displaced by hydrogen or other gasses, such as nitrogen or helium purges. In confined spaces, oxygen monitors are required. Poorly insulated liquid hydrogen components have the capability of forming liquid air. As this liquid air warms,

the nitrogen component will evaporate leaving a liquid with enriched oxygen content. This has the potential of creating a combustion hazard, as most substances combust in the presence of pure oxygen. Ensuring the liquid hydrogen lines are well insulated mitigates this risk. For this work, all proper personnel protective equipment was available, minimizing the low temperature hazards. All relief valves were sized properly. Continuous oxygen monitoring was available during periods of purging operations, and hydrogen detectors were used to detect leaks. All lines and components were vacuum jacketed except the vent line, and vent processes were limited in duration and frequency.

Facility Design

Knowledge regarding hydrogen hazards is essential in the proper design of a hydrogen facility. The order of preference in siting systems is always as follows; outdoors, in a separate building, in a special room, inside a shared room. Depending on the total quantity stored, some of these options are considered forbidden. For instance, quantities above 1140 liters are not permitted to be stored in anything but outdoors or a separate building. All quantities above 2270 liters must be stored outdoors. The system used for this work has a maximum storage volume of 140 liters, technically too small to fall under either NFPA or NSS specifications, however, for the purposes of safety the system was considered to be covered by these codes. The system was allowed to be stored inside a shared room. Liquid hydrogen storage should always be above grade, allowing for ease of access and quick detection of leaks. Tables correlating the total storage quantity to safe distance, referred to as Q-D tables, dictate the minimum separation between the storage area and facilities or areas where personnel are present. Access to this exclusion area is limited to trained personnel with the proper personnel protective equipment. All equipment inside the exclusion area must be approved for use

to ensure no ignition sources are present, and any operation inside the area must have reviewed and approved operational procedures. Barricades may be used to limit the extent of the exclusion area, and dikes and impoundments are necessary if there are any oxidizers or other flammable materials stored nearby.

All storage vessels should be designed per the ASME Boiler and Pressure Vessel Code, Section VIII, except for portable storage used in transportation, which must conform to DoT regulations. Storage vessels should be labeled with the content, capacity and maximum allowable working pressure (MAWP). The tank should be protected by barriers if there is the presence of rotating or reciprocating mechanical equipment nearby. A remote operated valve should be provided as close as possible to the storage tank to allow for isolation of the storage content in the event of a leak. All piping systems must conform to ASME B31.3. Electrical bonding shall be present across all joints, and the entire system shall be grounded. Piping shall allow for flexibility, to account for coefficient of thermal expansion as the system chills down. In most cases, bellows are provided for flexibility, although flexhoses, U bends, or low coefficient of thermal expansion materials such as Invar may be used. Supports shall account for this flexibility, using rollers where possible to constrain the system in only one degree of freedom. Piping shall also be labeled with content, MAWP, and flow direction.

Storage systems must have proper vent and pressure relief systems. Relief system design requirements have been discussed in previous sections. The pressure relief path shall be connected to an approved vent stack. Venting to the atmosphere is acceptable if the flowrate is below 0.5 lb/sec, any higher vent flowrates should be burned in a flare stack. In either case, the vent system shall be designed to prevent air or moisture

intrusion into the vent. Moisture can form ice blockage during venting of cold gasses, obstructing the vent path. Air intrusion allows for the formation of combustible mixtures. The overall flow velocity of the vent should be kept to a minimum, to preclude the possibility of generating enough ignition energy and to prevent turbulent mixing, which may aid in formation of detonations. The vent stack must have a purge capability to keep oxygen out of the system. Ground vent stacks shall be 25 feet above grade, and roof vent stacks shall be 16 feet above the roof level. In all cases, vent stacks should be positioned away from air intakes or other mechanical systems, and should have lightning protection in the form of a 30-degree cone around the top of the vent.

In the event the hydrogen is stored inside a special room or building, provisions for the design of that facility must be made. Use of lightweight, non-combustible materials is necessary, and walls, ceilings and floors should have a minimum 2-hour fire protection rating. All windows must be shatterproof glass or plastic, and doors shall open outward to facilitate easy egress. Emergency venting shall be accommodated in the event of a detonation, and the vent must open with a maximum pressure of 25 lb/ft2. Adequate ventilation is required to prevent the accumulation of hydrogen above a concentration of 1%. The minimum vent area shall be 1 ft2/1000 ft3 of room volume, and shall be located at the top of the room. The room shall be designed to avoid ceiling peaks and trapped pockets such as false ceilings. The hydrogen system shall be 100% covered with water spray systems, but care must be taken to avoid water deluge into a vent line. Any electrical systems within 3 feet of hydrogen connections must be certified as Class 1, Group B, Division 1 per NFPA Section 70, and Class 1, Group B, Division 2 within 25 feet. Any system containing hydrogen shall have adequate instrumentation and controls

to ensure that operation is within acceptable limits, and shall have adequate alarms and warnings if operation falls outside of acceptable limits. Means of detection hydrogen leakage must be employed. Fixed hydrogen detectors shall be used at likely leak points such as tanker connections, and portable hydrogen detectors should be used during operations where hydrogen may accumulate. The detectors must have short response times and must be capable of detection concentrations of 1%, or 25% of the LFL.

Management and Operations

Historical data regarding causes of past hydrogen accidents reveal system and hardware failures are seldom the sole cause of the incident. Often, there are a number of individual events that form a chain of events leading to an accident, and if any of those events was prevented the chain would be disrupted and the incident could be avoided. More often than not, improper management or operations is one of the key events leading to an accident, so care should be taken to ensure this cause is avoided.

The most important preventative measure is proper management of hydrogen systems and the operations. Safety reviews must be held at a number of points in the project life cycle. Design reviews to achieve a fail safe design must be held, and the design must incorporate all the requirements discussed above. The system should be single fault tolerant before failure that can lead to loss of life, injury or major system damage. A detailed hazards analysis by an engineer knowledgeable in hydrogen systems should be performed prior to first operation. All operations shall require approved written procedures, and the procedures must be maintained at the operational site. Once in the operational phase, good housekeeping must be maintained. Any combustible materials, including weeds, rags, wood, and cardboard, must be kept 25 feet away from any vessels or lines that may store hydrogen. Egress routs must be kept free and clear,

and must be marked properly. Practice of emergency planning or procedures should periodically be performed. It is important that area control be enforced to ensure people not knowledgeable about the operation are kept away.

Conclusion

Once the proper research and education was completed, these safety principles were used to design, construct, and operate a small liquid hydrogen storage system. This storage system, discussed in Chapter 5, contained an integrated refrigeration system. Although this type of system had not been developed previously, and the size of the system developed technically did not require adherence to the safety standards, the principles learned in this chapter were invaluable in the following chapters. If used properly, liquid hydrogen systems are as safe as other flammable hydrocarbon systems.

CHAPTER 5
TEST SYSTEM DESIGN AND ANALYSIS

The next major step was to design and fabricate a sub-scale system capable of testing concepts introduced in Chapter 2 and validating the models from Chapter 3 while conforming to safety standards addressed in Chapter 4. Funding was obtained in collaboration with Florida Solar Energy Center through the NASA Hydrogen Research for Florida Universities Program. The development process included a preliminary design and analysis phase, followed by a generation of a system specification used for procurement of the test cryostat, reviews of the detailed design drawings made by the cryostat vendor, acceptance testing of the cryostat after delivery, and finally the detailed design and fabrication of the cryostat support systems.

Preliminary Design and Analysis

Preliminary design requirements consisted of the need to effectively demonstrate the operational concepts discussed in Chapters 2 and 3. Major components needed would be a hydrogen storage vessel, a refrigeration system to remove heat, instrumentation and data acquisition, fluid supply and distribution, vacuum system, and safety and leak detection. The general design path was to determine the system size in terms of storage volume, then estimate the heat leak in that storage system. The refrigeration system is then sized to accommodate that heat leak combined with any heat removal required by the gas liquefaction rate. Once the sizing was complete, supporting systems such as instrumentation, pneumatics, and vacuum systems could be selected. Constraints on system size were dictated by budgets as well as safety specifications.

Hydrogen Storage

The required volume of the hydrogen storage was set at 150 liters. This volume is similar to familiar lab scale dewars that hold 180 liters, but was reduced to bring the total volume down below the minimum NFPA 50B guideline of 150 liters. This classified the cryostat as a lab scale research vessel, not a definite storage site. However, the volume was still expected to be large enough to perform long time liquefaction operations and to observe stratification in the densified liquid. The storage vessel was to be made as efficient as possible as determined by proven design characteristics.[57]

Many operations were to be performed below atmospheric pressure, so there was a requirement for the inner tank to be vacuum tight. Maximum operating pressure in the dewar was set at 358 kPa. Primary and secondary relief from overpressurization at 100% and 116% of the system MOP (required by ASME code) was satisfied by a relief valve and burst disk respectively. In addition, a vacuum relief valve for vacuum annulus protection was specified.

The minimum temperature expected for the liquid hydrogen was 14 K, just above the triple point temperature of 13.9 K. Saturated LH2 at this temperature has a density of .0769 g/cm3. Therefore, the maximum expected mass stored in the system was 11.5 kg.

Cryogenic Refrigerator

Once the storage system has been sized, a cryogenic refrigerator, or cryocooler must be identified that is capable of cooling the system. Based on a rule of thumb that the product loss rate of a new, well designed large dewar is less than 5% per day, an estimated heat leak can be calculated. The heat required to vaporize 7.5 liters of liquid

hydrogen at the NBP over 24 hours is found to be approximately 3 W. At a minimum, to achieve ZBO, a cryocooler that can produce 3 W at 20 K is needed.

If liquefaction is also required, refrigeration to remove the sensible heat of the gas between atmospheric temperature to the liquid temperature (3652 J/g) plus the heat of vaporization (443 J/g) must also be supplied. Additionally, the heat of conversion between ortho and para hydrogen must removed (703 J/g). Assuming the need to fill the dewar every 40 days, a mass flow rate of 0.0033 g/s of hydrogen gas is required. The refrigerator must then be capable of removing the following amount of heat;

$$Q = 0.0033 \text{ g/s} * (3652 \text{ J/g} + 443 \text{ J/g} + 703 \text{ J/g}) = 16 \text{ W} \quad (5\text{-}1)$$

Combining the liquefaction requirement with the heat leak requirement, a cryocooler capable of at least 19 W at 20 K must be used. Literature and web searches identified several candidates, mostly Gifford-McMahon style pulse tubes or stirling cycles, so no requirement was imposed for any particular manufacturer.

The cryocooler also needed to be integrated into the storage system in an efficient manner, to exchange heat between the cryocooler cold head and the liquid hydrogen at the bottom of the tank. Details for this interface design, including penetration at the bottom of the tank vs. at the top using a heat pipe or copper bar to transfer heat to the bottom, were left to the vendor building the cryostat.

One critical property that needed to be estimated was the free convection coefficient of liquid hydrogen. A simple heat exchanger had to be designed to effectively transfer the refrigeration from the cryocooler to the liquid, and the only mechanism was free convection. Literature reviews did not reveal any experimental values, so heat transfer correlations had to be used. The simplest HX to incorporate was flat straps of

oxygen free copper anchored to the coldhead, and this could be approximated as a vertical flat plate. Churchill developed a correlation for this geometry, which gives[58]

$$Nu_L = [0.825 + \frac{0.357 * (Ra_L)^{1/6}}{(1 + (\frac{0.492}{\Pr})^{9/16})^{8/27}}]^2 \quad 5\text{-}2$$

The Prandtl Number for liquid hydrogen at 20 K is found from the refrigerant property database refPROP to be Pr = 1.224. The Rayleigh Number is found from

$$Ra_L = \frac{g * \beta * (T_w - T_\infty) * L^3}{\alpha * \nu} \quad 5\text{-}3$$

The volumetric thermal expansion coefficient is defined as

$$\beta = -\frac{1}{\rho}(\frac{\delta \rho}{\delta T})_P \quad 5\text{-}4$$

and using refPROP to find the state variables is found to be $\beta = 0.14 \frac{1}{K}$ average between 15 K and 20 K. The average kinematic viscosity between 15 K and 20 K is $\nu = 0.0018 \frac{cm^2}{s}$ and the average thermal diffusivity is found to be $\alpha = 0.0015 \frac{cm^2}{s}$. The total length of the copper straps is set as 10 cm, long enough to reach within 5 cm of the bottom of the tank. Assuming a cold head temperature of 14 K and a liquid temperature of 20 K, the Rayleigh Number is estimated as 3.4×10^{13}. This high of a Rayleigh number implies the dominant form of heat transfer in this system will be convection and the natural convective flow will be turbulent. Later operational scenarios where the temperature gradient is not as large will reduce the overall heat flux and the flow regime will transition to laminar. From this the Nusselt number is calculated to be 3765. Finally, the convection coefficient is found, knowing the thermal conductivity of LH_2 and using the following relation

$$h = \frac{Nu_L * k}{L} \qquad 5\text{-}5$$

to be $h = 436\frac{W}{m^2 K}$. This is a significantly high heat transfer coefficient and means the heat exchange should be an efficient process. A calculated total surface area of roughly 100 cm2 is required for the heat exchange.

Instrumentation and Data Acquisition

Data acquisition needs were dictated by the type of planned operations. On the cryostat itself, a probe with five silicon diode sensors was necessary to measure temperature of the liquid as a function of liquid level. Other diodes were used to monitor the health of the cryocooler and to control temperature. The cryostat also needed pressure transducers for both the inner vessel and the vacuum jacket. It was also anticipated than mass flow of the product gas to be liquefied would be measured by a mass flowmeter.

The large thermal mass and the low heat transfer rates in the system eliminated the need for a high-speed data acquisition (daq) system. Labview 7.0 was used as the daq software, utilizing a program written by Dr. Baik at FSEC. Fieldpoint network modules were the interface between the instrumentation and the daq computer. The fieldpoint modules used have a 16-bit analog to digital converter.

Fluid Distribution

The following four fluid interfaces were required for the cryostat; a liquid fill and withdraw port (½" VJ), vent port (½" tube), liquefaction supply port (3/8" tube), and a gas supply port (3/8" tube). The liquefaction port and the gas supply port introduced gas at two separate locations, one wrapped around the cryocooler cold head for conduction heat exchange, and the other to introduce vapor bubbles at the bottom of the tank. The

tank relief valve and burst disk were flow through type with the outlet plumbed to the vent system. All shut off valves were specified as manual globe valves. In addition a pressure building leg was added to allow for self-pressurization, with regulation for pressure control.

Gaseous nitrogen, helium, and hydrogen K bottles would be used as a commodity supply system. Appropriate K bottle regulators were purchased, including high and low pressure gauges and shut off valves. Liquid nitrogen could be used to facilitate chilldown.

Vacuum System

The performance of any good cryostat depends directly on the quality of its vacuum system. To ensure good performance and to enhance flexibility in the laboratory, a high capacity, dual pump vacuum system was procured from Leybold[(59)]. The first stage of this system is a rotary vane mechanical pump capable of pumping speeds of 35 m^3/hr, and an ultimate low pressure of 10^{-3} torr. The second stage consists of a TurboVac turbo-molecular pump with pumping speed of 55 l/s and an ultimate low pressure of 10^{-9} torr. Vacuum pressures are measured using a Combivac CM31 universal vacuum gauge, combining a Thermovac pirani instrument for higher pressures (atmospheric to 10^{-3} torr) and a Penningvac cold cathode sensor for lower pressure (10^{-2} -10^{-9} torr). A built in RS232 interface allows data to be sent to the daq computer.

Safety and Leak Detection System

To measure any hydrogen leakage, a catalytic portable hydrogen leak detector was purchased for the laboratory. The detector works by sensing the heat generated by combustion of hydrogen and oxygen on the surface of a palladium catalyst. During normal operations the detector sensor was positioned above the cryostat to detect leaking hydrogen gas that is buoyant, but the sensor could also be used as a point detector during

some transient operations to measure leakage at a specific interface. A portable O_2 monitor was used to ensure any helium or nitrogen leakage would not create an oxygen deficient atmosphere in the enclosed laboratory. All electrical connections on the cryostat were specified to be built explosion proof per Class 1 Group B Division 2 of NFPA 70. Vendor supplied equipment, such as temperature and pressure monitors that were not explosion proof, were specified to be enclosed in a purged environment, meeting the intent of NFPA 70

Cryostat Specification

Following completion of the preliminary design, a cryostat specification was produced and distributed to a variety of vendors for bids. This specification used the sizing and operations requirements previously analyzed, and incorporated all the necessary design and fabrication requirements imposed by cryogenic standards. All construction was to be stainless steel, with the inner vessel conforming to ASME Boiler and Pressure Vessel Code Section VIII, and the vacuum jacket to Section VIII and Section IX. Tubing was specified by ANSI B31.3. A number of test requirements, such as x-ray of welds, cold shock, leak test, and pressure test were also specified. The vendor was required to submit a number of test reports and certifications as well as the fabrication and assembly drawings. A final cleaning requirement and shipping details were included as well. The full system specification, as well as a preliminary test schematic, is included in Appendix A.

Cryostat Detailed Design

Cryogenic Technical Services, of Longmont, Colorado was selected to fabricate the cryostat, primarily due to the experience of the owner Glen McIntosh with liquid hydrogen. Glen added several innovative design features, especially in the area of the

pressure buildup system (PBU). His expertise in designing and fabricating low heat leak vessels eliminated the need for a shield around the inner tank. The cryocooler chosen was a G-M, connected to the top flange of the dewar with a heat pipe to transfer heat to the bottom of the tank. A detailed design is shown in Figure 5-1.

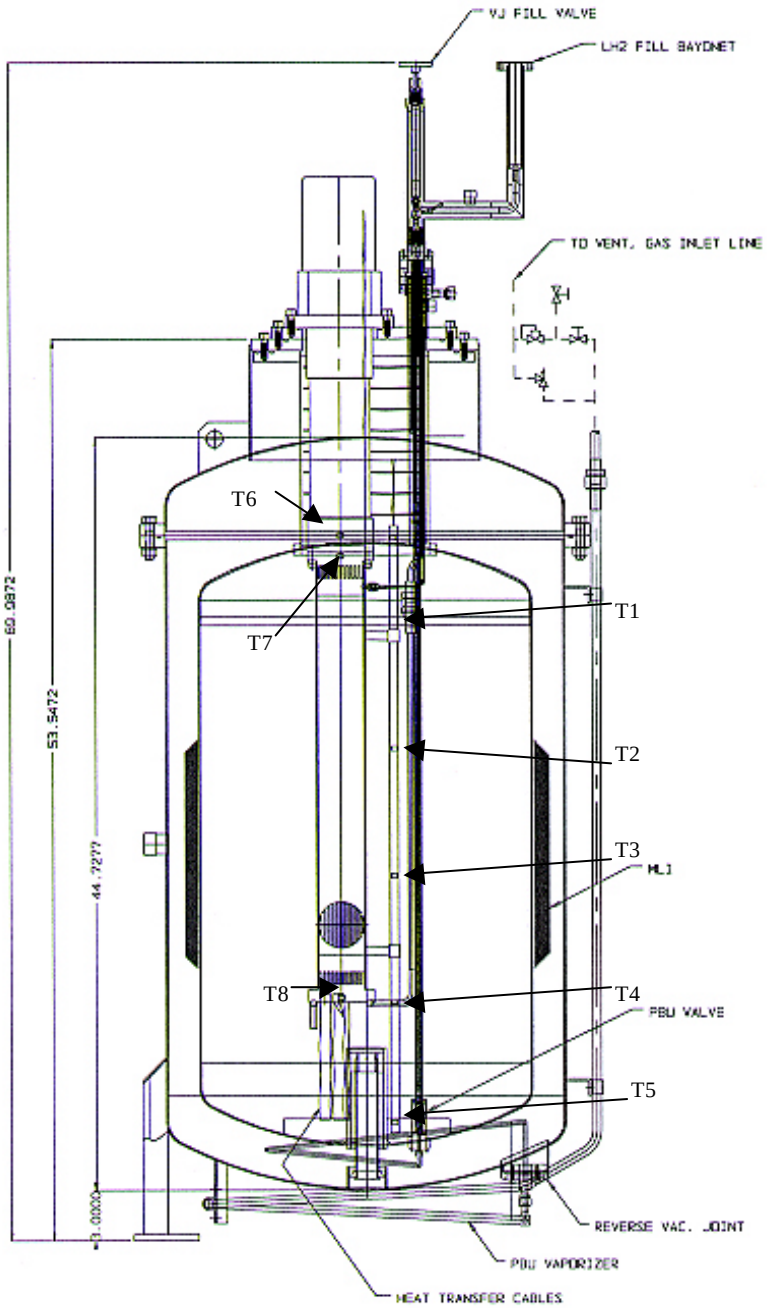

Figure 5-1 Cryostat design detail (Cryogenic Technical Services)

Cryostat Construction

The inner vessel is 20 inch SS 304 tubing, with a cylindrical section 25.5 inch long and two elliptical end caps. The total volume is 157 liters, and has a surface area of 1.56 m2. 45 layers of dexterous paper and aluminized mylar, 1 ½ inches thick, serve as the multi-layer insulation (MLI). The inner vessel is primarily supported by the 12-inch long, 8-inch diameter 304 SS neck. There is also a low conductivity G-10 bottom support. The cryocooler cold head is installed down the length of the neck, offset from the center, and thin stainless steel baffles suppress and radiative heat transfer in the neck of the dewar. One design feature added is the incorporation of a flange at the top of the vacuum shell, to allow the entire inner vessel to be removed. Another flange at the top of the neck allows removal of the cryocooler coldhead, heat pipe, and inner vessel instrumentation.

A total of four lines were connected to the inner vessel. The liquid fill and drain line, VJ outside the dewar, was 3/8 inches ID, .049 inch wall thickness, and had a conduction path of 12 inches long. This line had a bayonet connection interface, and ran to the bottom of the inner vessel. The vent line was 5/8 inches OD, had 0.049-inch wall thickness and had a path length of 12 inches. It connected to the high point of the inner vessel, and had external tees to the pressure transducer, the vent stack, the PBU leg, and a shut off valve. The liquefaction inlet line is 3/8 inch OD tube, with .049 wall thickness and a conduction path of 12 inches. This line is brazed onto the cold end of the heat pipe for good conduction heat transfer, and has a shut-off valve at the warm interface. The PBU system was a unique challenge. In most storage vessels, the PBU line is connected to the bottom of the tank, has a number of coils wrapped in the VJ annulus, and has a shut off valve and regulator outside the dewar at the top of the system. In this case, the PBU system uses a liquid trap to minimize heat leak when not in operation. In deeply

subcooled systems, there is no vaporization occurring immediately in the PBU line, so there is no vapor backpressure preventing the liquid from flowing over the liquid trap and into the uninsulated portion of the PBU line. This would dramatically increase the total heat leak in the cryostat to the extent that the cryocooler would not be able to overcome this heat leak, and subcooling would not be achievable. The simple solution to this is to move the PBU isolation valve to the bottom of the tank, but this design is complicated since the valve stem would be inverted and liquid could be present at the valve stem packing. This situation is unacceptable since heat leak would increase and there could be leakage problems at the dynamic seal at the top of the valve stem. CTS proposed an innovative solution to this problem, placing the valve body and poppett at the bottom of the tank and using a stainless steel cable as a link between the valve seat and the manual actuator at the top of the system. The PBU line, 3/8 inches OD and 0.049 inch wall thickness, then runs downstream of this valve a total of 23.5 inches until it exits the vacuum annulus and enters the vaporizer section at the bottom of the tank. The PBU regulator is at the top of the tank. There is some additional heat leak associated with this cable, but this small heat leak is negligible.

Knowing the details of construction, a more exact calculation of the total tank heat leak can be made. This number is estimated by adding the contributions from the radiation around the area of the dewar with the conduction down the dewar neck and all tube penetrations, and adding in a cryocooler heat leak contribution given by the vendor

$$Q_{hl} = hA(T_\infty - T_c) + \sum kA\frac{(T_\infty - T_c)}{L} + Q_{cc} \qquad 5\text{-}6$$

where h is the overall heat transfer coefficient across the MLI calculated from the modified Lockheed correlation[42].

The total heat leak for the cryostat is now estimated to be 8.7 W, more than doubled compared to the original estimate based on the 5 % per day rule of thumb. This is due to the fact that the small vessel has more parasitic heat loads than larger dewars due to the scaling of heat leak being related to area (r squared) compared to volume (r cubed). Details of this heal leak calculation, made using an Excel spreadsheet, are included in Appendix B.

The final instrumentation design for the cryostat included 8 Lakeshore DT-400 series silicon diode temperature sensors, with 4 wires each, calibrated at the factory. The sensitivity of these diodes is +/- 22 mK[60,61]. Five of these diodes were installed on a G-10 support down the height of the tank, spaced every 5 inches, with T1 reading the product (usually vapor) temperature at the top of the vessel and T5 reading the product (usually liquid) temperature at the bottom of the vessel. T6 is the cryocooler cold head temperature, T7 is the temperature at the top of the heat pipe, and T8 is the temperature at the bottom of the heat pipe. This arrangement allowed for visibility into liquid temperature stratifications, as well as cryocooler performance, heat pipe performance, and the effectiveness of the cryocooler to heat pipe thermal connection. A Taber Industries pressure transducer, factory calibrated with a resolution of 0 .05 psia, monitors the inner tank pressure from a tee off the vent port[62]. An American Magnetics capacitance based liquid level probe was included to better estimate the total volume of liquid in the tank, but it never seemed to function consistently and the data was not used.

Cryogenic Refrigeration

A Cryomech AL330 Stirling type G-M cryocooler was selected for the refrigeration system. The AL330 is capable of producing 40W at 20 K, 15 W at 15K and has a no load temperature of 12 K. A capacity curve is shown in Figure 5-2[63]. The cold

head package, consisting of a rotary valve, displacer, regenerative heat exchanger, and copper cold mount, weighs 44 lbs and is connected to the compressor by two gaseous helium lines and an electrical power feed. The CP970 compressor is oil lubricated and water cooled. The compressor power requirement is 220 VAC, 3 phase, 60 Hz, and uses a total of 7.5 KW. At 20K, this gives a specific power of 187.5 W/W, not very efficient but the cryocooler is very reliable.

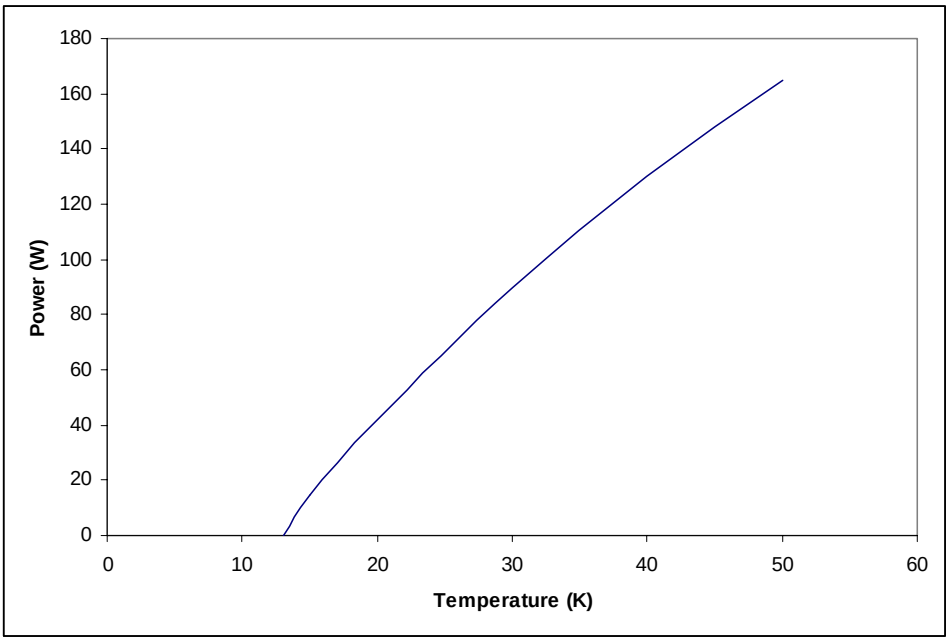

Figure 5-2 Cryocooler AL330 capacity curve (Manufacturer Spec)

The heat pipe is a 2 1/2 inch diameter tube, 26 inches long with an internal volume of 127 in3. It is thermally anchored at the top to the cold head, using invar screws for low thermal expansion and Apezion N vacuum grease to enhance heat transfer between the two polished oxygen free copper surfaces. The heat pipe copper heads are machined on the inside surface with parallel fins, to increase the condensation and evaporation surface area. The heat pipe has a charge port that has an interface outside the dewar, for changing the working fluid if the temperature range requires it, or to refill any

leakage that may have occurred. The bottom copper mass on the heat pipe has the liquefaction line soldered to the outside surface, and four flexible copper straps, .75 inch wide by 5 inches long, designed to exceed the required heat transfer area by giving 194 cm2 of surface.

Acceptance Testing

The cryostat was delivered to FSEC in October, 2003. Following unpacking and visual inspection, the system was set up in the Chemistry Laboratory. The instrumentation was powered up and the vacuum level on the vacuum jacket was verified to be good. The vacuum pump was connected to the inner vessel and this was evacuated to 10 microns, following which a vacuum decay check was performed. The pressure rose 7 microns in 6 hours. Vacuum leak rates can be quantified by the equation[64]

$$Q = 79 * \{273/(273+T)\} * V * \Delta P / t \qquad 5\text{-}7$$

Where Q is the leak rate in sccm, V is the volume in liters, and P is the pressure in Torr. The estimated leak rate becomes 0.0036 sccm. After the vacuum decay, the cryocooler was started and a temperature of 14 K was reached on the cold head. At this point the heat pipe had not been charged. All diodes functioned as expected.

Support Systems

Once the acceptance testing was complete, the cryostat was positioned into the lab where the testing was to take place. Previously, a hole was cut into the outer wall and a 1” vent pipe was installed and placed several feet above roof level. A K-bottle rack was purchased as well as nitrogen, helium and hydrogen K-bottle regulators. For the gaseous hydrogen supply system, a MKS mass flow meter was installed to control and measure the quantity of hydrogen entering the system. The flowmeter had a range of 0-50 slm and an accuracy of 0.05 slm[65]. Flexible copper tubing was used to connect different

elements, and swagelok compression fittings were used for all gas connections. Check valves were used to minimize the potential for system contamination. A liquid nitrogen laboratory scale dewar was purchased to aid in the initial chilldown, and a foam insulated, metal bellows flexhose was used to connect the LN2 to the cryostat. A picture of the completed test set up is shown in Figure 5-3.

Figure 5-3 Liquid hydrogen cryostat test arrangement

CHAPTER 6
LABORATORY TESTING AND DATA ANALYSIS

A series of tests were conducted at the Florida Solar Energy Center in the summer of 2004. Total quantities of LH2 were limited by the laboratory managers to keep the liquid mass under 2 kg, for safety purposes. Testing was terminated on August 12 2004, when the approach of Hurricane Charley created the need for system deservicing and safing. Zero boil off, liquefaction and densification were all achieved. Future plans call for further testing in 2005-2006 in a dedicated lab space where quantity-distance concerns are minimized. The test description and data analysis follow.

Liquid Nitrogen Chilldown

Testing with cryogens started on June 22, 2004. The cryocooler was not operating and the system was at ambient temperature. It was decided that a stored cryogen supply would be used for the system chilldown to save time, as opposed to using the cryocooler refrigeration power. No readily available supply of liquid hydrogen was found in small quantities for this purpose. The estimated total mass of the cryostat that would need to be chilled down was 150 kg, mostly stainless steel. Jacobs [66] has provided a method of estimating total liquid require for chilldown of cryogenic pipelines, and using this method approximately 4800 liters of liquid helium is required. This estimate assumes only the latent heat is used for chilldown, as opposed to cross country pipelines where sensible heat can also be a contributing factor due to longer dwell times in the equipment. Liquid helium was determined to be too expensive. The solution was to use liquid nitrogen to chill down to 77K, then drain and purge the liquid nitrogen using

gaseous helium, evacuate then turn on the cryocooler and supply gaseous hydrogen to complete the chilldown process. The total volume of LN2 needed was estimated to be only 84 liters. Figure 6-1 shows the data from the initial phase of this chilldown.

At the start of the test, all valves on the system were closed and the system was evacuated to a pressure of 0.02 psia. The vacuum annulus was evacuated to a vacuum in the range of 1x10-4 Torr. All temperatures were reading in the range of 297 K. A portable, 160 liter dewar of liquid nitrogen was connected to the liquid fill and drain line, and the dewar supply valve and the liquid hydrogen drain valve were opened. The system vent valve was then opened. Unfortunately, the supply dewar pressure was not vented prior to the transfer, and the valve was not opened slowly enough. As liquid nitrogen entered the warm hydrogen storage tank, it vaporized and expanded beyond the flow capability of the ½ inch vent line. Frost was observed at the outlet of both the relief valve and the burst disk, indicating cold vapor flow out of these devices. The liquid nitrogen supply valve was closed and the system pressure began to decrease. The nitrogen storage pressure was vented and supply valve was very slowly opened to reestablish the chilldown process.

Figure 6-2 shows more detail of the over pressurization of the system. Note the pressure increasing in surges, as is expected in a chilldown process as liquid flashes off, creating a localized pressure spike that reduces further liquid flow. In spite of these spikes, the overall pressure increases in a fairly linear profile until the burst disk relieves at 64.5 psia (49.8 psig), slightly higher than the 45 psig specification. It is worth noting there was no corresponding decrease in pressurization rate when the relief valve opens, indicating the flow capacity was not sufficient to relieve that quantity of gas.

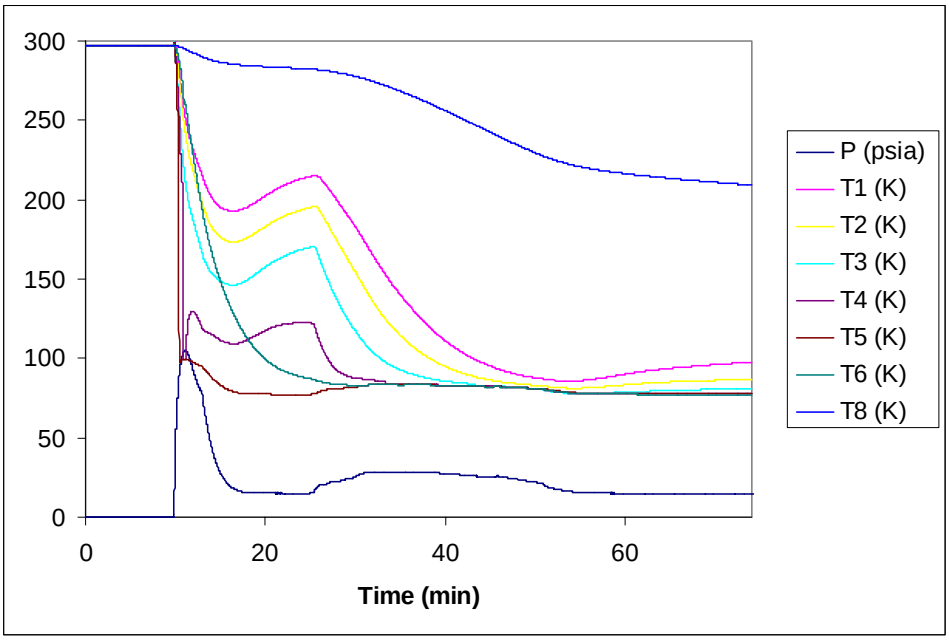

Figure 6-1 Liquid nitrogen chilldown

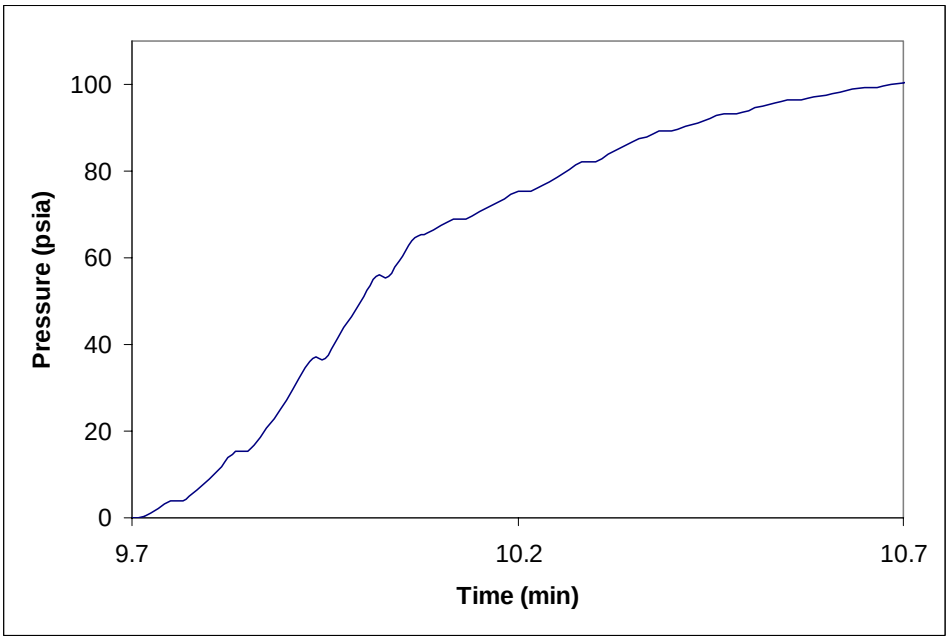

Figure 6-2 Hydrogen dewar overpressurization

Pressure continued to increase until the delta pressure between tanks reached a point where the liquid mass flow rate into the system equaled the gaseous mass flow rate out of the system. Once the frost was observed on the relief line, the liquid nitrogen supply

valve was closed, and pressure decreased to match the atmospheric pressure. Later, after the chilldown was complete and while the system was open to ambient, a new burst disk was installed to provide a redundant method of overpressure protection.

Looking at the temperature profiles during the chilldown in more detail (Figure 6-3), notice the lowest diode (T5) quickly reaches the liquid state (97.8 K, 96.5 psia) and remains liquid during the flow interruption. The liquid temperature decreases after the flow stops since the vapor pressure is decreasing. T5 eventually reaches 77 K (NBP) as the pressure in the tank vents to ambient. Similarly, T4 initially reaches the liquid point, but turns to vapor shortly after the flow is terminated. The other three diodes in the temperature rake are gradually decreasing in temperature, even when the flow is stopped initially. This is due to the fact that liquid nitrogen is boiling off in the bottom of the tank, removing heat from the saturated liquid as the vapor pressure drops. Once the depressurization rate decreased enough, the tank heat leak and heat capacity of the semi-warm metal overcomes this cold vapor supply and the ullage temperatures seek to stabilize at a higher temperature. Another interesting point is the temperatures on the cryocooler and heat pipe themselves, which gradually decrease in temperature compared to the diodes on the rake. This is due to the much larger thermal mass associated with these locations taking longer to chill.

After the burst disk rupture had been diagnosed and determined not to be a constraint on further testing, the liquid nitrogen supply valve was reopened. Figure 6-4 below shows details on this process. The nitrogen dewar had been vented to a much lower pressure and the lack of a burst disk gave a larger path to vent, so the system pressurized in a much more controlled manner. Extra care was also used to open the

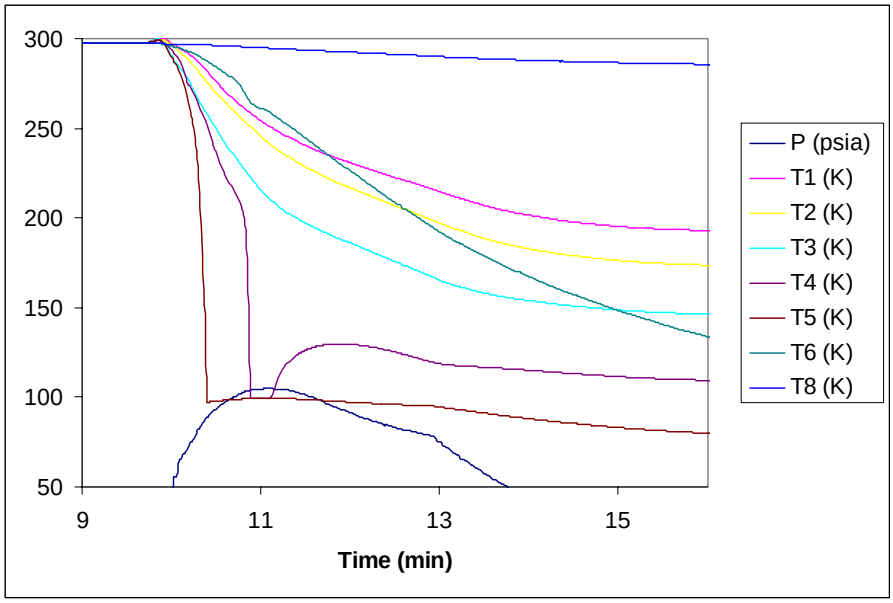

Figure 6-3 Liquid nitrogen chilldown detail

supply valve more slowly. The maximum system pressure was only 28 psia during this chilldown sequence. Data shows that T5 increased slightly as the pressure increases, following the liquid saturation line. T6 and T4 quickly reached liquid temperature, followed by T3 about 18 minutes after the start of flow. Flow was terminated at T+51

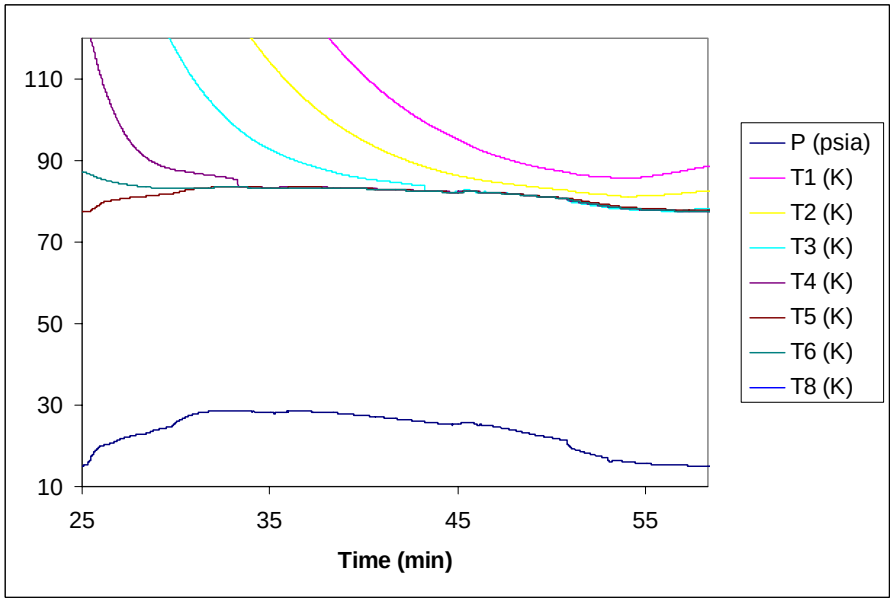

Figure 6-4 Completion of chilldown

minutes, when the liquid level was approaching T2. Pressure in the system vented to ambient, accompanied by a drop in saturated liquid temperature. Shortly after the pressure reached ambient, the T3 measurement increased past the saturation temperature, indicating enough liquid boiled off to leave the diode in the vapor region. Another interesting phenomenon was observed in the temperature profiles in the liquid. During flow, all liquid temperatures were equal, indicating mixing of the liquid. Shortly after the flow was stopped the temperature of the upper liquid layers decreased (T3, T4) compared to the lowest liquid layer (T5). Evaporation at the surface caused liquid temperatures to decrease, but there was a time delay before the natural convection currents created a normal temperature gradient in the liquid. The tank, half full of liquid nitrogen was left open to atmosphere overnight to ensure a complete chill down. By Thursday June 24 at 11:00 am, a stable temperature profile was recorded with T4 and T5 reading 77K, T3 reading 95K, T2 reading 117K, and T1 reading 138K. At this point, the tank drain and purge was performed.

LN_2 Drain and Purge

Drain and purge of the liquid nitrogen was started on June 24 at 10:45 am. A data overview of the next four hours is shown in Figure 6-5. First the system vent valve was closed. The system immediately began self-pressurizing. A gaseous helium K-Bottle was connected to the system and the line was evacuated to eliminate any contaminants. The system was then pressurized to 18.2 psia. A series of 5 positive pressure purge and vent cycles was completed. Once the remaining liquid was expelled, two helium purge and vacuum cycles were completed to remove all the gaseous nitrogen, which would solidify at liquid hydrogen temperatures. Finally, after all the nitrogen was removed and the system was still under vacuum, the cryocooler was turned on.

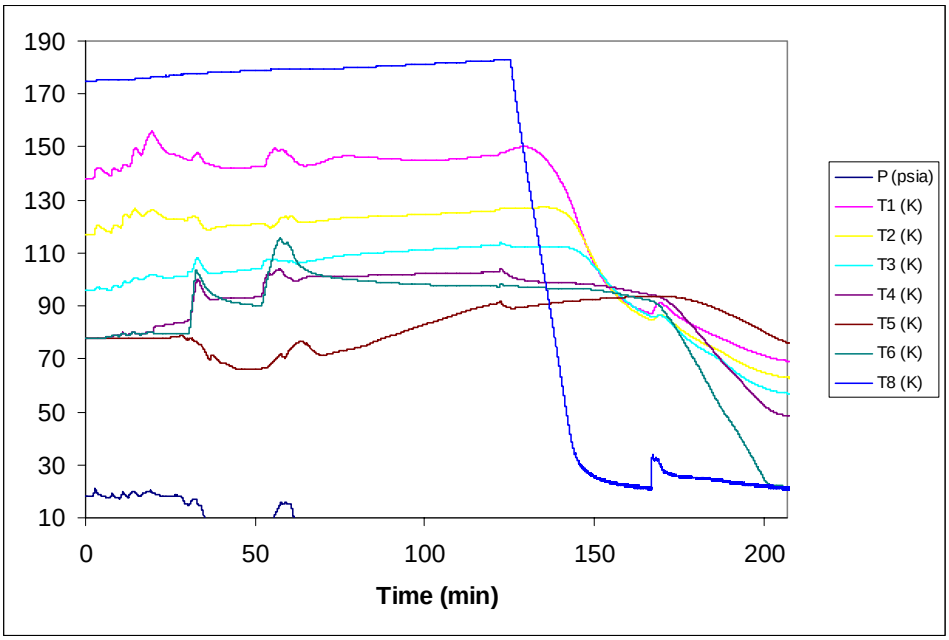

Figure 6-5 Liquid nitrogen drain and purge

More insight on the system behavior can be found by examining the data in greater detail. Figure 6-6 shows the tank pressure profile during the purges, drains, and evacuation. Starting at 18.2 psia, the gaseous helium inlet valve was opened to pressurize to 20.7 psia. The system vent valve was then opened starting the first purge cycle. When the pressure decreased to 17.5 psia, the vent was closed to repressurize. This was repeated five times, to get the nitrogen ullage replaced with helium. While this is occurring, enthalpy from the warm helium is causing liquid nitrogen to boil. Notice the pressurization and depressurization rate decreases as the boil off leaves a greater ullage volume. At the end of the fifth cycle, the gas supply valve is closed and the vent valve is closed. The system is repressurized to 18.5 psia and the liquid withdraw valve is opened.

There is a noticeable slope change in the depressurization curve when comparing a gas vent to a liquid withdraw. As most of the liquid is drained, the system reaches near

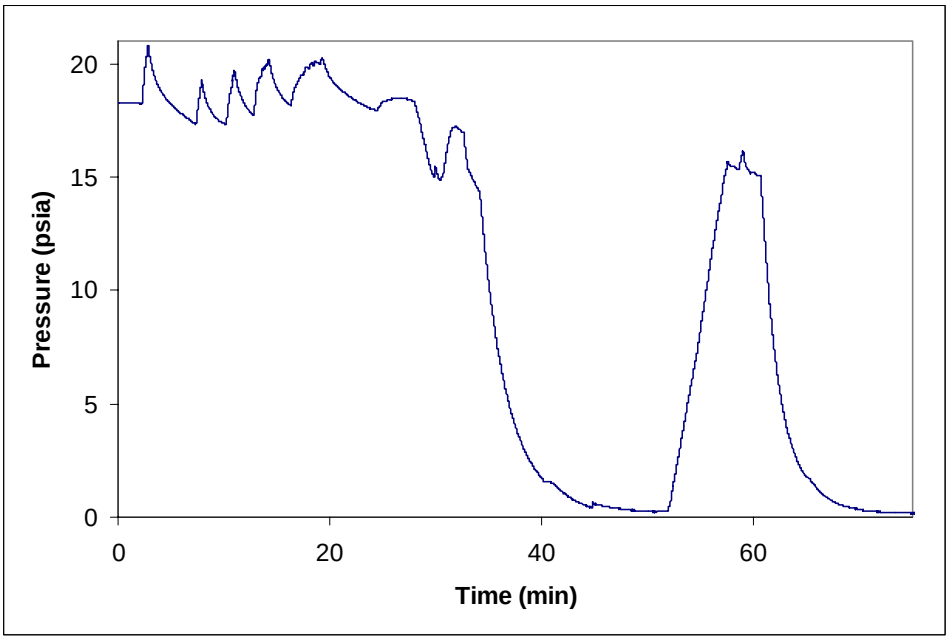

Figure 6-6 Tank drain and purge pressure cycles

ambient pressure and valve is closed. Next, two evacuations are performed using the vacuum pump, with a backfill of gaseous helium in between. The system remained evacuated until the following day when the gaseous hydrogen was introduced into the system.

Temperature profiles during this operation are shown in detail in Figure 6-7. All five purge and vent cycles are clearly evident in the ullage temperature measurements. By the second purge cycle, enough warm gas had entered the system that the liquid level had reached the T4 level. After this point, T4 behaves in a similar manner to the other ullage temperatures, except the final pressurization cycles during the liquid withdraw procedure created much higher temperature spikes in T4 that T3, T2, and T1. Liquid stayed in the bottom of the tank through all five purge cycles, as is evident by the lowest tank temperature continuing to track the saturation line. After the five purge cycles, the liquid withdraw valve was opened. Most, but not all of the tank was drained. Note the

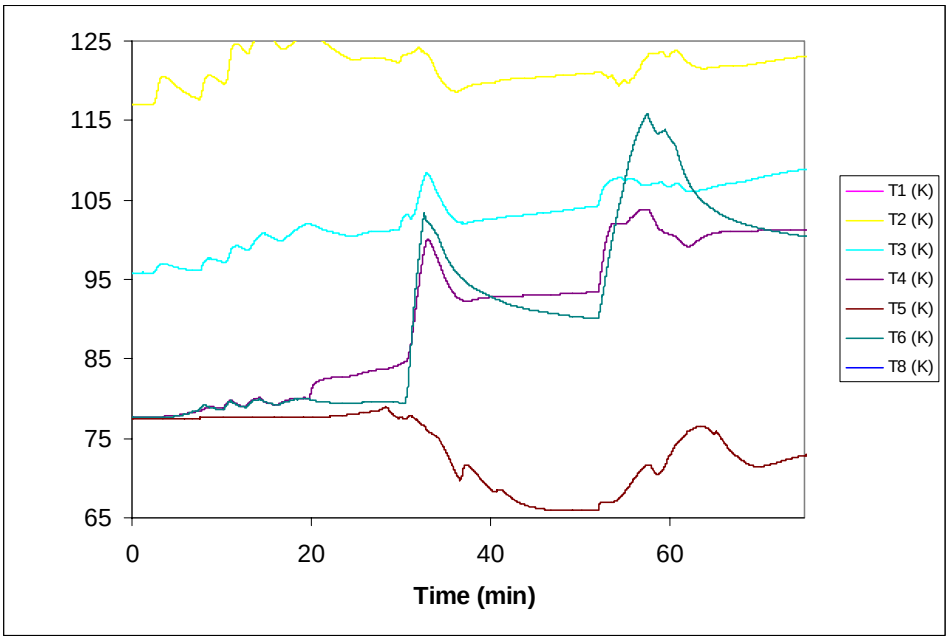

Figure 6-7 Tank drain and purge temperature profile

differences in behavior between the diodes in gas vs. diode in liquid. The ullage temperature drops initially as the pressure decreases, and during this phase it is measuring the gas temperature directly thru convection. Eventually the temperature decrease stops, although the pressure continues to decrease. The liquid diode decreases in temperature as the pressure drops, roughly following the saturation line. At this point it was decided to do a second drain operation, and the system was repressurized to 16 psia. The drain valve was reopened and the system vented to ambient. The vacuum pump was reconnected and turned on and this time it appeared the remaining liquid was removed from the tank. The T5 reading began increasing, along with all the other temperatures, and the decision was made to turn on the cryocooler.

When the cryocooler was started (Figure 6-8), the cold head temperature was reading 182K. Within 30 minutes, the temperature had decreased to 22K, and many of the other temperatures near the top of the tank were decreasing. However, the lower tank

temperatures and the bottom heat pipe temperature did not start decreasing until the heat pipe was charged with gaseous hydrogen. The charge operation caused an immediate spike in cold head temperature due to the enthalpy of the warm gas entering the pipe, and this spike is also evident in the upper tank temperatures. Once the heat pipe was fully charged, the lower heat pipe temperature immediately began decreasing as the refrigeration power was pumped down the length of the pipe by the internal hydrogen gas. Within 30 minutes, the lower heat pipe temperature had completed its chilldown. The delta temperature between the cooler and the heat pipe end was approximately 0.7K, which is very efficient considering there was thermal contact resistance between the top of the pipe and the cold head, and thermal resistance down the length of the pipe. One puzzling piece of data is that the expected temperature profile was established with the exception of the lowest diode T5. This temperature did not decrease as quickly as the others, and remained the warmest of all the temperatures during this phase of operation.

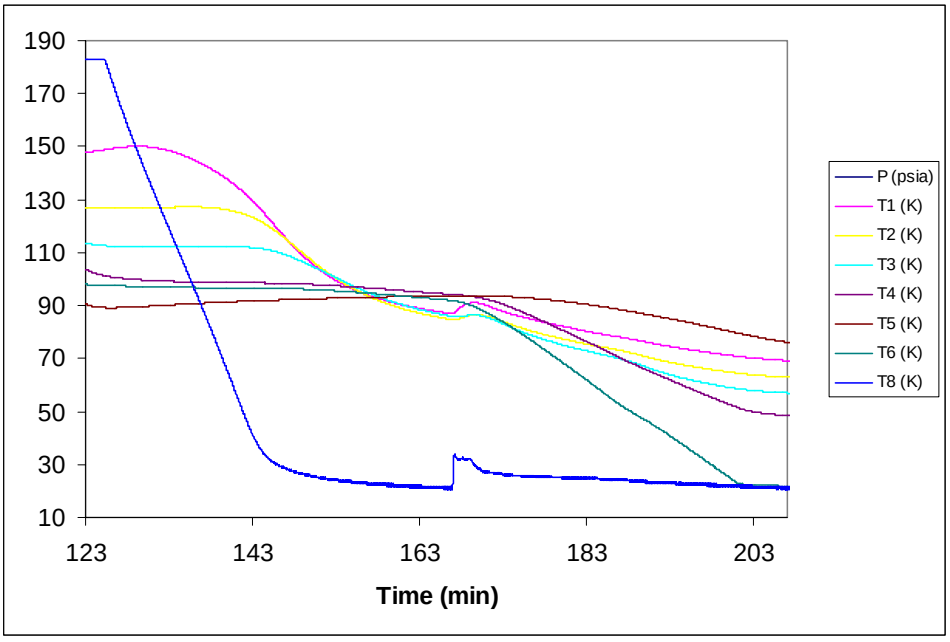

Figure 6-8 Cryocooler chilldown in vacuum

This is potentially explained by the internal configuration of the tank, with the internal G10 support tube partially blocking the radiation path between T5 and the heat pipe cold mass. With little pressure in the tank, the primary heat transfer mechanism would be radiation. The cryocooler was left on overnight to achieve maximum chill down and the next morning the hydrogen liquefaction process began.

Hydrogen Liquefaction

After the cryocooler operated overnight, the cold head temperature and heat pipe temperature were reading approximately 15.5 K. The cold head temperature was actually experiencing temperature oscillations of a magnitude near 1.5 K, which were damped out by the thermal mass of the heat pipe. Ullage temperatures varied between 28 K and 37 K, and were still decreasing slightly. Around 10:20 am on 6/25/04, hydrogen gas at room temperature was introduced into the vessel. Figure 6-9 below shows this operation, from start of gas flow until termination of gas flow 4.5 hours later. The temperature and

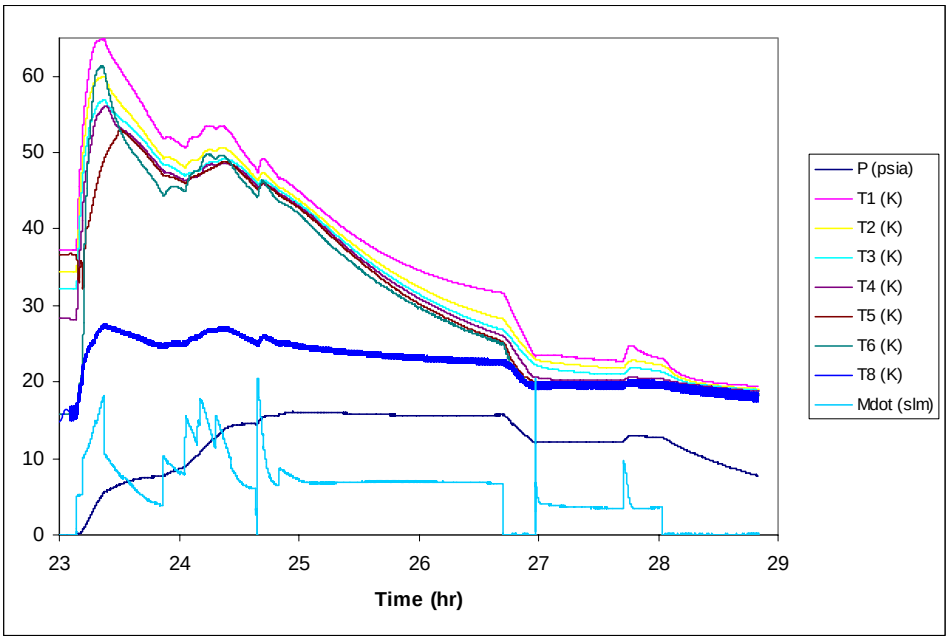

Figure 6-9 Hydrogen liquefaction on 6/24/04

pressure profiles are driven by the mass flow rate into the vessel, as is expected since the enthalpy from the warm gas introduces the energy in the system while the cryocooler tries to remove this thermal energy. If the mass flow rate exceeds what the cryocooler can liquefy, the pressure increases. Accurate control of the mass flow rate of gaseous hydrogen was somewhat difficult since the only means of control were globe valves that had imprecise adjustments, with fluctuating pressures upstream and downstream of the valve, and in some cases, vibration from the cryocooler displacer that caused changes in valve positions. Future modifications to the experimental set up will include the addition of a mass flow controller.

As soon as the gas flow was initiated into the vessel, the temperatures started to rise on all thermocouples, with the exception of T5. Recall that during the overnight chilldown T5, the lowest thermocouple on the rake, was expected to read a lower temperature than T1 thru T4, but in fact it did not. This was attributed to the fact that the dominant heat transfer mechanism in the tank ullage at that time was radiation, not convection, and T5 was shielded from a direct view of the lower end of the heat pipe. However, as soon as gas was introduced into the system, convection became the primary means of heat transfer, and T5 initially cooled off as stratification of the gas occurred. When the gas pressure was sufficient so as to allow T5 to read the temperature accurately (around 0.5 psia), the measurement began to rise. At this point, the expected temperature profile was recorded in T1 thru T5. As the pressure continued to increase, greater convective heat transfer began to occur between the heat pipe end (T6) and the measurement on the rake, and T5 began to decrease again. This continued until the heat pipe and cold head warmed up beyond the boiling point of the hydrogen in the heat pipe.

At this point, heat transfer down the heat pipe was limited to convection instead of a phase change, and the heat transfer down the pipe was restricted. T6 began to increase as a result, and this caused T5 to start increasing as well. This initial warm up phenomenon is shown in greater detail in Figure 6-10.

At this point the decision was made to increase gas flow in the tank to get to the point where the internal pressure was above atmospheric, so as to minimize the possibility of air leaking into the system. The valve was opened numerous times to increase flow, but the flow rate decayed immediately afterward. Eventually the k-bottle regulator pressure was decreased to minimize delta pressure, and flow rates became somewhat more controllable. Pressure changes in the tank were directly related to the value of the mass flow rate. This is shown graphically in more detail in Figure 6-11, with the slope of the pressure curve related to the magnitude of the mass flow rate. Some effort was made to determine the mass flow rate that gave a constant pressure in the tank, such a flow rate would roughly approximate the liquefaction rate of the cryocooler (neglecting ortho-para conversion losses). There were two periods of time when the tank pressure was roughly constant, corresponding to flow rates of 6.6 standard liters per minute and 4.3 slm. However, there were still too many transient effects at this time to come to any conclusions.

From this data it is easy to numerically integrate the mass flow rate with respect to time to obtain the total quantity of hydrogen in the system. This result is shown in Figure 6-12. During the course of the day, a total of 2000 standard liters of gaseous hydrogen was introduced into the tank. Knowing the standard volume of hydrogen gas in the tank, combined with the total volume of the tank, the specific volume of the hydrogen can be

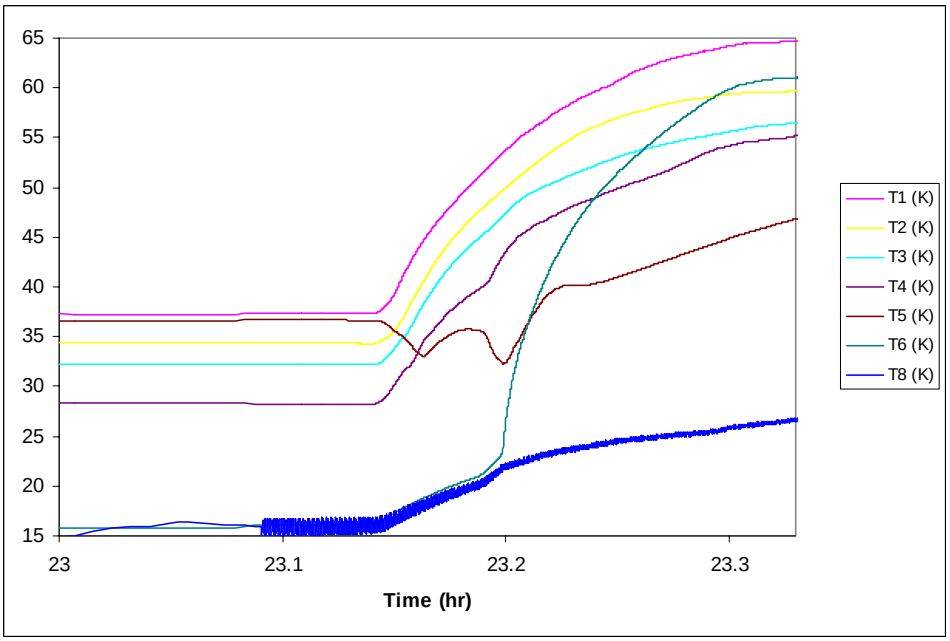

Figure 6-10 Temperature transients during initial gas flow

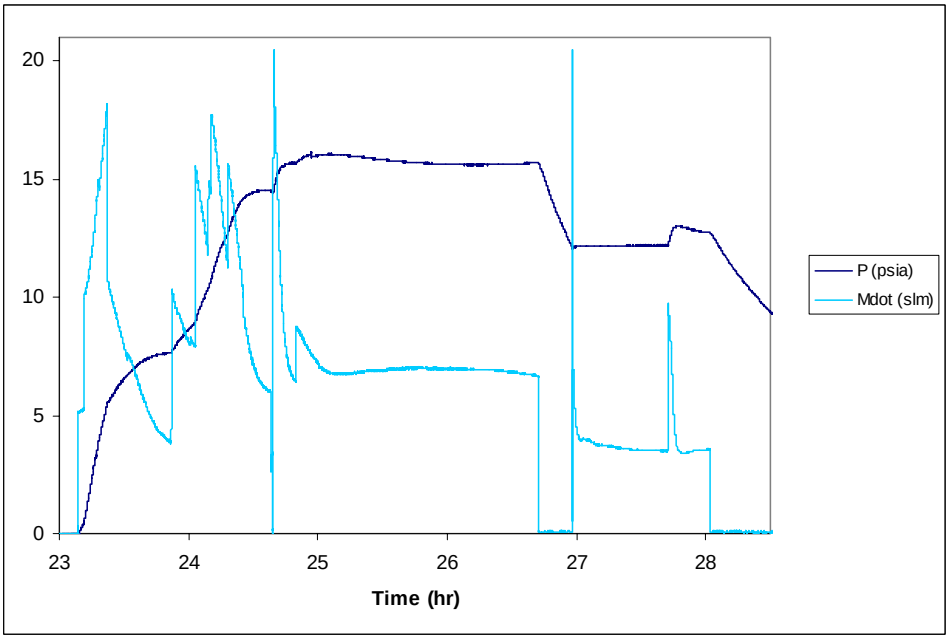

Figure 6-11 Mass flow rate and pressure during liquefaction

computed. The hydrogen mass is found to be 0.164 kg , and the specific volume is .91 m3/kg . When this is combined with the tank pressure, the thermodynamic state of the hydrogen can be found.

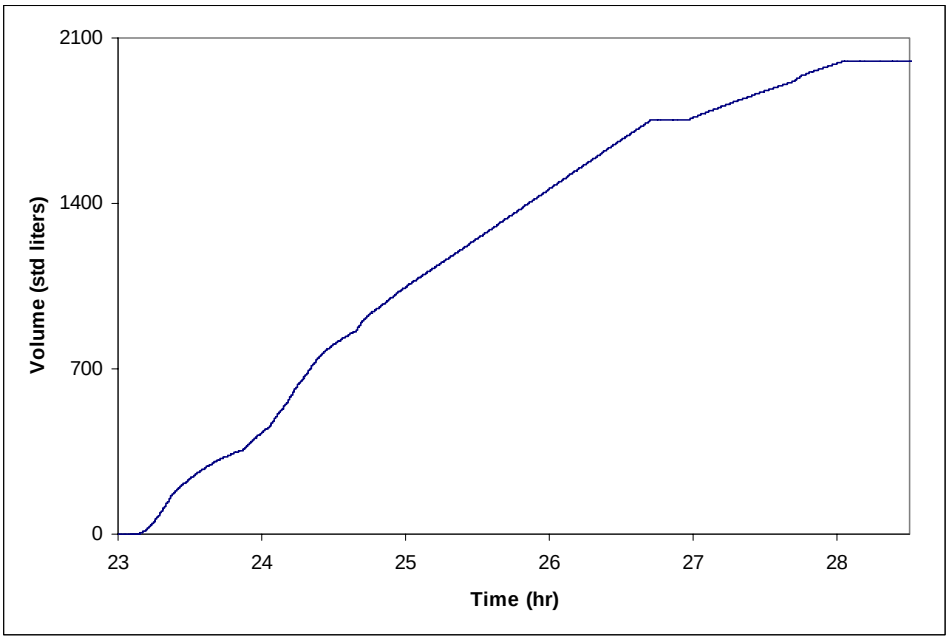

Figure 6-12 Total hydrogen volume in tank

At the time the mass flow is shut off, the pressure is 12.6 psia, so a quick check of hydrogen properties shows the state point to be in the vapor region. At this point, no hydrogen liquid has been produced, just cold vapor, however as the cryocooler continued to operate the vapor pressure continued to decrease and when the pressure reached the saturation point (11.89 psia) liquid droplets started to form. By the next morning the pressure had dropped to 3.78 psia, well inside the two-phase region. Another interesting point is where the hydrogen inside the heat pipe becomes saturated again, which is evident by the sharp decrease in heat pipe temperature and change in the slope of the ullage temperature curves. Figure 6-13 shows this event in more detail.

Hydrogen Densification

Around 4:00 pm on June 25, the hydrogen flow was terminated and the cryocooler remained on overnight to continue to refrigerate the hydrogen remaining in the tank. As

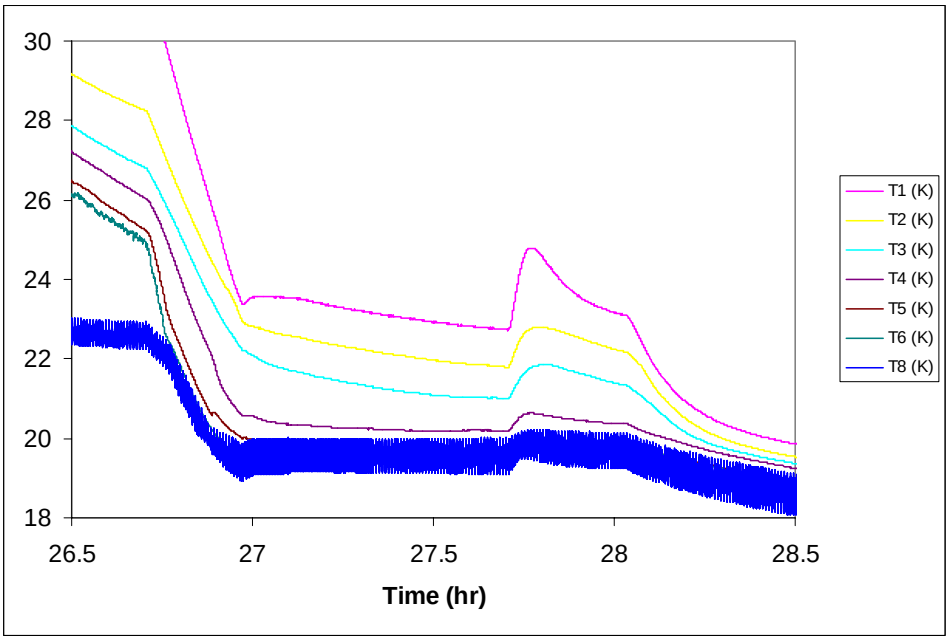

Figure 6-13 Heat pipe saturation

was discussed above, the hydrogen was not yet saturated when the flow was terminated, but shortly thereafter it reached the saturated state. The following morning the tank pressure and temperature had stabilized to an expected condition. The pressure was 3.88 psia and the temperatures varied between 16.5 K and 18.7 K. There were several unexplained jumps in temperature and pressure measurements, but at this time it is undetermined whether this represents some physical process or an error in the way the data files were manipulated. In either case, the state of the fluid is known at this time. The specific volume is still 0.91 m3/kg, since no changes occurred either to the system volume or the mass overnight. The saturated vapor specific volume is 2.49 m3/kg, and the saturated liquid specific volume is 0.0134 m3/kg. The quality of the fluid is then found to be 36% , or a total liquid mass of 0.06 kg. The density of the saturated liquid is 74.7 kg/m3, an increase of 5.5% over the normal boiling point of the liquid. Figure 6-14 below shows temperature and pressure profiles during this densification period.

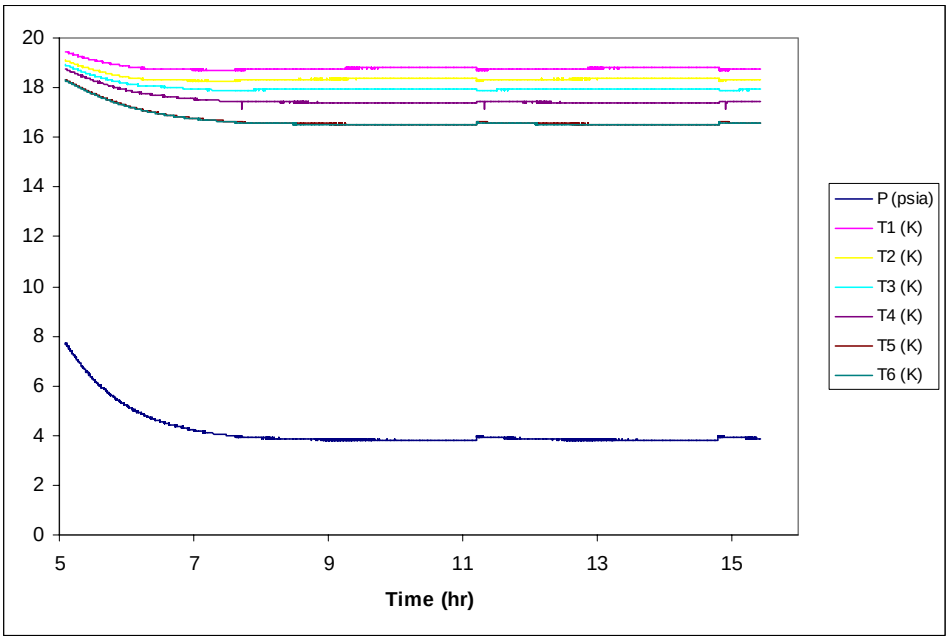

Figure 6-14 Overnight densification

The system was allowed to continue to pump down over the weekend, with the exception being a quick period on June 28 when the cryocooler was turned off for a relocation of the system within the lab for safety purposes. The system warmed up slightly during this time, with the largest increase in temperature being in the cold head. This is expected since the temperature measurement that is most susceptible to increases is the cold head due to conduction down the length of the regenerator portion of the cryocooler. The warm up data is shown in Figure 6-15 below. From this figure it is obvious the heat pipe never reached the unsaturated state. On June 29, liquefaction operations restarted, as shown in Figure 6-16. This operation was slightly different from before since there was a small amount of liquid already in the tank and the system was completely chilled down, as opposed to the hard vacuum on the system prior to the start of the first operation. As such, there were slightly different temperature profiles. Note that the lowest temperature measurements did not increase at nearly the same rate as the

upper measurements. This is probably due to the thermal mass of refrigeration stored in the system from cooling overnight. The heat pipe temperature and T4 and T5 on the rake did not increase above 21 K, in fact T5 seemed to stay within the temperature saturation

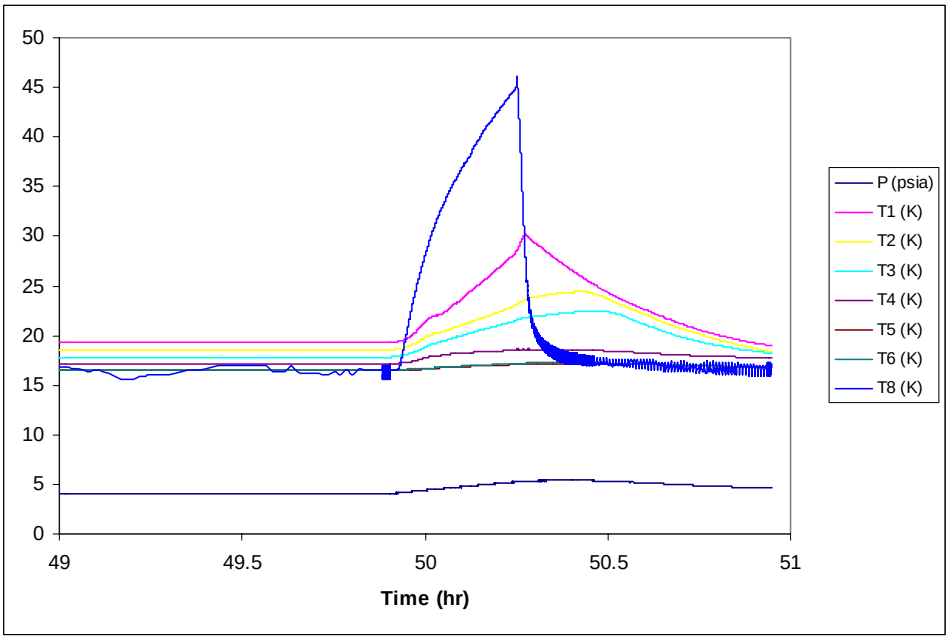

Figure 6-15 System relocation warm up

line indicating it remained in liquid. Reference Figure 6-17 for details. The heat pipe remained partially filled with liquid, allowing for maximum heat transfer to the bottom of the tank. Again, there was some trouble maintaining a constant hydrogen flow rate. At the end of the day, integration showed the total volume of hydrogen inside the tank had risen to 3153 standard liters.

There was some behavior in the tank that was not expected. Once the hydrogen gas flow was terminated, the pressure began to decrease as expected, since the cryocooler was condensing the ullage gas. However, the ullage temperatures fairly quickly collapsed to the saturated state, equaling the liquid temperature. The ullage

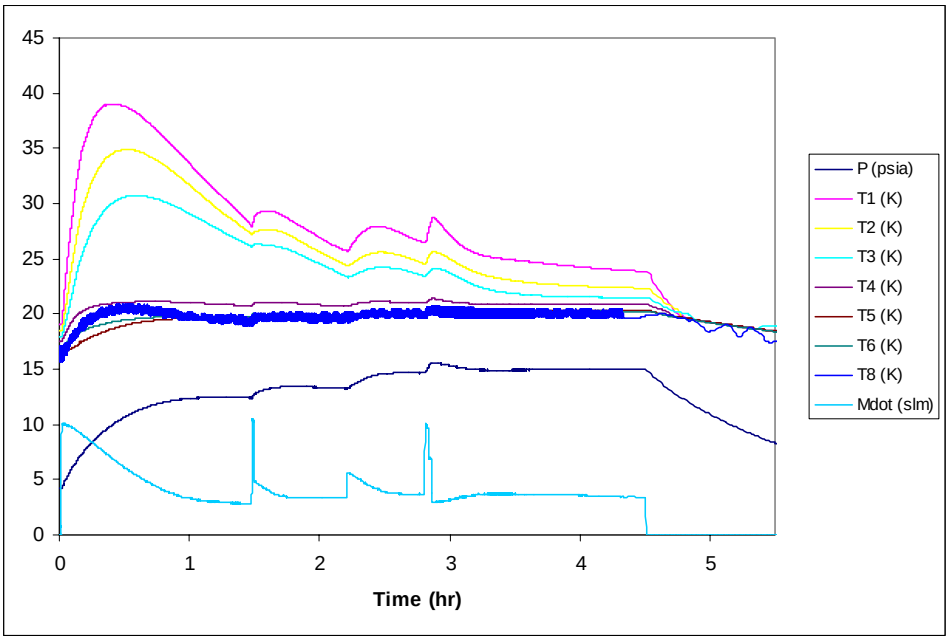

Figure 6-16 Continuing liquefaction

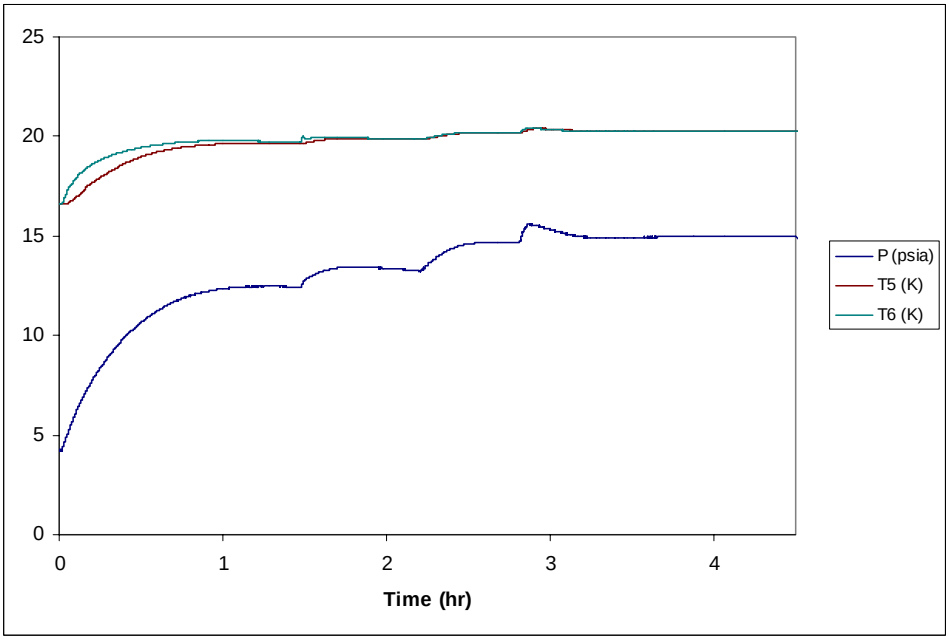

Figure 6-17 Liquid temperature and pressure saturation curve

remained saturated for approximately 30 minutes, and then the expected temperature gradients began to reappear in the ullage. This behavior was not observed on the first day, due to the fact that there was still no liquid in the tank at the time the gas flow was

terminated. Similar behavior was observed to some extent on all subsequent days the hydrogen flow was terminated. Figure 6-18 below shows this ullage collapse graphically.

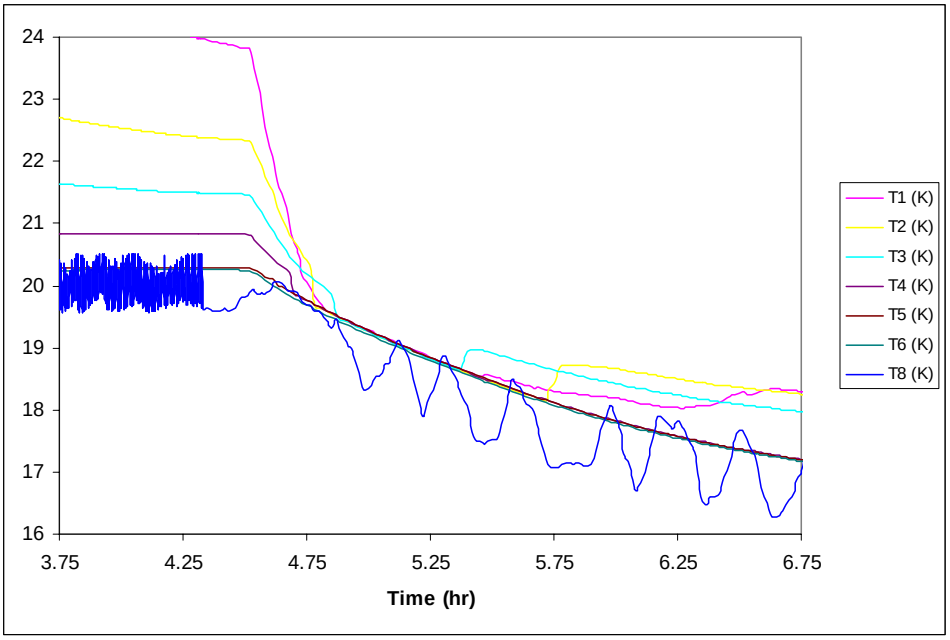

Figure 6-18 Ullage collapse

Hydrogen flow and liquefaction operations continued for the next several days on first shift only, with only slight changes in data. Plots are shown in Figures 6-19 and 6-20 for the next two days. At the end of these two days, a total of 7565 standard liters of hydrogen had been liquefied. At this point, hydrogen flow was terminated for the next week, and densification operations continued around the clock. After one week of densification, the stabilized temperature at the bottom of the system remained 16.7 K, roughly equal to the temperature achieved at the end of an overnight chilldown. A second bottle of gaseous hydrogen was purchased and connected to the system, and liquefaction operations recommenced.

Following another week of densification, the liquefaction operations began again on July 12. A second K-bottle of gaseous hydrogen was connected. Liquefaction

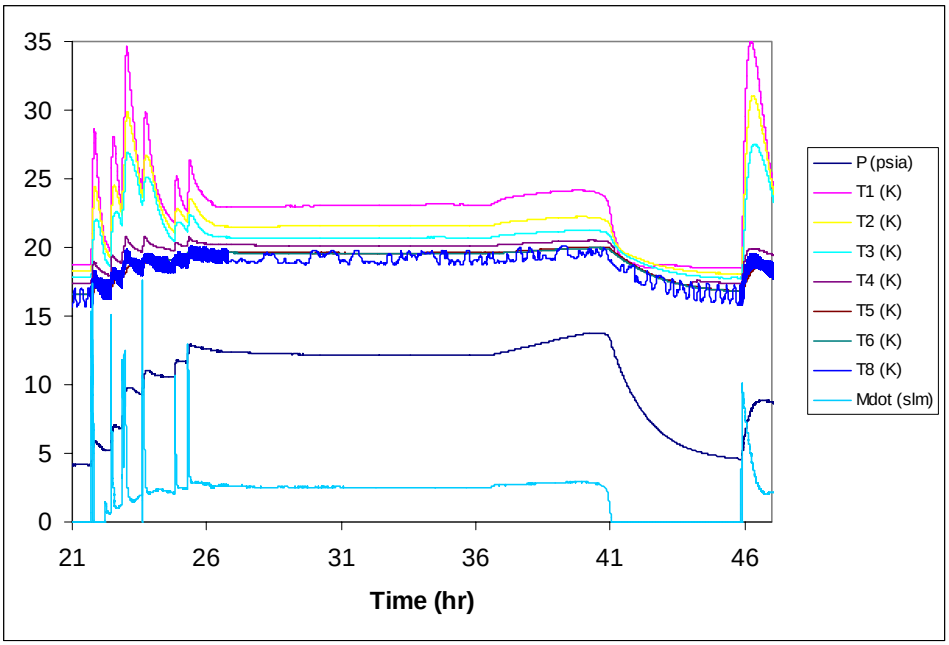

Figure 6-19 Liquefaction on 6-30-04

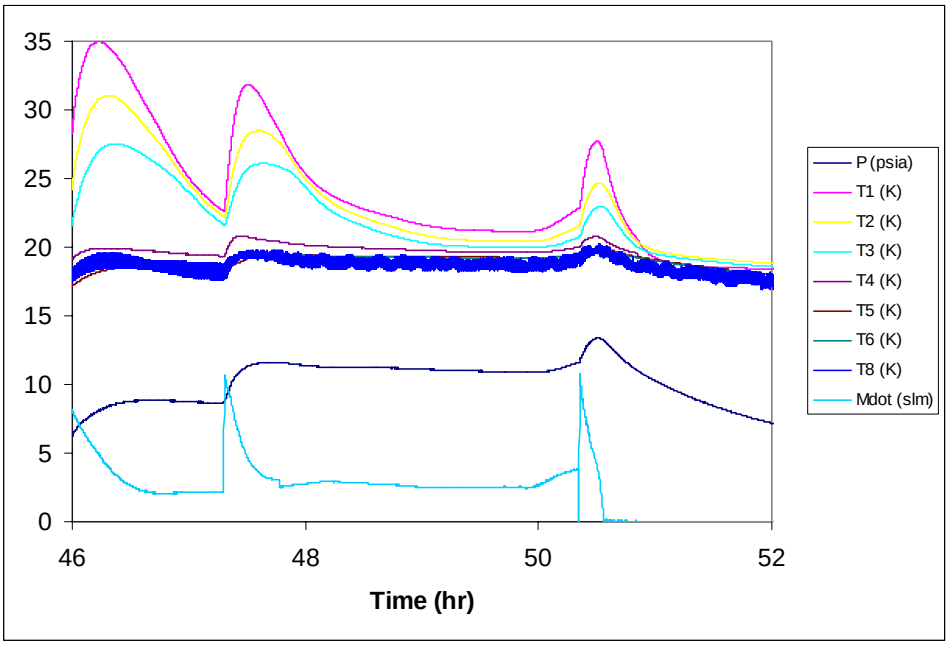

Figure 6-20 Liquefaction on 7-1-04

occurred on first shift all five days that week, with very similar temperature and pressure profiles as was recorded previously. At the end of the week, a total of 15,214 standard liters of gaseous hydrogen had been liquefied, or 1.25 kg. This is equal to 17.65 liters of

liquid in the tank. At this time it was decided no further liquefaction would be allowed in the small laboratory that was being used, due to safety constraints. Further liquefaction would occur once the outdoor hydrogen test facility was completed.

Zero Boil Off

Although no further liquefaction was allowed, the system remained partially full of liquid hydrogen. Testing was performed to determine the minimum cryocooler run time necessary to maintain the hydrogen in the tank without boil off losses. This was done for two reasons; first, to minimize the energy expended, and second, to minimize the excessive noise in the lab that the G-M refrigerator caused. Figure 6-21 shows the typical temperature and pressure profiles of the ZBO testing for two days. The cryocooler was turned off for 8 to 9 hours on first shift, then turned back on at the start of second shift and allowed to cool overnight. Pressure rise in the tank reached 33 psia, below the relief valve set point, so no venting occurred. The cryocooler generally took about 7 hours to recondense the boil-off and achieve the densified condition again. Since there was no way to turn on and off the cryocooler automatically, the cooler continued to operated over third shift and was then turned off at the start of the next first shift. Future performance upgrades to the system will include a control system to automatically start the cryocooler when the pressure reaches a set point (33 psia), and turn off the cooler when the low point pressure is reached. The ZBO operations continued until August 12, when securing for Hurricane Charley dictated the system be drained and purged of H2. Looking at a plot of the non-dimensional temperature profile for a shorter time period gives a better physical understanding of the heat transfer processes taking place inside the tank. From an energy balance of a defined region inside the tank, assuming no mixing, the functional dependence of the non-dimensional temperature (T*) becomes

$$T^* = f(x^*, Fo, Bi) \qquad 6\text{-}1$$

where Fo is the Fourrier number and Bi is the Biot number. This functional dependence

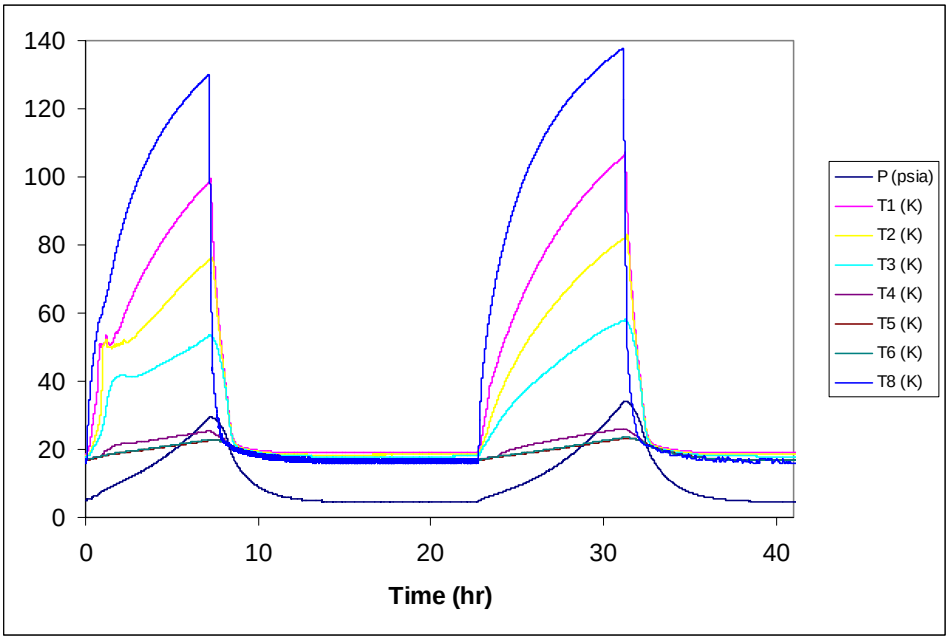

Figure 6-21 Zero boil off operations

can be found knowing the exact geometry of the system. The geometry of the vapor region is a cylinder with variable temperatures up the length of the wall and a constant warm temperature at the top of the tank. For this case, T1* thru T4* exhibit the same behavior since they are all in the same vapor region and only the difference in location gives a variation in temperature. T8* is influenced more by conduction down the cryocooler and has different temperature profiles. Similarly T5* and T6* are both in the liquid region and the heat transfer mechanism also is different than the vapor region.

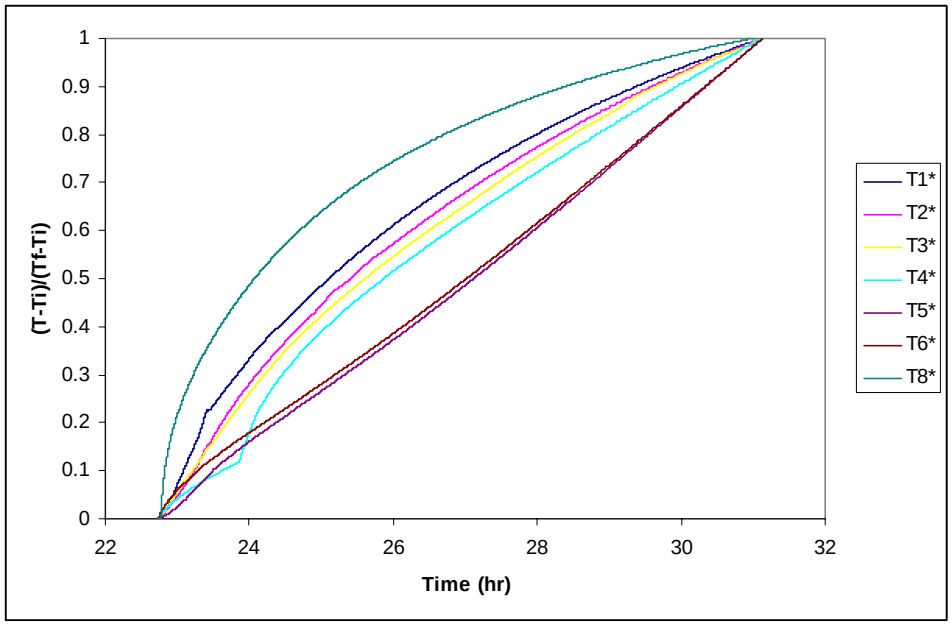

Figure 6-22 Non-dimensional thermal stratification during self pressurization

Measurement Uncertainty Analysis

Any well-executed experiment must include accounting for uncertainty in the measurements. These errors manifest themselves in two ways, bias errors and precision errors. Bias errors are fixed, constant components of the total error, whereas precision errors are random and due to repeatability of measurements. Although bias errors are often thought to be eliminated by calibration of the instruments, there are still installation bias errors present. In this case, these installation bias errors for the calibrated silicon diode temperature measurements come from an imperfect heat exchange with the surface they are bonded to.[67]

The main focus of this chapter is to obtain a general knowledge of the thermodynamic behavior of hydrogen in an integrated refrigeration and storage system. This focus means much of the work is an examination of data collected for the thermodynamic variables, and not as much emphasis is placed on data reduction equations where errors and uncertainty can propagate. This simplifies the uncertainty

analysis. For example, two primary properties to be measured are the temperature and pressure, and the instrumentation vendor has provided a calibration report for both of these measurements. For example, the pressure is calibrated to an accuracy of +/- 0.05 psia. There is also a bias error associated with the analog to digital signal. With a 16-bit analog to digital converter, there is a precision bias of approximately 0.00153 psia. The addition of these individual uncertainties gives the overall measurement uncertainty. Knowing the uncertainty, error bars in the y direction can be added to these plots. Figure 6-23 is another view of Figure 6-21 (ZBO operations), with only T6 and the tank pressure shown, and the measurement uncertainty bars are included. Figure 6-24 shows these error bars for the pressure and temperature (T6) respectively for a blown up section of Figure 6-23. From this it is apparent that the uncertainty in these measurements is so small, it is not visible in the "big picture" plots that make up the bulk of this chapter.

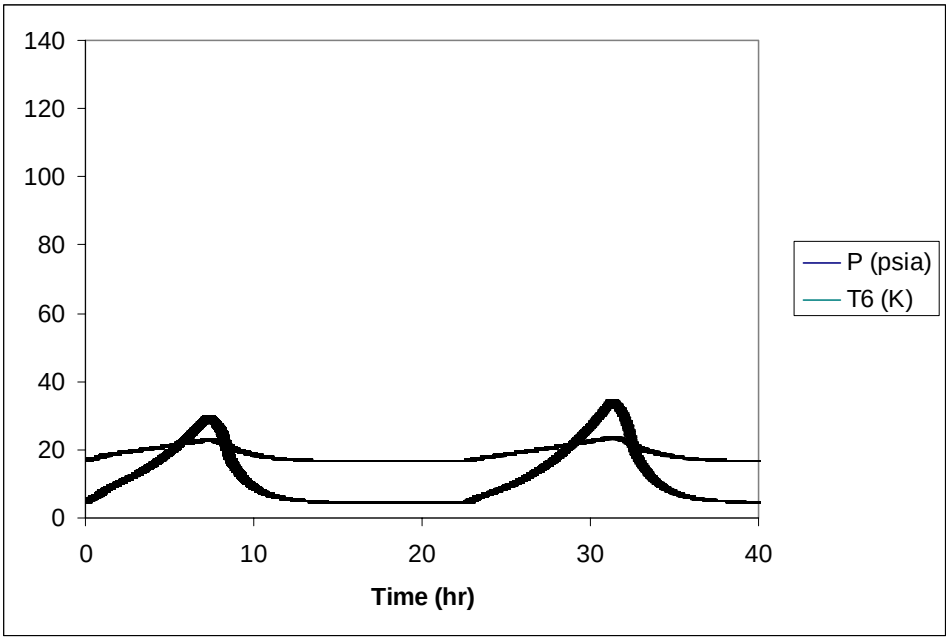

Figure 6-23 ZBO operations with P and T error bars

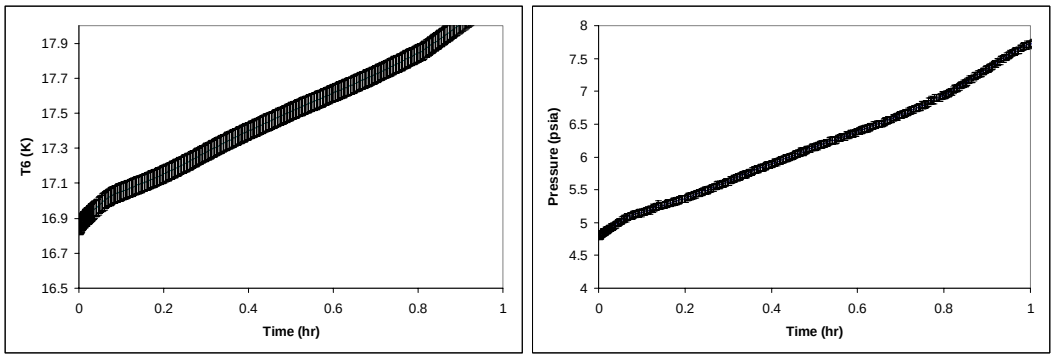

Figure 6-24 Expanded section plots of P and T with error bars

There are several places in this chapter where data reduction calculations are made. In these cases the uncertainty can propagate into the derived expressions.[68] An example is Figure 6-24, which shows the total mass in the tank as it is calculated by the expression

$$M = \int \dot{m} * dt \qquad 6\text{-}2$$

Knowing the mass flow rate measurement has a calibration uncertainty of 0.05 slm, and the A/D conversion bias is 0.002 slm, the total uncertainty of the mass flow is +/-0.052 slm. Adding these uncertainties into the Excel database and integrating over time, the total uncertainty of the hydrogen mass can be calculated. Figure 6-25 is a revised graph of Figure 6-12, with an upper and lower uncertainty plotted. From this analysis, there is a final uncertainty of 1.6% in the tank mass over the period of time considered. This total uncertainty is much greater than the uncertainty at any one specific measurement point, since the errors can propagate over time.

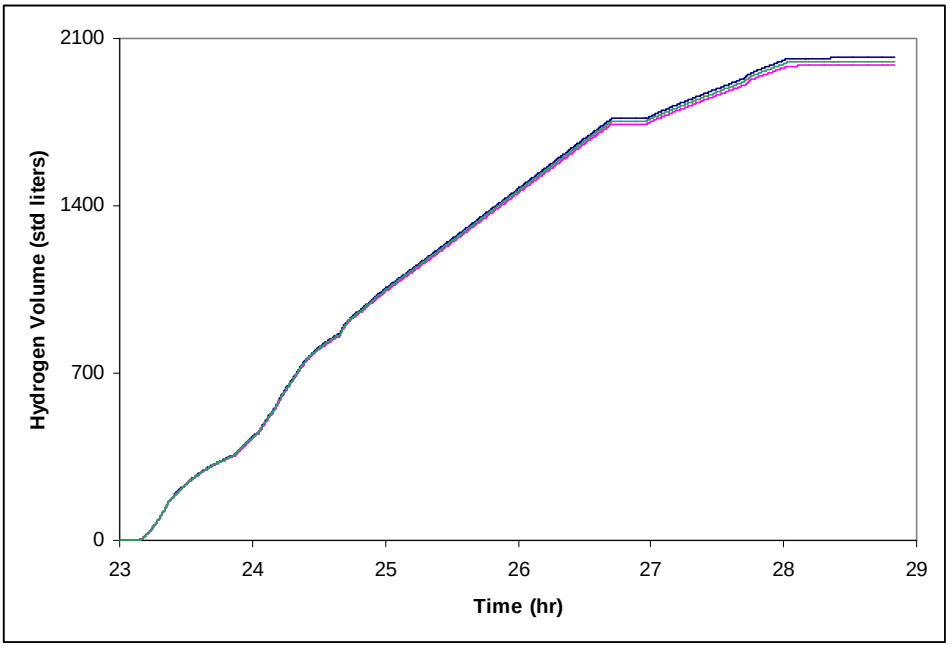

Figure 6-25. Mass uncertainty estimates

CHAPTER 7
CONCLUSIONS AND RECOMMENDATIONS

A novel hydrogen liquefaction, storage and distribution system has been proposed for space launch vehicle servicing applications. This system integrates a closed cycle helium refrigerator into the liquid space of the storage tank, removing the heat leak into the system from the surroundings and controlling the state of the hydrogen by varying the total heat interactions. This offers a potential for reduced operations cost combined with advanced servicing capabilities.

Chapter 1 provides background research in the current state of the art in liquid hydrogen storage. Present systems lose up to 50% of the liquid hydrogen per year. These losses are a byproduct of normal heat leak into the system, heat leak via tanker transportation operations, or chill down of warm parts of the system. Research into past zero boil-off studies have been conducted, and economic analysis applied future launch vehicles have been presented. In addition, on site liquefaction gives greater flexibility to the entire propellant supply chain, minimizing the reliance on commercial liquid hydrogen suppliers. Current and proposed methods of propellant conditioning, or densification, were also discussed. Chapter 2 details the concept of the proposed system and the economic and safety advantages over the current state of the art. The behavior of the system is addressed from a qualitative standpoint and potential issues are addressed. A projected vision of what a full-scale system would be is also presented.

Chapter 3 provides the quantitative analysis of the system behavior from the thermodynamic perspective. First, an Excel based model of the storage system

thermodynamic behavior is developed. This model uses the integral forms of the conservation of mass and conservation of energy and makes an assumption of bulk fluid properties in the liquid and vapor region. The heat leak is modeled using the modified Lockheed Martin MLI correlation combined with Fourier's law of conduction down solid supports. The state of the liquid and gas in the system is modeled for a variety of system operations. Where possible, the model is compared to experimental data gathered in Chapter 6. Discrepancies in the data and the model are noted. These discrepancies are attributed to assumptions made in the heat leak calculation (assumption of isothermal system) and transient effects that are not accounted for by the bulk fluid property assumption. A two-part correction factor is proposed to account for these changes. First, a linear correction factor with respect to system liquid level is added, then, a time dependent logarithmic correction is added to account for transient effects. This proposed factor is added to the model and predicted results match experimental results more accurately. This model can be used for ground or space based mission design, including estimating on orbit hold times, required cooling capacities for zero boil off, and predictions of propellant densification low temperature load points.

Second, a thermodynamic model of the proposed liquefaction cycle is developed. This is a novel cycle that achieves cooling in a combined manner by expanding hydrogen at high pressure while other steps in the cycle remove heat via a closed loop helium refrigeration cycle. The details of the cycle are provided, and an Excel based model is developed. This model uses a number of inputs, including heat exchanger, compressor, and turbine efficiencies, variable temperature storage states, and input hydrogen flowrates. The model then iterates to find problem solutions for a range of variables

including hydrogen and helium compression ratio, helium high and low temperature turbine mass flow rates, and required intermediate temperatures downstream of the recuperative heat exchanger. The model shows there is a small range of acceptable operating temperatures for a given set of hydrogen and helium pressures, and the favored operating pressure for this cycle is around 1200 kPa for the helium side and 2200 kPa for the hydrogen side.

The last section of Chapter 3 addresses the true physical behavior of the hydrogen in the storage system. An energy balance between the heat leak across the insulation and the free convection heat leak inside the tank shows normal temperature gradients between the walls and the fluid is less than 0.1K. During transient operations, this gradient may increase. Using this temperature gradient, predictions are made on the heat transfer and hydrodynamic flow regimes. The Reynolds number and the Grashof number are computed for this liquid and vapor regions. Then, the full conservation equations in differential form are presented, and using an order of magnitude analysis the equations are simplified. These equations are transient and 2 dimensional, and include a viscous boundary layer region and an inviscid core flow. Finally, a unique form of these equations is presented in dimensionless form, using dimensional constants derived from the initial state of the fluid and the thermal boundary conditions. The significance of the choice of dimensional constants and dimensionless parameters is discussed.

Chapters 4, 5, and 6 focus on an experimental apparatus designed to test the proposed system. Chapter 4 is a safety analysis of liquid hydrogen systems, with a particular emphasis on densified fluids cooled below the normal boiling point. Previously unpublished data on subcooled hydrogen explosive equivalence is included.

Chapter 5 details the experimental system design and fabrication effort. Several unique design features were needed to accommodate the densified hydrogen, including redesign of the self-pressurization system and design of a liquid hydrogen heat exchanger. Finally Chapter 6 shows the results of approximately 6 weeks worth of testing, including data analysis on hydrogen liquefaction, densification, and zero boil-off operations. Pressure control via mass injection is achieved during some liquefaction operations.

At the end of this effort, the conclusion that has been reached is the integrated refrigeration and storage system as proposed within appears to offer many benefits. Numerical analysis and experimental data confirm that the system behavior is acceptable.

A number of recommendations can be made to further this effort in the future. First, a detailed computational fluid dynamics model should be developed to more accurately predict system behavior. Prior to this model development, experimentation to determine heat and mass transfer coefficients of liquid hydrogen in the natural convection mode should be made. The verification of these transport properties will allow for greater model fidelity. Once more accurate analysis and experimentation are done at this level, a large-scale testbed (greater than 10,000 gallons) should be developed. This will allow further testing of operational concepts that could not be completed in the small testbed due to size, funding and safety constraints, including recovery of chill down losses, pressurization with non condensable gasses, methods of temperature stratification management, and efficient liquefaction including staged refrigeration and ortho-to-para hydrogen conversion at multiple temperatures.

APPENDIX A
CRYOSTAT SYSTEM SPECIFICATION

Liquid Hydrogen Dewar and Cryocooler Assembly

Configuration and Performance Requirements

General: The entire assembly shall be designed to store subcooled liquid hydrogen, with a maximum pressure of 52 psia and a minimum temperature of 14K, and shall be considered portable. A cryocooler cold head shall be integrated into the dewar to provide refrigeration for subcooling of the NBP hydrogen. This entire assembly shall be designed for, and suitable for use with liquid and/or gaseous hydrogen service. Refer to Fig. 1 for representative configuration. The assembly shall be designed and built to allow for maximum flexibility to access and modify internal components, including access to disconnect the pressurization coil.

Size and dimensions: Inner tank volume shall be between 140 and 150 liters. Four liquid/gas interface ports shall be provided for connection with the experimental system. Liquid fill/withdraw port shall be ½ inch ID vacuum jacket line with manual shut-off valve at the end. Vent port shall be 1/2 inch line with manual shut-off valve at the end. Liquefaction supply port shall be 3/8 inch line with manual shut off valve at the end. Gas supply port shall be 3/8 inch line with manual shut-off valve at the end. Mechanical connections on valve outlets are TBD.

Pressurization: Dewar assembly shall have the capability of self-pressurization thru internal vaporizer. Pressure level shall be adjustable thru a vaporizer regulator.

Overpressurization protection: Dewar inner vessel shall be equipped with relief valve to prevent overpressurization. RV shall be set at maximum operating pressure. RV shall be in line type to allow for connection to external vent system. Capacity of relief system shall be capable of relieving pressure buildup in the event of loss of vacuum. Dewar inner vessel shall be equipped with burst disk set at 116% of maximum operating pressure.

Vacuum jacket: Vacuum annulus shall include spacers, multi-layer super-insulation (MLI), and a chemical gettering system. A suitable vacuum pump out port, preferably a 1" CF flange, standard for high vacuum use, shall be provided for the vacuum annulus. A vacuum relief valve shall be provided to ensure overpressurization of the vacuum annulus does not occur.

Heat leak: Total assembly heat leak shall be minimized (10 W at 14 K or less) to reduce size of selected cryocooler assembly. Radiation shielding such as LN2 jacket, vapor cooled shield, or mechanical cooling (cryocooler 1st stage) are acceptable if required to meet heat leak specification.

Cryocooler interface: Cryocooler cold head shall be in the inner vessel to facilitate transfer of energy from the liquid hydrogen to the cryocooler. Cryocooler compressor shall be outside the vacuum annulus and can be located some small distance away from the assembly. Cryocooler shall be sized to provide at least 30W cooling at 20K. Cryocooler shall be optimized for long term, reliable operation and not necessarily for overall thermodynamic efficiency.

Heat exchanger: A fin type heat exchanger shall be added to the cryocooler coldhead to increase surface area and allow for greater heat exchanger to the liquid

hydrogen. One fin shall be hollow with perforations to allow for connection to liquefaction supply line.

Instrumentation: Dewar shall be instrumented to provide temperature profile of the liquid hydrogen. Temperature probe shall have sensors spaced at a minimum of every 4 inches. Temperature probe shall have the capability of quantifying liquid level. Additional temperature sensors shall be capable of measuring cryocooler cold head temperature. Tank pressures shall be monitored using pressure transducer.

Design, Fabrication, Inspection and Testing Requirements

Inner Vessel: The inner vessel shall be designed, fabricated, and tested in accordance with ASME Code, Section VIII, Division I for a design pressure of 52 psia, and a service temperature range of 14 K to 300 K. The inner vessel shall be designed to withstand an internal vacuum (0 psia) and external (vacuum jacket) pressure of 15 psia.

Vacuum Jacket: VJ shall be designed, fabricated, and tested in accordance with ASME Boiler and Pressure Vessel Code, Section VIII and Section IX. For a service temperature of 14 K to 300 K, the VJ shall be designed for both 1) an internal vacuum (0 psia) and 15 psig external pressure, and 2) an internal pressure (the greater) of 35 psig or two times the VPR valve relief pressure and 0 psig external pressure.

Bellows: Any bellows shall be designed, fabricated, and tested in accordance with ASME B31.3 and the Standards of the Expansion Joint Manufacturers Association (EJMA). Normal movement shall not exceed 75% of the maximum rated movement for a design cycle life of 7,000 cycles.

Materials: All dewar materials shall be 304/304L or 316/316L stainless steel, unless otherwise approved.

Radiographic Testing: All vessel welds shall be subject to 25% random radiographic testing. Do not use liquid penetrant on welds.

Pressure Test: Pressure vessels shall be pressure tested in accordance with ASME Code, Section VIII except that a pneumatic pressure test shall not be at less than 125% of the design pressure. After a hydrostatic pressure test, component surfaces shall be completely dried and passivated.

Cold Shock: Prior to leak test, the completed assembly shall be cold shocked with liquid nitrogen. After completion of cold shock test, assembly shall be allowed to return to ambient temperature, using an ambient nitrogen purge if necessary. Moisture shall be prevented from forming on (the inside of) components as the assembly warms.

Leak Test: The completed assembly shall be leaked tested by pressurizing process lines/component to 30 psig with (pure and dry) helium. During the test no leakage shall be detected using a helium mass spectrometer connected to the vacuum annulus, previously evacuated to 0 psia. The helium mass spectrometer shall be calibrated to a sensitivity of $1x10^{-9}$ standard cubic centimeters per second (sccs).

Final Cleaning: After the successful completion of all testing, the entire assembly shall be commercially oxygen cleaned (per standard “Linde” specification). Prior to shipping, with the assembly at ambient temperature and at (or above) 0 psig, the vacuum level shall not significantly change (i.e., approx. ±1 micron) over a 48 hour period, and shall be stable at less than 15 microns (micro-meters of Mercury).

Submittals

Fabrication and assembly drawings for assembly, including dimensions, line sizes/schedules, and material specifications.

Vessel heat leak and design code calculations.

Welding procedure specifications (WPS's), procedure qualification records (PQR's), and welder performance qualifications (WPQ's).

Non-destructive test personnel qualifications.

Mill test reports.

Radiographic records, radiographs, and weld map.

Test reports and certifications.

Shipment

Assembly shall be packaged for shipment such that the cleanliness level is maintained and to prevent moisture intrusion. Assembly shall be restrained from motion during shipment and evenly supported (no concentrated support loads) All ports shall be capped with the appropriate mating fitting. Assembly shall be shipped with a nitrogen blanket pressure between 5 to 10 psig. The pressure port shall be equipped with an appropriate gauge and vent valve (for venting the assembly to ambient pressure upon arrival). An obvious and conspicuous caution, stating "CAUTION: ASSEMBLY UNDER POSITIVE PRESSURE", shall be placed on the assembly for shipping (which will be immediately seen upon opening the shipping container, but able to be easily removed without damaging the assembly).

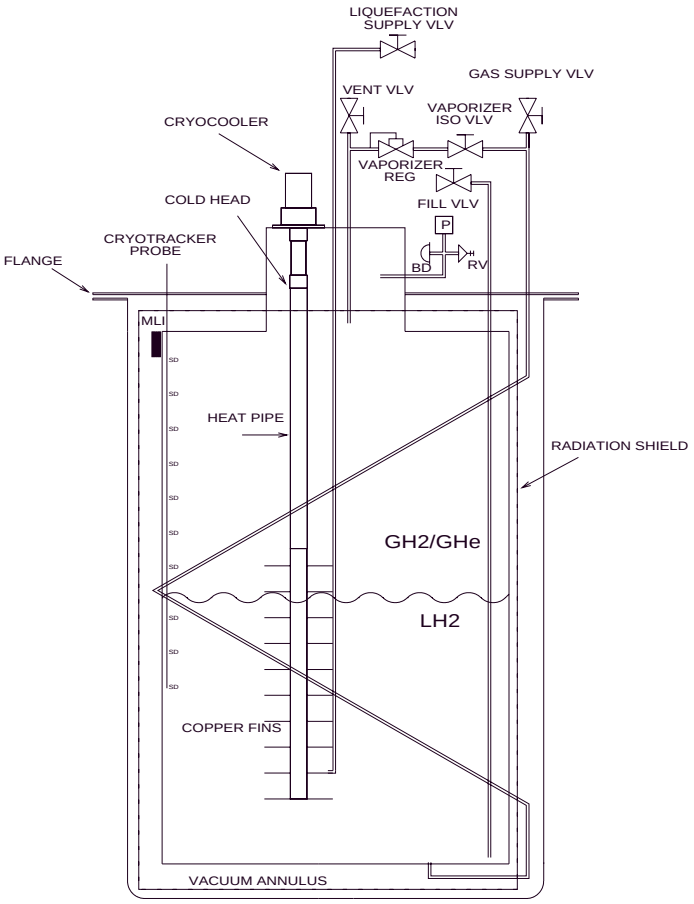

Figure A-1 System Specification Schematic

APPENDIX B
HEAT LEAK CALCULATION

Radiation

Tank Geometry		
Volume	157,000	cm3
Radius	25.4	cm
Length	64.7	cm
Area	15,600.0	cm2
Insulation density	11.8	#/cm
Insulation layers	45	#
Warm boundary T	300	K
Cold Boundary T	20.2	K
Insulation K	1.121625	W/m2
Radiation H/L	1.75	W

	TOTAL	
Radiation	1.75	W
Neck	2.424209	W
Tubes	2.440476	W
Cooler	1.97	W
Total	8.58	W

Conduction

Neck

ID	20.32	cm
Thickness	0.0381	cm
Length	30.48	cm
Warm Boundary T	300	K
Cold Boundary T	20.2	K
Material	304	
K-h	3060	W/m
K-c	16.30	W/m
Heat leak	2.424209	W

Feedthru #1

ID	0.9525	cm
OD	0.1244	cm
Length	25.4	cm
Warm Boundary T	300	K
Cold Boundary T	20.2	K
Material	304	
K-h	3060	W/m
K-c	16.30	W/m
Heat leak	0.581717	W

Feedthru #2

ID	1.59	cm
OD	0.1244	cm
Length	25.4	cm
Warm Boundary T	300	K
Cold Boundary T	20.2	K
Material	304	
K-h	3060	W/m
K-c	16.30	W/m
Heat leak	1.029544	W

Feedthru #3

ID	0.9525	cm
OD	0.1244	cm
Length	25.4	cm
Warm Boundary T	300	K
Cold Boundary T	20.2	K
Material	304	
K-h	3060	W/m
K-c	16.30	W/m
Heat leak	0.581717	W

Feedthru #4

ID	0.9525	cm
OD	0.1244	cm
Length	59.7	cm
Warm Boundary T	300	K
Cold Boundary T	20.2	K
Material	304	
K-h	3060	W/m
K-c	16.30	W/m
Heat leak	0.247498	W

APPENDIX C
DENSIFICATION SAMPLE MODEL

Initial Conditions		
P	101	kPa
T	20.27	K
M	5411	g
V	150000	cm3
Fluid	n-hyd	
Heat leak	8.80	W

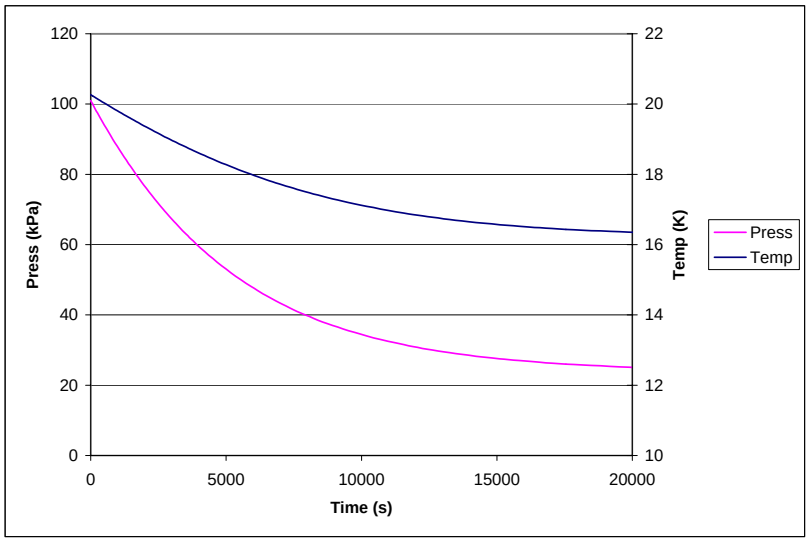

P kPa	T K	X m3	h J/g	H J	rho-g g/cm3	M-g g	H-g J	rho-f g/cm3	M-f g	H-l J	t /	Q W
101	20.27	0.0185	-273.13	-1477891	0.00134	100.2	16439	0.0708	5310.8	-1494330		-32.394
100	20.23	0.0184	-273.55	-1480158	0.00132	99.3	16278	0.0708	5311.7	-1496436		-32.151
99	20.20	0.0182	-273.97	-1482433	0.00131	98.5	16117	0.0709	5312.5	-1498550		-31.905
98	20.16	0.0180	-274.39	-1484718	0.00130	97.6	15956	0.0709	5313.4	-1500674		-31.657
97	20.13	0.0179	-274.81	-1487012	0.00129	96.7	15795	0.0710	5314.3	-1502807		-31.407
96	20.10	0.0177	-275.24	-1489316	0.00128	95.9	15634	0.0710	5315.1	-1504950		-31.154
95	20.06	0.0176	-275.67	-1491630	0.00126	95.0	15473	0.0710	5316.0	-1507102		-30.900
94	20.03	0.0174	-276.10	-1493953	0.00125	94.1	15312	0.0711	5316.9	-1509264		-30.643
93	19.99	0.0172	-276.53	-1496286	0.00124	93.3	15150	0.0711	5317.7	-1511437		-30.383
92	19.96	0.0171	-276.96	-1498630	0.00123	92.4	14989	0.0712	5318.6	-1513619		-30.121
91	19.92	0.0169	-277.39	-1500984	0.00122	91.5	14828	0.0712	5319.5	-1515811		-29.856
90	19.88	0.0168	-277.83	-1503348	0.00120	90.7	14666	0.0712	5320.3	-1518015		-29.589
89	19.85	0.0166	-278.27	-1505723	0.00119	89.8	14505	0.0713	5321.2	-1520228		-29.319
88	19.81	0.0164	-278.71	-1508110	0.00118	88.9	14344	0.0713	5322.1	-1522453		-29.047
87	19.77	0.0163	-279.15	-1510507	0.00117	88.1	14182	0.0714	5322.9	-1524689		-28.771
86	19.74	0.0161	-279.60	-1512916	0.00116	87.2	14021	0.0714	5323.8	-1526936		-28.493
85	19.70	0.0160	-280.05	-1515336	0.00114	86.3	13859	0.0714	5324.7	-1529195		-28.212
84	19.66	0.0158	-280.50	-1517768	0.00113	85.4	13697	0.0715	5325.6	-1531465		-27.928
83	19.62	0.0156	-280.95	-1520212	0.00112	84.6	13536	0.0715	5326.4	-1533747		-27.641
82	19.58	0.0155	-281.40	-1522668	0.00111	83.7	13374	0.0716	5327.3	-1536042		-27.351
81	19.54	0.0153	-281.86	-1525137	0.00110	82.8	13212	0.0716	5328.2	-1538349		-27.058
80	19.50	0.0151	-282.32	-1527618	0.00108	81.9	13051	0.0717	5329.1	-1540669		-26.762
79	19.46	0.0150	-282.78	-1530113	0.00107	81.0	12889	0.0717	5330.0	-1543001		-26.462
78	19.42	0.0148	-283.24	-1532620	0.00106	80.1	12727	0.0717	5330.9	-1545347		-26.159
77	19.38	0.0146	-283.71	-1535141	0.00105	79.3	12565	0.0718	5331.7	-1547706		-25.852
76	19.34	0.0145	-284.18	-1537676	0.00103	78.4	12403	0.0718	5332.6	-1550079		-25.542
75	19.30	0.0143	-284.65	-1540225	0.00102	77.5	12241	0.0719	5333.5	-1552467		-25.229
74	19.26	0.0142	-285.12	-1542789	0.00101	76.6	12079	0.0719	5334.4	-1554868		-24.911
73	19.22	0.0140	-285.60	-1545367	0.00100	75.7	11917	0.0720	5335.3	-1557284		-24.590

APPENDIX D
ACRONYMS AND SYMBOLS

Acronyms

A/D	analog to digital
AIAA	American Institute of Aeronautics and Astronautics
ASME	American Society of Mechanical Engineers
CTE	coefficient of thermal expansion
daq	data acquisition
DoT	Department of Transportation
ET	External Tank
FOM	Figure of Merit
FSEC	Florida Solar Energy Center
G-M	Gifford McMahon
GRC	Glenn Research Center
GSE	ground support equipment
HHV	higher heating value
HX	heat exchanger
ISRU	In Situ Resource Utilization
J-T	Joule-Thompson
KISS	keep it simple, stupid
KSC	Kennedy Space Center
LC	launch complex
LEO	low earth orbit
LFL	lower flammability limit
LH2	liquid hydrogen
LHS	left hand side
LN2	liquid nitrogen
LOX	liquid oxygen
LRU	line replacement unit
MAWP	maximum allowable working pressure
MLI	multi layer insulation
MOP	maximum operating pressure
NASA	National Aeronautics and Space Administration
NBP	normal boiling point
NFPA	National Fire Protection Association
NSS	NASA safety standards
PBU	pressure build up
Q-D	quantity-distance
RHS	right hand side
RLV	reusable launch vehicle

SBIR	Small Business Innovative Research
SS	stainless steel
UFL	upper flammability limit
USAF	United States Air Force
VJ	vacuum jacket
ZBO	zero boil-off

Units

g	grams
gpm	gallons per minute
J	joules
K	degrees Kelvin
kg	kilogram
kJ	kilojoules
kPa	kilopascals
kW	kilowatts
kW-hr	kilowatt-hour
m^3	cubic meters
psi	pounds per square inch
psia	pounds per square inch absolute
psig	pounds per square inch gauge
sccm	standard cubic centimeters per minute
SLPM	standard liters per minute

Symbols

A	Area
E	energy
$\overline{F}$	force vector
g_y	gravitational acceleration
Gr	Grashof number
h	specific enthalpy
h	heat transfer coefficient
k	thermal conductivity
L	characteristic length
$\dot{m}$	mass flow rate
m	mass
Nu	Nusselt number
P	pressure
Pr	Prandtl number
$\dot{Q}$	heat transfer rate
Q_{ref}	refrigeration heat transfer

Q_{HL}	heat leak
Q_{rad}	radiation heat transfer
Q_{con}	conduction heat transfer
Ra	Rayleigh number
Re	Reynolds number
s	specific entropy
t	time
T	temperature
u	velocity in horizontal direction
v	velocity in vertical direction
V	volume
$\overline{V}$	velocity vector
W	work
y	liquid yield %
α	thermal diffusivity
β	volumetric expansion coefficient
γ	specific heat ratio
μ	coefficient of viscosity
ρ	density
υ	kinematic viscosity

LIST OF REFERENCES

1. Peschka, W., Liquid Hydrogen – Fuel of the Future, Springer-Verlag Wein, New York, NY, 1992

2. Culp, A.W., Principles of Energy Conversion, 2nd Edition, McGraw-Hill Inc., New York, NY, 1991

3. Sutton, G.P., and Bilbarz, O.; Rocket Propulsion Elements; Wiley Interscience, New York, NY, 2001

4. Rudiger, H., and Seifers, H.; Liquid Hydrogen Storage System for Urban Bus; .; Hydrogen Energy Progress X; Proceedings of the 10th World Hydrogen Energy Conference; International Association of Hydrogen Energy, Orlando FL,1994

5. Kocer, K., and Veziroglu, T.N.; Liquid Hydrogen Powered Commercial Aircraft; Hydrogen Energy Progress X; Proceedings of the 10th World Hydrogen Energy Conference; International Association of Hydrogen Energy, Orlando FL, 1994

6. GasPak V 3.41, Thermophysical and Transport Properties Database, Horizon Technologies, 2003

7. Flynn, T.M., Cryogenic Engineering, Marcel Dekker Inc., New York, NY, 1997

8. West, J.E., The Economics of Small to Medium Liquid Hydrogen Facilities, CryoGas International, pg 28-33, May 2003

9. Barron, R.F., Cryogenic Systems 2nd Edition, Oxford University Press, New York, NY, 1985

10. Hynek, S. and Fuller, W., Hydrogen Storage within the Infrastructure, Proceedings of the 10th World Hydrogen Energy Conference, International Association of Hydrogen Energy, Orlando FL, 1994

11. Gen H2, CryoGas International, pg 45, May 2003

12. Pehr, K., Aspects of Safety and Acceptance of LH2 Tank Systems in Passenger Cars, Proceedings of the 10th World Hydrogen Energy Conference, International Association of Hydrogen Energy, 1Orlando FL, 994

13. Methods of Distributed Scale Liquefaction for Natural Gas and Hydrogen; Professional Development Short Course; Prometheus Energy Company

14. Strobridge, T.R.; Cryogenic Refrigerators – An Updated Survey; NBS Tech Note 655; Boulder CO, 1974

15. Add on Study to Prepare Design Details for a Re-Liquefier on the Complex 39 LH2 Tank, Martin Marietta Corp. 1977

16. Rosso, M.J., and Golben, P.M., Capture of Liquid Hydrogen Boil-Off with Metal Hydride Absorbers, Ergenics Inc., SBIR Final Report, 1986

17. Egan, G.J., and Gier, H.L., Capture and Reliquefaction of Hydrogen Boiloff at Shuttle Launch Site, Final Report, NAS10-11401, Hydrogen Consultants, SBIR Final Report, 1991

18. Notardonato, W.U., Baik, J.H. and McIntosh, G.E, Operational Testing of Densified Hydrogen Using GM Refrigeration, Advances in Cryogenic Engineering, Volume 49, pg 64-71, Plenum Publishers, New York NY, 2004

19. Larson, Wiley and Pranke, Linda; Human Spaceflight – Mission Analysis and Design; McGraw Hill, New York NY, 2002

20. Investigation of External Refrigeration Systems for Long Term Cryogenic Storage, Lockheed Missiles and Space Report A981632, 1971

21. Giellis, R.T., Long Term Cryogenic Storage Study, US Air Force, AFRPL TR-82-071

22. Kittel, P., Cryocoolers for the Human and Robotic Exploration of Mars, Cryocoolers10, pg 815-821, Plenum Press, New York NY, 1999

23. Plachta, D.W., Hybrid Thermal Control Testing of a Cryogenic Propellant Tank, Advances In Cryogenic Engineering Volume 45, pg 465-472, Plenum Press, New York NY, 2000

24. Hastings, L.J., An Overview of NASA Efforts on Zero Boiloff Storage of Cryogenic Propellants, Cryogenics 41, pg 833-839, Elsevier Science Ltd., New York NY, 2002

25. Plachta, D.W., Results of an Advanced Development Zero Boil-Off Cryogenic Propellant Storage Test, NASA TM-2004-213390, 2004

26. Kittel, P., Propellant Preservation Using Re-Liquefiers, Cryogenics 41, pg 841-844, Elsevier Science Ltd., New York NY, 2002

27. Lak, T., and Lozano, M., Advancement in Cryogenic Propulsion System Performance Through Propellant Densification, AIAA-96-3123, 1996

28. Ewart, R., and Dergance, R., “Cryogenic Propellant Densification Study”, Final Report NASA Lewis Research Center Contract Number NAS3-21014, 1977

29. DeWitt, R,. and Hardy, T., “Slush Hydrogen Technology Development for Application to the National Aerospace Plane”, NASA TM 102315, 1989

30. Tomsik, T., “Recent Advances and Applications in Cryogenic Propellant Densification Technology”, NASA TM-2000-209941, 2000

31. Notardonato, W.U.; NASA Strategic Launch Initiative Propellant Densification Program, Results of the Base Period Work and Future Plans, Proceedings of the 19th International Cryogenic Engineering Conference; pg 533-537, Narosa Publishing, New Delhi India, 2002

32. Notardonato, W., “Densified Propellant Operability Analysis”, NASA KSC White Paper, 2002

33. Notardonato, W.U., Propellant Densification for the Human Exploration of Mars, Proceedings of AIAA 37th Joint Propulsion Conference, Indianapolis IN, 2002

34. Rhodes, R; Propellant Cost Factors: NASA KSC White Paper; 2003

35. NSTS 3600 Launch Commit Criteria; NASA KSC, 2005

36. Gisteau-Baguer, G.; Helium Refrigeration; Cryogenic Society of America; Chicago, IL, 2004

37. Filina, N.N., and Weisend, J.G.; Cryogenic Two Phase Flow; Cambridge University Press; New York NY, 1996

38. Anderson, J.D.; Modern Compressible Flow; McGraw Hill; New York NY, 1990

39. Li, X., and Xu, L.; Investigation on Performances of Non-Loss Storage for Cryogenic Liquefied Gas; Cryogenics 44 pg 357; 2004

40. Tholmes, L.A. and Schwartz, S.H.; The Thermodynamics of Space Storage of Liquid Propellants; Douglas Aircraft Company Internal Report ;1967

41. Younglove, B.A.; Thermophysical Properties of Fluids: Argon, Ethylene, Parahydrogen, Nitrogen, Nitrogen Trifluoride, and Oxygen; J. Phys. Chem. Ref. Data, Vol. 11, Suppl. 1, pp. 1-11, 1982

42. Spadley, I.E., Nast, T.C., and Frank, D.J.; Experimental Studies of MLI Systems at Very Low Boundary Temperatures; Advances in Cryogenic Engineering, Vol.35; pg 407-413, Plenum 1990

43. McMordie, R.K.; Steady State Conduction with Variable Thermal Conductivity; Journal of Heat Transfer 84: pg 92-93

44. White, F.M.; Viscous Fluid Flow; McGraw Hill; New York NY, 1991

45. Majumdar, A., and Steadman, T.; Numerical Modeling of Thermal Performance of Cryogenic Test Tank at Kennedy Space Center; CESAT Interim Report, 2005

46. Tannehill, J.C., Anderson, D.A., and Pletcher, R.H.; Computational Fluid Mechanics and Heat Transfer; Taylor and Francis; New York NY, 1997

47. White, F.M.; Fluid Mechanics; McGraw Hill; New York NY, 1999

48. Oosthuizen, P.H., and Naylor, D.; Introduction to Convective Heat Transfer Analysis; McGraw Hill; New York NY, 1999

49. Nunn, R.H,; Intermediate Fluid Mechanics; Hemisphere Publishing Corporation; New York NY, 1989

50. Bejan, A.; Convection Heat Transfer; Wiley, New York NY, 1984

51. NSS 1740.16 NASA safety Standard for Hydrogen and Hydrogen Systems; 1995

52. NFPA 50B; Standard for Liquid Hydrogen Systems at Consumer Sites; 1999 Edition

53. CFR 29 1910.103; Occupational Health and Safety Standards 2206, Hydrogen; 1981

54. Title 49 CFR Parts 171-190; US Department of Transportation; Specifications and Regulations

55. Explosive Equivalence of Subcooled Liquid Hydrogen and Liquid Oxygen; USAF Report Number 07805-004-001-1; 2001

56. KSC STD Z-0009; Standard for Design of Cryogenic Ground Support Equipment; 1973

57. Scurlock, R.; Low Loss Tanks and Dewars; Cryogenic Society of America; Chicago IL, 2004

58. Churchill, S.W., and Chu, H.S,; Correlating equations for Laminar and Turbulent Free Convection from a Vertical Plate; International Journal of Heat and Mass Transfer, Vol 18, p1323; 1975

59. Combivac CM31 Operating Instructions; Leybold Vacuum

60. Model 218 Temperature Monitor- Users Manual; Lake Shore Cryotronics, Inc.

61. Calibration Report 376905; Lake Shore Cryotronics, Inc.

62. Calibration Report 20002647, Taber Industries

63. Operations and Maintenance Manual-G-M Cryocooler AL330 and Helium Compressor CP970; Cryomech Inc

64. Hansen, S.; Leaks: The Good, the Bad, and the Ugly; Bell Jar, Volume 7, No. 1 Winter 1998

65. MKS 358C Mass Flow Meter Instruction Manual; MKS Instruments

66. Jacobs, R.B.; Liquid Requirements for the Cool-Down of Cryogenic Equipment; Advances in Cryogenic Engineering, Vol. 8, Plenum Press

67. Coleman, H.W., and Steel, W.G.; Experimentation and Uncertainty Analysis for Engineers; Wiley Interscience, New York, NY, 1989

68. Uhl, V.W., and Lowthian, W.E.; Uncertainty Analysis for Engineers; American Institute of Chemical Engineers; New York, NY, 1982

69. Exploration Crew Transportation System Requirements Document; Version Preliminary – Revision B 8 Nov 2004

BIOGRAPHICAL SKETCH

William Notardonato is a Mechanical Engineer working for NASA at Kennedy Space Center (KSC). Mr. Notardonato's specialty is design and development of advanced cryogenic systems, with an emphasis on thermodynamic control of liquid hydrogen. He has been working at KSC since 1988, and has held a variety of jobs in different fluid systems, including hydraulics, pneumatics, life support, hypergolics, and cryogenics.

Mr. Notardonato earned a bachelor's degree in aeronautical engineering from the Ohio State University in 1988. After joining NASA, he earned a master's degree in mechanical engineering from the University of Central Florida in 1992. He was accepted for a KSC Graduate Fellowship and attended classes at the University of Florida in 2000. Since that time, he has been working on his dissertation part time while keeping his present duties at work.

Mr. Notardonato has published 10 papers relating to cryogenics and advanced materials testing.